Live Single-Cell Screening Based on Cell Encapsulation and Irradiation of Patterned Light

(パターン光照射と細胞カプセル化を用いた単一生細胞スクリーニング技術の開発)

July, 2024

Doctor of Philosophy (Engineering)

Venkatesh Kumar Panneer Selvam

ベンカッテイュ クマー パンニール セルバム

Department of Mechanical Engineering

Toyohashi University of Technology

別紙４－１（課程博士（英文））

Date of Submission: 2024/07/11

Department of Mechanical Engineering	Student ID Number	D209107
Applicant's name	Venkatesh Kumar Panneer Selvam	

Supervisors	Moeto Nagai Takayuki Shibata

Abstract（Doctor）

Title of Thesis	Live Single-Cell Screening Based on Cell Encapsulation and Irradiation of Patterned Light

Approx. 800 words

Single-cell screening has emerged as a powerful tool in life science, offering an effective method for detecting, isolating, and manipulating individual cells based on their specific characteristics. Traditional approaches involving manual identification of single cells from images were labor-intensive and time-consuming. Image-based cell sorting (IBCS) addresses these limitations by employing image processing tools for efficient identification and processing of single cells from large populations. This thesis presents two novel light irradiation approaches for single-cell screening.

Chapter 2 details the development of an automated photopolymerization system for encapsulating suspended single cells in photo-cross-linkable hydrogel. The system utilizes an image processing algorithm to identify individual cells from cell groups in captured images. A Digital Micromirror Device (DMD) transfers generated polymerization patterns, allowing targeted irradiation of suspended single cells in gelatin methacryloyl (GelMA) for encapsulation. Three data transfer methods were developed and evaluated based on their encapsulation rates and processing times.

Chapter 3 explores the potential of GelMA for single-cell screening in comparison to polyethylene glycol diacrylate (PEGDA). HeLa cells were encapsulated using a common polymerized pattern at 1000-2000 mJ/cm². The study revealed that 5% GelMA facilitated superior cell collection within two days due to enhanced profile retention. GelMA also demonstrated greater

biocompatibility with HeLa cells for long-term observation of proliferation and biodegradation. Cell displacement of 16 μm was observed over two days. Additionally, two trypsin-based targeted cell recovery methods were developed. These findings establish GelMA as a promising bioink for single-cell screening, offering advantages over PEGDA in cell encapsulation and targeted recovery.

Chapter 4 introduces a liquid crystal display (LCD) screen-based photopolymerization system for live single-cell encapsulation in hydrogel. This approach addresses the limitations of the DMD-based method, which required complex optical design and skilled operation. The LCD-based system employs 3D CAD software to create photopolymerization patterns, which are then processed using CHITUBOX software to set exposure conditions. The final pattern is uploaded to an LCD printer, allowing for cell encapsulation in GelMA hydrogel using LED light irradiation. This chapter analyzes the formation of photopolymerized patterns and demonstrates the successful collection of both wanted and unwanted cells.

In summary, this thesis presents two approaches—DMD-based and LCD-based—for encapsulating live single cells in hydrogel using patterned light irradiation. Both methods successfully encapsulate cells in polymerized GelMA hydrogel and enable the recovery of both wanted and unwanted cells. The study of encapsulated cell behavior, conducted primarily using the DMD-based approach, provides valuable insights into the potential of these techniques for advanced single-cell screening applications.

Acknowledgment

I would like to express my deepest gratitude to the following individuals and institutions for their invaluable support throughout my research journey:

First and foremost, I am profoundly grateful to my supervisor, Prof. Moeto Nagai, for his continuous guidance and support in navigating the complexities of research.

I sincerely thank my thesis committee members, Prof. Takayuki Shibata and Prof. Tadaharu Adachi, for their insightful comments and feedback during my graduation defense process.

My heartfelt appreciation goes to my project mates Takeru Fukunaga, Yuya Suzuki, Muhammad Luqman Arief Bin Kamaludin, Ghulam Murtaza, Rifat Hussain Chowdhury, Tanmay Debnath, and all my current and former lab mates for their assistance with experiments and for creating memorable moments during my time here.

I am grateful to Toyohashi University of Technology for providing this wonderful opportunity to continue my research, and to the Amano Institution and other funding agencies for their financial support.

Lastly, I would like to thank my family and friends for their unwavering emotional support during my research in Japan.

Submission date: 2024/07/11

Department of Mechanical Engineering		Student ID	D209107	Supervisor	Moeto Nagai Takayuki Shibata
Applicant's name	Venkatesh Kumar Panneer Selvam				

Abstract

Title of Thesis	Live Single-Cell Screening Based on Cell Encapsulation and Irradiation of Patterned Light

Single-cell screening has emerged as a powerful tool in life science, offering an effective method for detecting, isolating, and manipulating individual cells based on their specific characteristics. Traditional approaches involving manual identification of single cells from images were labor-intensive and time-consuming. Image-based cell sorting (IBCS) addresses these limitations by employing image processing tools for efficient identification and processing of single cells from large populations. This thesis presents two novel light irradiation approaches for single-cell screening.

Chapter 2 details the development of an automated photopolymerization system for encapsulating suspended single cells in photo-cross-linkable hydrogel. The system utilizes an image processing algorithm to identify individual cells from cell groups in captured images. A Digital Micromirror Device (DMD) transfers generated polymerization patterns, allowing targeted irradiation of suspended single cells in gelatin methacryloyl (GelMA) for encapsulation. Three data transfer methods were developed and evaluated based on their encapsulation rates and processing times.

Chapter 3 explores the potential of GelMA for single-cell screening in comparison to polyethylene glycol diacrylate (PEGDA). HeLa cells were encapsulated using a common polymerized pattern at 1000-2000 mJ/cm². The study revealed that 5% GelMA facilitated superior cell collection within two days due to enhanced profile retention. GelMA also demonstrated greater biocompatibility with HeLa cells for long-term observation of proliferation and biodegradation. Cell displacement of 16 µm was observed over two days. Additionally, two trypsin-based targeted cell recovery methods were developed. These

findings establish GelMA as a promising bioink for single-cell screening, offering advantages over PEGDA in cell encapsulation and targeted recovery.

Chapter 4 introduces a liquid crystal display (LCD) screen-based photopolymerization system for live single-cell encapsulation in hydrogel. This approach addresses the limitations of the DMD-based method, which required complex optical design and skilled operation. The LCD-based system employs 3D CAD software to create photopolymerization patterns, which are then processed using CHITUBOX software to set exposure conditions. The final pattern is uploaded to an LCD printer, allowing for cell encapsulation in GelMA hydrogel using LED light irradiation. This chapter analyzes the formation of photopolymerized patterns and demonstrates the successful collection of both wanted and unwanted cells.

In summary, this thesis presents two approaches—DMD-based and LCD-based—for encapsulating live single cells in hydrogel using patterned light irradiation. Both methods successfully encapsulate cells in polymerized GelMA hydrogel and enable the recovery of both wanted and unwanted cells. The study of encapsulated cell behavior, conducted primarily using the DMD-based approach, provides valuable insights into the potential of these techniques for advanced single-cell screening applications.

List of figures

Figure 1.1. The application of single-cell screening. 1

Figure 1.2 Working principle of Fluorescence Activated Cell Sorting (FACS). 6

Figure 1.3 Working principle of Magnetic Activated Cell Sorting (MACS). 7

Figure 1.4 Working principle of Microfluidics Cell sorting (MCS). 8

Figure 1.5 Working principle of Image-Based Cell Sorting (IBCS). (A) Microfluidic method (B) Microarray method. 9

Figure 1.6 Gel-based cell manipulation process. (A) Cells were arranged in microcavity array (B) Photopolymerization process (C) Desired cells were encapsulated in the gel after the process. 10

Figure 2.1 The working flow of the single-cell encapsulation system. (A)Image acquisition. (B) Identification of single cells. (C) Image processing of desired cells. (D) Automatic data transfer to BBB. (E) DMD reflects the transferred image. (F) Photopolymerization of gel around desired single cells. 14

Figure 2.2 Experimental setup of the single-cell encapsulation system. In beam expander, concave lens have focal length of f_1 = -35 mm and convex lens have focal length of f_2 = 125 mm. Biconvex lens 1 and 2 have focal lengths of f_3 = 400 mm and f_4 = 100mm respectively. 15

Figure 2.3 Schematic diagram of a sample substrate. (A)Side view of sample substrate. (B) Top view of sample substrate holds cell suspension. 20

Figure 2.4 Image processing of photopolymerization pattern. (A) Flow of image processing algorithm in NI vision assistant. (B) Image capturing from sample. (C) Object detection. (D) Image after threshold applied. (E) Removal of unwanted objects. (F) Invert the image background and object. (G) Convert required photopolymerization pattern 21

Figure 2.5 Results of image processing for single-cell encapsulation pattern. (A) Grayscale image. (B) Binary images of the captured image. (C) Removal of unwanted objects. (D) Conversion of circular objects to square and size enlargement (E) Required photopolymer 23

Figure 2.6 Results of addition of angle to a tone curve. Image with a tone curve at (A) 45º, (B) 65º, (C) 70º and (D) 75º slope. 24

Figure 2.7 Effect of contrast addition. 25

Figure 2.8 Formation of light pattern. (A) Polymerization pattern with a dimension of 53 × 53 pixels. (B) Microscopic view of projected photopolymerization pattern on the sample. 26

Figure 2.9 Photopolymerization process of GelMA at single cell. (A) Before photopolymerization. (B) Single-cell encapsulation pattern. (C) Cell encapsulated in around 50 µm square hydrogel. 27

Figure 2.10 Alignment error of single cells in polymerized hydrogel (A) SFTP and WinSCP with PAD. (B) SFTP and WinSCP with manual input. (C) USB flash drive. (D), (E) and (F) Enlarge image of polymerized 50 µm square hydrogel from (A), (B) and (C) respectively. 28

Figure 2.11 Alignment error using various data transfer method. 29

Figure 2.12 Total time of polymerization process using various transfer methods. 30

Figure 3.1 Schematic diagram of a sample plate. (A) Side view of sample substrate. (B) Top view of sample substrate holds cell suspension. 35

Figure 3.2 Procedure of cell viability. 36

Figure 3.3 Setup for collection of uncured and cured cells. (A-B) Removal of uncured cells from the sample. (C-D) Removal of cured cells from the sample. 37

Figure 3.4 Microscopic images of cured gel at 5 % w/v GelMA hydrogel. (A) 1070, (B) 1280, (C) 1490, (D) 1700 (E) 1920 mJ/cm². 38

Figure 3.5 Dimension of cured hydrogel at different light integral. 39

Figure 3.6 Microscopic images of HeLa stained with Calcein-AM and PI. (A-C) Negative control of hydrogel. (D-F) 5 % w/v of GelMA cured gel at 1200 mJ/cm². (A, D) bright field images. (B-E) Green fluorescent images. (C, F) Red fluorescent images. 40

Figure 3.7 GelMA degradation and cell proliferation of 5 % w/v of GelMA. (A) Microscopic image of polymerized gel without a cell. (B) Microscopic image of polymerized gel with gel. 41

Figure 3.8 Degradation of gel area without/with cells. 42

Figure 3.9 Cell proliferation of encapsulated cells. 43

Figure 3.10 Time-lapse images of HeLa cells encapsulated in the GelMA hydrogel from Day 0 to Day2. (A-C) Observation of three cells on Day 0-2. (D-F) Observation of five cells on Day 0-2. 44

Figure 3.11 Mobility analysis of HeLa cells encapsulated in GelMA hydrogel. 45

Figure 3.12 Microscopic view of cells encapsulated in GelMA photocured at 800 mJ/cm². (A) Immediately after irradiation (B) After 4 minutes (C) After 10 minutes of addition of trypsin. The red circle indicates the unwanted cells..... 46

Figure 3.13 Degradation and collection of polymerized cells encapsulated in GelMA at 600 mJ/cm².Immediately after cured gel. (B) At 2 min 30 s, (C) At 3 min 15 s, (D) At 4 min, (E) At 4 min 45 s, (F) At 5 min 37 s after addition of trypsin. The red dished circle indicates the photopolymerized hydrogel that encapsulate the HeLa cells. 47

Figure 3.14 Degradation and collection of polymerized cells encapsulated in GelMA at 1000 mJ/cm².Immediately after cured gel. (B) At 3 mins 30 s, (C) At 7 mins 25 s after addition of trypsin. The red circle indicates the photopolymerized hydrogel..... 48

Figure 3.15 Degradation and collection of polymerized cells encapsulated in GelMA at 1500 mJ/cm².Immediately after cured gel. (B) At 6 mins, (C) At 9 mins after addition of trypsin. The red circle indicates the photopolymerized hydrogel 49

Figure 3.16 Degradation and collection of polymerized cells encapsulated in GelMA at 2400 mJ/cm².Immediately after cured gel. (B) At 9 mins, (C) At 16 mins 40 secs after addition of trypsin. The red circle indicates the photopolymerized hydrogel..... 49

Figure 3.17 Degradation and collection of polymerized cells encapsulated in GelMA at 3600 mJ/cm².Immediately after cured gel. (B) At 10 mins, (C) At 20 mins, (D) 23 mins after addition of trypsin. The red circle indicates the photopolymerized hydrogel..... 50

Figure 3.18 Degradation and collection of polymerized cells encapsulated in GelMA at 1700 mJ/cm².Immediately after cured gel. (B) At 6 mins, (C) At 9 mins after addition of trypsin. The red circle indicates the photopolymerized hydrogel 50

Figure 3.19 Degradation and collection of polymerized cells encapsulated in GelMA at 3400 mJ/cm².Immediately after cured gel. (B) At 11 mins, (C) At 19 mins after addition of trypsin. The red circle indicates the photopolymerized hydrogel 51

Figure 3.20 Degradation and collection of polymerized cells encapsulated in GelMA at 5100 mJ/cm².Immediately after cured gel. (B) At 9 mins, (C) At 18 mins and (D) 24 mins after addition of trypsin. The red circle indicates the photopolymerized hydrogel..... 51

Figure 3.21 Degradation of polymerized GelMA hydrogel at various light integral value..... 52

Figure 4.1 Working flow of single-cell encapsulation using LCD based system. 56

Figure 4.2 Single-cell encapsulation of LCD screen based 3D printer. 57

Figure 4.3 Creation of polymerization pattern. (A) .stl file of 4 × 4 mm pattern with each box of 100 × 100 µm size. (B) Top view of polymerization pattern on the LCD screen in the software and converted into .prz file format. 58

Figure 4.4 Schematic diagram of a specimen. (A)Side view of sample substrate. (B) Top view of sample substrate holds cell suspension. 59

Figure 4.5 Polymerization pattern formation on LCD screen. Each box dimension of (A) 100 µm (B) 88 µm (C) 66 µm (D) 50 µm (E) 44 µm. 60

Figure 4.6 Histogram of number of pixels of each box in a pattern. (A) 100 µm (B) 88 µm (C) 66 µm (D) 50 µm and (E) 44 µm. 62

Figure 4.7 Microscopic images of photopolymerization pattern on GelMA hydrogel. (A) 200 s, (B) 250 s, (C) 300 s, (D) 350 s and (E) 400s..... 64

Figure 4.8 Dimension of polymerized boxes at different light integral..... 65

Figure 4.9 Microscopic images of cells encapsulated on GelMA hydrogel. (A) 200 s, (B) 250 s, (c) 300 s, (D) 350s and (E) 400 s..... 66

Figure 4.10 Microscopic images of HeLa stained with Calcein-AM and PI. (A-C) Negative control of hydrogel. (D-F) 5 % w/v of GelMA cured gel at 600 mJ/cm². (A, D) bright field images. (B-E) Green fluorescent images. (C, F) Red fluorescent images 67

Figure 4.11 Microscopic image of cured gel at 5 % w/v GelMA. (A-B) Observation of encapsulated cells in 1×1 mm polymerization pattern on Day 0-1. (C-D) Observation of encapsulated cells in 100×100 µm polymerization pattern on Day 0-1 68

Figure 4.12Microscopic image of cured gel at 5 % w/v GelMA. (A-B) Observation of encapsulated cells in 1×1 mm polymerization pattern on Day 0-1. (C-D) Observation of encapsulated cells in 1×1 mm polymerization pattern on Day 0-1 69

Figure 4.13 Collection of unwanted cells in GelMA photocured at 800 mJ/cm² by trypsin treatment. (A) Immediately after polymerization (B) 10 minute (C) 15 minutes. 71

Figure 4.14 Degradation of GelMA photocured hydrogel at 600 mJ/cm² in trypsin (A) Immediately after polymerization (B) 10 minute (C) 20 minutes (D) 30 minutes and (E) 40 minutes. 71

Figure 4.15 Change of size of GelMA hydrogel degradation in trypsin 72

List of tables

Table 1.1 Comparison of various single-cell screening methods. 10

Table 3.1 Experimental parameters of hydrogel degradation 48

List of abbreviation

scRNA-seq - single-cell RNA sequencing

FACS - Fluorescence Activated Cell Sorting

MACS - Magnetic Activated Cell sorting

MCS - Microfluidics Cell Sorting

IBCS - Image-Based cell sorting

DMD - Digital Micromirror Device

PEGDA -polyethylene glycol Diacrylate

BBB - BeagleBone Black

USB - Universal Serial Bus

RPM – Revolutions per minute

SFTP - Secure File Transfer Protocol

WinSCP - Windows Secure copy Protocol

PAD - Power Automate Desktop

PBS - Phosphate Buffered Solution

GelMA - Gelatin Methacryloyl

LAP - Lithium Phenyl (2, 4, 6-thrmethey-benzoyl) Phosphinate

MEM - Minimum Essential Medium

UV - ultraviolet

PI- Propidium iodide

LCD - Liquid-Crystal Display

CAD – Computer Aided Design

Table of Contents

Acknowledgment III

Abstract V

List of figures VII

List of tables XII

List of abbreviation XIII

Chapter 1 Introduction 1

1.1 Need of Single-cell screening 1
1.2 Traditional single-cell screening system 5
1.2.1 Flow cytometry 5
1.2.2 Fluorescence Activated Cell Sorting (FACS) 6
1.2.3 Magnetic Activated Cell Sorting (MACS) 7
1.2.4 Microfluidics cell sorting (MCS) 7
1.2.5 Image-Based Cell Sorting (IBCS) 8
1.2.6 Gel-based cell manipulation 9
1.3 Research goal 10

Chapter 2 Automatic Single-cell encapsulation using optical system and photopolymerization of parallel single-cell screening 13

2.1 Introduction 13
2.2 Methods 14
2.2.1 Working flow of Single-Cell encapsulation 14
2.2.2 Working Experimental setup 15
2.2.3 Photo polymerization pattern 17
2.2.4 Preparation of photopolymerization sample 19
2.3 Results and Discussion 21
2.3.1 Image processing of photo polymerization pattern 21
2.3.2 Formation of photopolymerization pattern 26
2.3.3 Encapsulation of single-cell on hydrogel 27
2.3.4 Alignment error of single cells in photo-curable hydrogel 28
2.4 Conclusion 31

Chapter 3 Behavior of cells encapsulated in GelMA 32

3.1 Introduction 32
3.2 Methods 34
3.2.1 Preparation of bioink and cell suspension 34
3.2.2 Experimental setup 35
3.2.3 Observation of cell encapsulation in GelMA for long period observation 35
3.2.4 Observation of cell viability 36
3.2.5 Collection of unwanted cells and cured cells in polymerized GelMA hydrogel 37
3.3 Results and Discussion 38
3.3.1 Behavior of photo polymerization GelMA 38
3.3.2 Cell viability of encapsulated cells in GelMA hydrogel 40
3.3.3 Cell proliferation of polymerized GelMA 41
3.3.4 Mobility of cells encapsulated in GelMA 44
3.3.5 Recovery of unwanted cells in polymerized GelMA hydrogel 46
3.3.6 Collection of cured cells in polymerized GelMA hydrogel 47
3.4 Conclusion 53

Chapter 4 Single-cell encapsulation using LCD screen based printer and behavior of cells encapsulated in GelMA. 55

4.1 Introduction 55
4.2 Methods 56
4.2.1 Working flow of single-cell encapsulation using LCD based system 56
4.2.2 Working experimental setup 57
4.2.3 Creation of photopolymerization pattern 58
4.2.4 Materials 58
4.3 Result and discussion 60
4.3.1 Formation of photopolymerization pattern on LCD screen 60
4.3.2 Formation of photopolymerization pattern on GelMA hydrogel 64
4.3.3 Cells encapsulation in polymerized hydrogel 66
4.3.4 Cell viability of encapsulated cells in GelMA hydrogel 67
4.3.5 Cell proliferation of encapsulated cell 68
4.3.6 Removal of Unwanted cells in polymerized hydrogel 70
4.3.7 Collection of cured cells in polymerized GelMA hydrogel 71
4.4 Conclusion 73

Chapter 5 Conclusions 74

5.1 Conclusion 74
5.2 Future work 75
Reference 76

Publication list

Chapter 1 Introduction

1.1 Need of Single-cell screening

The need of single-cell screening has becoming decisive factor in biological and medical research and it's offering the unique insights into cellular heterogeneity, rare cell populations and its dynamic process. Single-cell screening has opened the emerging field likes regenerative medicine, advanced therapies, drug delivery [1, 2] and immunotherapy [3]. Figure 1.1 shows the application of single-cell screening.

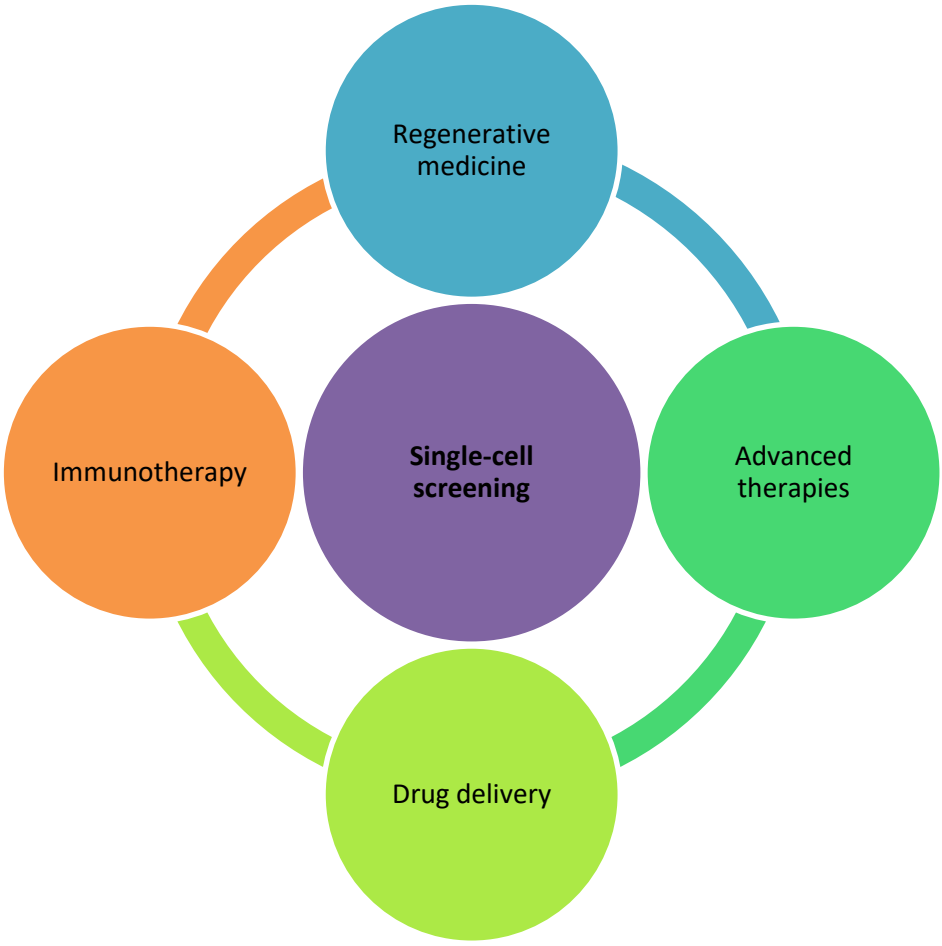

Figure 1.1 The application of single-cell screening.

Single-cell screening has arisen as a powerful tool in the study of the relationship between genetic expression and phenotype. To analyze the genetic and phenotypic characteristics of individual cells, the researchers got new knowledge in cellular heterogeneity and the complex mechanisms in phenotype. Single-cell screening methods like single-cell RNA sequencing (scRNA-seq), the

researchers can understand cellular biology to understand heterogeneity that exists in homogeneous cell populations [4]. These procedures enable the profiling of gene expression at the expression of individual cells, offering a granular perspective on how genetic expression can fluctuate across a population and how these changes might contribute to various phenotypes.

One of the main purposes of single-cell screening is the recognition of cells with identical genotypes. This phenomenon can be credited to gene expression, where the difference in gene activity leads to variation in gene expression between the cells [5]. For example, the differential gene expression occurs due to the difference in DNA methylation patterns across the individual cells [6]. Generally, single-cell epigenomics has exposed the epigenetic states which are highly dynamic and the changes can happen rapidly in the environments [7]. The dynamic nature of epigenetic parameters increases the difficulty for researchers in understanding the genotype-phenotype connections.

The single-cell screening has already proved that the gene environment relations can improve the substantial change in phenotypic diversity within the cell population [8]. For example, to reduce the stress response in cells which leads to changes in gene expression and the outcomes are in varied phenotypic [9]. To clearly understand phenotypic, there is a need to combine approaches in single-cell genomics with environmental data.

Even the relation between phenotype and genetic expression is still some challenges in single-cell screening methods. One of the major challenges is the inherent noise in single-cell data sets [10]. In making the quantified gene expression, the insufficient single-cell experimental data can lead to failure, where some genes are not identified in cells. Single-cell screening has provided the gene expression in over an array of factors such as transcription factors, non-coding RNA and chromatin remodelers. To overcome the limitations, the high-resolution imaging methods and single –cell data with spatial transcriptomics want to integrate. The researchers can study the cells in the inherent tissue background that provides the knowledge into how cell-cell interactions and micro-environmental aspects contribute to phenotypic diversity.

In the medical and biotechnology industries, the innovation in high-producing cell lines is a difficult objective to achieve. These cell lines are important parameters to produce proteins, vaccines, monoclonal antibodies, enzymes, etc. to increase the demand in biopharmaceuticals where to ensure product quality and low production cost, the high-producing cell lines want to meet those

requirements. Still, the cell lines are a most challenging task because of the complexity of cellular processes and their behavior, and it requires extreme control in genetic and environmental conditions.

For example, in the mammalian cell lines especially in Chinese hamster ovary (CHO) cells, the production of biologics is more common in biotechnology and medical industries. Those cell lines are chosen because of their capacity to produce proteins with human-like post-translational modifications, which are serious in the efficiency and welfare of therapeutic proteins [11]. In the development of high-producing cell lines, the process includes the introduction of the desired gene into the host cells. However, this procedure is often ineffective, with only a small number of transfected cells reaching the targeted production level [12]. Additionally, the selected high-producing cell lines are unstable, and it leads to difficulty in the manufacturing process.

The production of cell lines not only depends on its gene, but the culture conditions are also important in the process. The cell growth and protein expression are dependent on nutrient availability, oxygen levels, pH, and temperature [13]. By performing various experimentation and continuous monitoring, the optimal culture conditions for individual lines are achieved but it can be a time-taking and difficult process. In the post-translational modifications, the produced biologics quality is an important factor. In the therapeutic proteins to maintain efficiency and safety, effective controlling is needed in post-translational modifications such as glycosylation [14]. In the high-production cell lines, the controlled post-translation modifications across various production batches is still a difficult task.

Another challenge in high-producing cell lines is maintaining productivity and quality of the product where the production is scaled up. If the changes occur in the production time, it affects the cell behavior and protein expression leads to variation in the final product [15]. For successful commercialization, we have to develop a robust process that makes sure efficiency in various scale ups is the same.

In rapid identification and selection of high-producing cell lines, the high-throughput screening technologies are used. Using automatic systems, it can screen higher counts of targetable traits such as high expression levels and positive post-translational modification profiles. It considerably increases the cell line development process. Some of the gene editing technologies have been used to modify the host cell genome, increasing gene integration and stability [16]. To improve the overall cell line, the desired amplification is enabled on specific genes and eliminates the unwanted genetic essentials. The production of high levels of targeted protein is achieved by

modifying the metabolic pathways within host cells. To meet the high demand in high-producing cell lines, continuous research and innovations are needed.

To understand cellular processes and innovate new therapeutic methods, the isolation of cells is an important task. For example, in cancer research, the isolating and study of cells that reveal resistance to chemotherapy can provide ideas into the mechanisms of drug resistance and it leads to innovation of effective treatments [17]. On the other hand in regenerative medicine, finding and expanding stem cells that have a possible way to differentiate into desired tissue types for developing the cell-based therapy. The researchers are doing long-term observations of cells that allows them to understand the behavior of isolated cells over time, their growth, division, migration, and how they perform in various environments. Here, once the cells are targeted, these cells are isolated and observed in a controlled environment for complete study of their properties.

One of the major challenges in isolating the cells with targeted parameters is the inherent heterogeneity in the cell populations. In a clonal population, the individual cells can reveal major differences in behavior and phenotypes [18]. If the isolated cells are observed for long-term, control techniques are required without affecting their properties. Some techniques such as Fluorescence-Activated Cell Sorting (FACS) microfluidic systems require the use of labels that can affect the cell behavior [19]. The viability and functionality need to be maintained during the isolation of cells. Due to the changes in culture conditions, the isolated cells may be lost over the time. This specific challenge for stem cells and other progenitor cells required some specific term to sustain their potency [20].

To overcome these challenges, label-free isolation techniques are used that allow for isolating targeted cells based on their physical properties without the use of labels. These methods improve the cell viability and function during isolation. The optimized culture conditions are required to maintain the isolated cells that closely mimic the cell environment. This technique includes the use of medium, growth factors and a three-dimensional culture system. By using single-cell genomics and proteomics with live cell observation that allows the researchers to understand the complete details of isolated cells at molecular level. It provides the genetic and proteomic profiles related to targetable cells [21].

Single-cell screening methods express the understanding of the relation between genetic expression and phenotype that opens up the complexity and heterogeneity within the cellular populations. However, the new development in high-throughput screening methods is used to

overcome the limitations in high-producing cell lines. Continuous research in single-cell screening and successful isolation of the targeted cells leads to the development of new therapeutic strategies.

1.2 Traditional single-cell screening system

Single-cell screening systems are often categorized by three key parameters: efficiency, purity, and recovery [22]. Efficiency refers to the number of cells that can be isolated in a given time period. Purity is defined as the fraction of target cells collected after separation. Recovery represents the fraction of target cells obtained after separation compared to the initial number of target cells in the sample.

Single-cell screening methods can be classified into two main categories: physical and biological methods [23, 24]. Physical methods are based on cell properties such as size, deformability, electric charges, and density. Biological methods, on the other hand, rely on cell biological properties, including protein expression.

Additionally, single-cell screening systems can be further categorized based on their temporal analysis capabilities. Instantaneous analysis systems provide a snapshot of cellular characteristics at a single point in time. These are useful for capturing the state of cells at a specific moment, such as flow cytometry or imaging-based cytometry. Time-series analysis systems allow for the observation of cellular processes over time. They are valuable for studying dynamic cellular behaviors, such as live-cell imaging techniques or microfluidic devices that enable continuous monitoring of individual cells.

Both instantaneous and time-series analysis systems offer unique insights into cellular heterogeneity and behavior. They complement each other to provide a comprehensive understanding of single-cell characteristics and dynamics.

1.2.1 Flow cytometry

Flow cytometry is a methodology that gives the information of multi-parameters of single cells from the sample. For conducting flow cytometry, a laser is used as a light source that produces scattered and fluorescent light signals and it can be read by detectors. These electronic signals are analyzed by a computer and converted into readable standardized format data file format. This technique deals with fluorescent expression proteins, DNA binding dyes, viability dyes, ion indicator dyes and conjugated antibodies. It is a powerful tool that implicates in immunology, cancer, virology and infectious disease monitoring [25]. To perform the flow cytometer, the cell suspension doesn’t

contain cell debris. If it is present in the sample, the instrument will clog, and we will get the worst results.

1.2.2 Fluorescence Activated Cell Sorting (FACS)

Fluorescence-activated cell sorting is one of the methods for finding the characteristics and differentiating the cell types in a heterogeneous cell population by using its size, granularity and fluorescence. It provides quantitative and qualitative data on single cells [26] and it is mainly the screening/isolation of single cells from highly concentrated cell populations [27]. Figure 1.2 shows the working principle of fluorescence-activated cell sorting. FACS is based on labeling the cell with a fluorescent dye and screened by their fluorescence intensity. Here, the cells are labeled with fluorescent dye and stored in a container with nozzle. From the nozzle, the droplets are formed and strike by laser beam. And the beam is detected by two detectors, one is forward scatter (FSC) that detect the size of the cells and other is side scatter (SSC) that the fluorescence or granularity of the cells. Based on the fluorescence intensity value and size of the cells that are detected by the sensor, it gives a signal to the electrode either a positive or negative charge. Finally, the cells are separated based on charge and the separated cells are collected in labeled collection tubes. The limitations of the FACS method are high flow rate, dissociated cells and high skilled operator need.

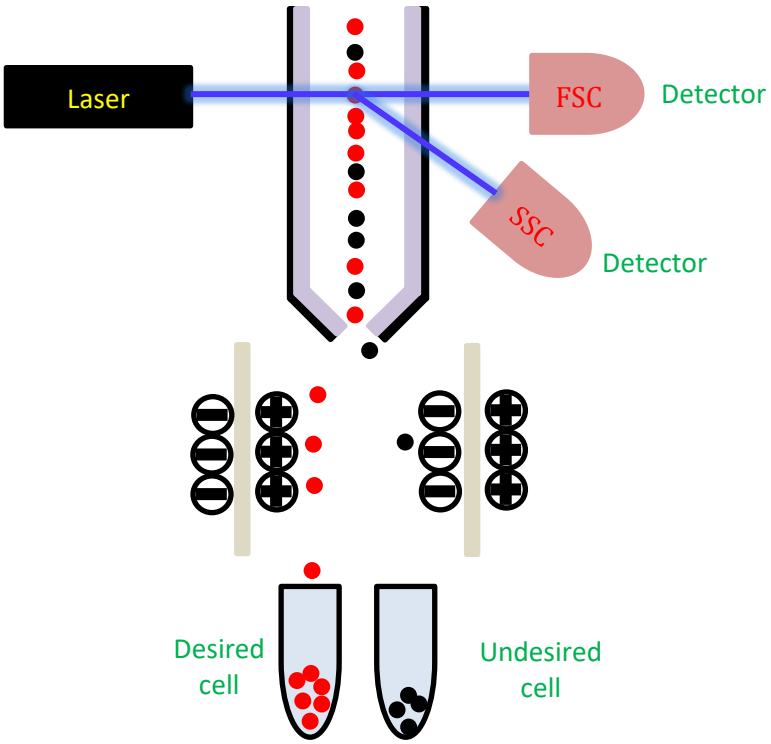

Figure 1.2 Working principle of Fluorescence Activated Cell Sorting (FACS).

1.2.3 Magnetic Activated Cell Sorting (MACS)

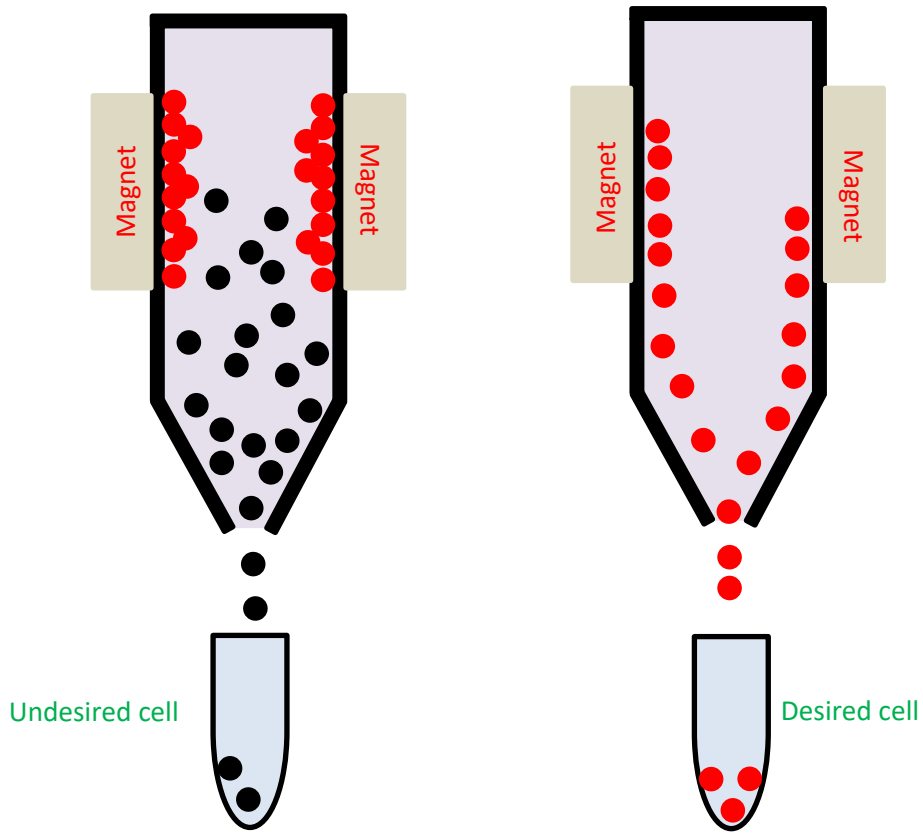

Figure 1.3 Working principle of Magnetic Activated Cell Sorting (MACS).

Figure 1.3 shows the working principle of MACS. Magnetic activated cell sorting is a common separation method used for screening various types of cells. This method achieves 90% of screening from the desired cell populations [28]. The working principle of MACS is to mix the magnetic particle with the cell and separate it by magnetic property. First, the antibodies coated magnetic beads with surface makers are mixed with the cells, a method that is classified with specific proteins on the desired cells. Then the solution is transformed into the hopper and resealed in nozzle where the magnetic field is applied. While applying a magnetic field, the desired cells are magnetized and those cells are attached to the channel wall and the non-desired cells flow through the channel. This methodology is time consuming and costly because we need to replace the channel and magnetic beads for each experiment. The capture of non-targeted cells and cell disaggregation were the main limitation of the MACS method.

1.2.4 Microfluidics cell sorting (MCS)

Microfluidics cell sorting is an emerging methodology for cell screening systems that is used for less analysis expenses, low sample consumption and is easy to handle even in Nano-liters volumes

[29]. The cell sorting process is carried out by earthier active sorting (electric force, acoustic force, mechanical force, magnetic force) or passive sorting (inertial force, adhesion, and filtration). In this process, the cell suspension (for example magnetic force sorting, the solution contain magnetic beads) is introduced in the valve 1. The microfluidics device is placed in magnetic field, the targeted cells are attached on the flow chamber walls and undesired cells are collected in valve 4. After removing the magnetic field, the buffer solution is introduced in valve 2 and it collect the desired cells in valve 4. Figure 1.4 shows the working principle of microfluidics cell sorting. The disadvantage of the microfluidics cell sorting is the disaggregation of cell and high skill needed.

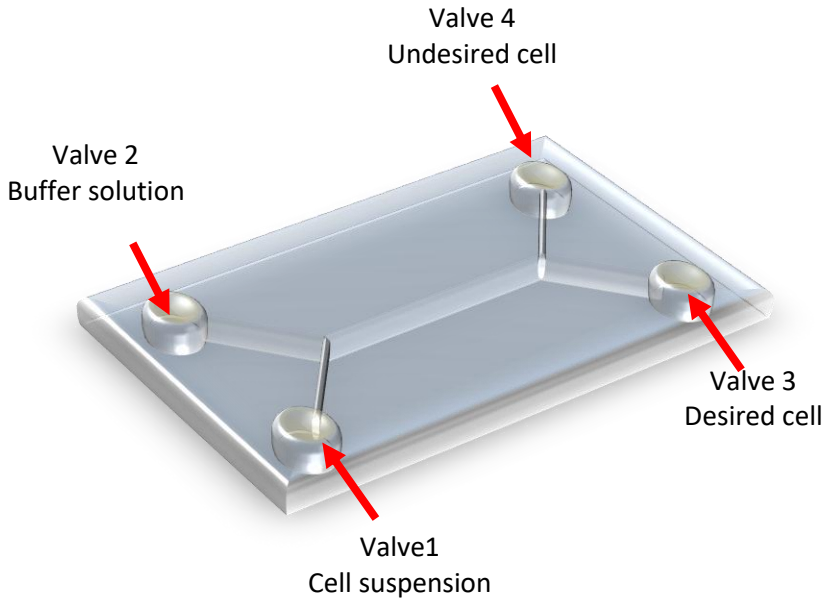

Figure 1.4 Working principle of Microfluidics Cell sorting (MCS).

1.2.5 Image-Based Cell Sorting (IBCS)

Image-based cell sorting is a new methodology for characterizing and isolating the single cells from a higher population of cells with the help of advanced imaging technique, machine learning and deep neural networks. For single-cell screening, the combination of an IBCS and microfluidic or microarray platforms are used and each setup has specific application and property [30]. Figure 1.5 shows the experimental setup of Image-based cell sorting. In the microfluidic based IBCS (Fig. 1.5(A)), the cells flow through the channel, and it is continuously monitored by camera. From the images, the desired and undesired cells are isolated. In microarray setup (Fig. 1.6(B)), the cells are arranged in the arrays and the camera is used to scan the arrays. The desired cells are ejected and collected by a Nano-pin probe.

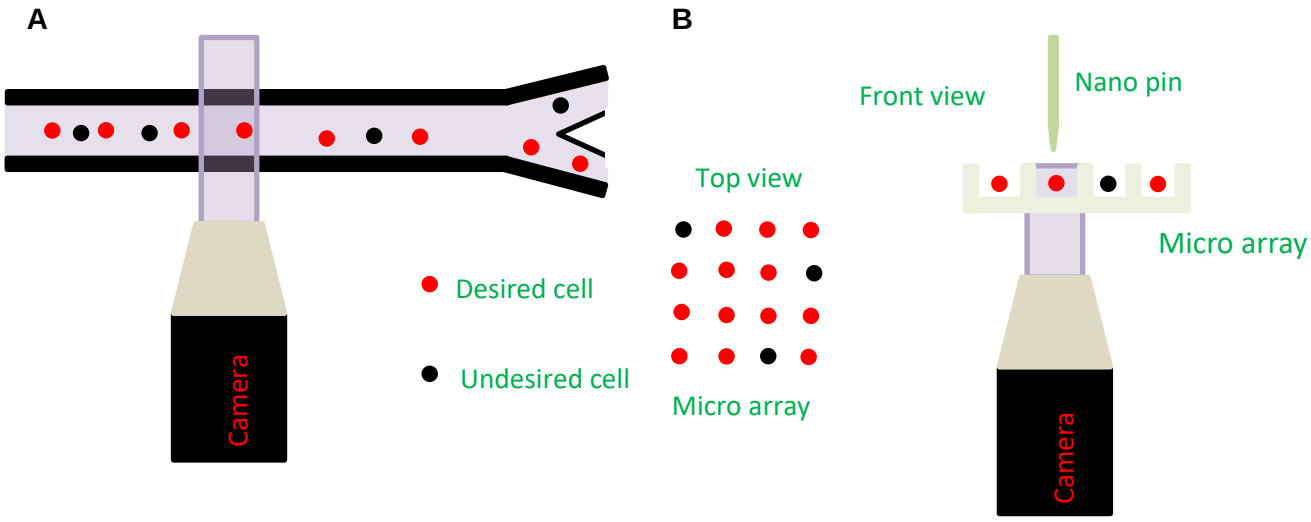

Figure 1.5 Working principle of Image-Based Cell Sorting (IBCS). (A) Microfluidic method (B) Microarray method.

1.2.6 Gel-based cell manipulation

Recently, a development of a simple single-cell isolation technique was gel-based cell manipulation. The basic principle of gel-based cell manipulation was to align the cells on the microcavity array sample and transfer the photopolymerizable prepolymer like polyethylene glycol Diacrylate (PEGDA) on the sample. So, the cells were immersed in the PEGDA. Passing the light source of 405 nm wavelength on to the hydrogel, the cells were encapsulated which were presented in the irradiated part of PEGDA hydrogel. Figure 1.6 shows the gel-based cell manipulation process. The size and shapes of an encapsulating material were the key factors, and they can reflect in survival rate of the encapsulated cells. To maintain the cell viability, the diffusion rate of gel was controlled [31].

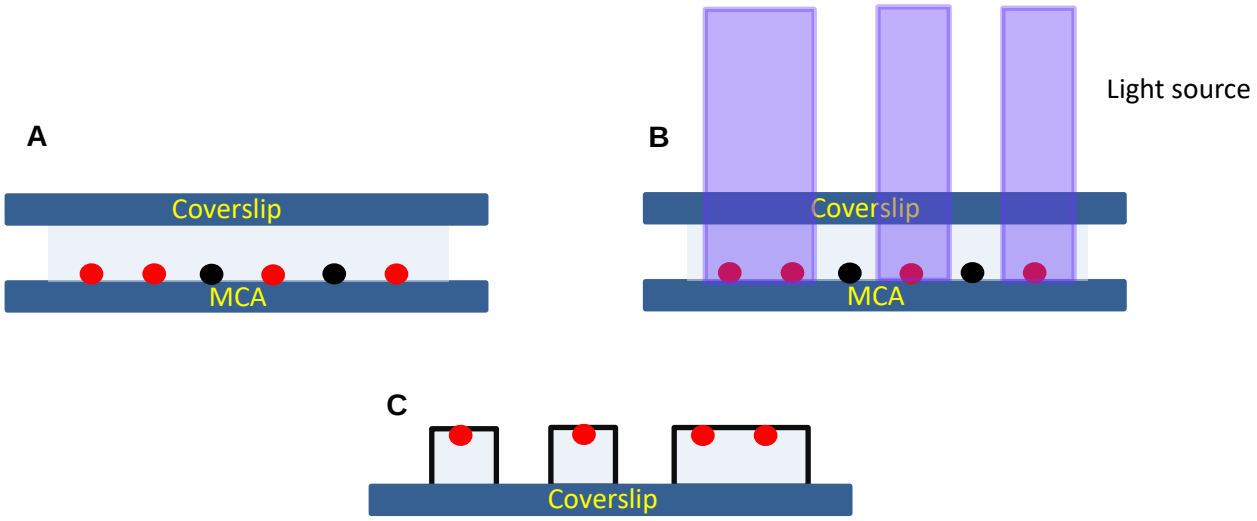

Figure 1.6 Gel-based cell manipulation process. (A) Cells were arranged in microcavity array (B) Photopolymerization process (C) Desired cells were encapsulated in the gel after the process.

1.3 Research goal

The single-cell analysis and various screening methodologies are briefly discussed in the previous sub-sections.

Table 1.1 Comparison of various single-cell screening methods.

	Fluorescence-activated cell sorting (FACS)	**Magnetic-activated cell sorting (MACS)**	**Microfluidic cell sorting (MCS)**	**Image-based cell sorting (IBCS)**	**Gel-based cell manipulation (GCM) This study**
Sorting capacity	Moderate	Low (specific markers)	Moderate	High (morphology-based)	High
Throughput	High	High	Low to moderate	Low	Low
Separation time	Fast	Moderate	Moderate	Slow	Slow
Cell viability	Moderate	High	High	High	Very high
Observation capability	Short-term	Short-term	Short-term	Short-term to long-term	Short to long-term
Cost	High	Moderate	High (initial setup)	Moderate	Moderate to high

Table 1.1 summarizes the advantages and disadvantages of the single-cell screening techniques. In this study, the main goal is to capture and isolate a single cell from the sample and the proposed system to eliminate the disadvantages of other conventional methods. So, the following requirements need to be satisfied by the proposed system.

- Easy to operate and low-cost
- Suitable for long-time observation
- The long-term survival rate of isolated single cells

My study aims to develop a single-cell encapsulation system with the integration of photopolymerization. Here, the cells are captured and analyzed by the image processing tool (LabVIEW software). The single-cell data is extracted and converted into the polymerization pattern. Using this pattern, the single cells are encapsulated in hydrogel. The efficiency of the system is evaluated by the behavior of polymerization hydrogel, cell proliferation, biodegradation of gel, cell motility, and long-time survival rate.

This study primarily focused on live single-cell encapsulation in hydrogel. Chapter 2 discusses the development of a DMD-based single-cell encapsulation system using a multi-light irradiation pattern. The system was constructed using optical elements, a DMD board, a motorized stage, and a high-resolution camera. The basic working principle of this system was to identify single cells from the sample and encapsulate the targeted single cells in the hydrogel. First, the sample was captured, and single cells were automatically detected from the image using an image processing algorithm. Based on this information, the photopolymerization pattern was formed. Finally, the pattern was uploaded to the DMD, and the photopolymerization process was carried out. Additionally, experiments were conducted using various data transfer methods to analyze the photopolymerization process.

Chapter 3 presents studies on the behavior of cells encapsulated in GelMA hydrogel. While Chapter 2 focused on the construction of the DMD-based single-cell encapsulation system, automatic single-cell detection algorithm, and study of the photopolymerization process using various data transfer methods, Chapter 3 analyzes the samples after the polymerization process for long-term observation. This includes cell viability, degradation rate of polymerized hydrogel, cell growth, and the motion of encapsulated cells inside the hydrogel. The samples were also treated to remove unwanted cells and collect cured cells.

As the system described in Chapter 2 was complex in design, unstable, and only able to irradiate a small region, Chapter 4 discusses a single-cell encapsulation system based on an LCD screen 3D printer. A modified LCD screen 3D printer was used as the experimental setup. The photopolymerization pattern was created using CAD software and converted into the required file format. This chapter details the photopolymerization process and subsequent sample analysis.

Chapter 2 Automatic Single-cell encapsulation using optical system and photopolymerization of parallel single-cell screening

2.1 Introduction

In single-cell screening, an image-based cell sorting method is used to select the desired cells from the cellular image and it is a very potential tool for determining the phenotype of a cell [30]. In the IBCS method, to monitor cellular behavior and study the detailed structures of cells is possible with the help of high-resolution images. In the past few years, the single-cells were identified based on cellar image from the sample and it was collected by using magnetic [32] or glass needle [33 - 35]. Even though a single probe has the most common method, the output is very low and the more appropriate in array approach. To capture the multi cells, the micro hole array has been established [36, 37].

A Digital Micromirror Device (DMD) based method was established to capture the DNA from isolated cells on a microcavity array. In polyethylene glycol Diacrylate (PEGDA, Mn = 750 or 750) hydrogels, the cells were polymerized and encapsulated in gel. The DMD consists of thousands of micromirrors and it has high throughput [38 - 40].

To achieve live single-cell collection, the DMD based methods were developed nowadays. In DMD approaches, some limitations are addressed as follow:

1) Detection of the desired single cell process is not automatic. With the help of the operator, the identification process is done.
2) For live-cell collection encapsulation, the fast degradation is required with mild conditions. But the PEGDA hydrogel is slow degradation [41].
3) To capture the cell, a microcavity is needed.

The substrate-free method is preferred to increase substrate type. In the case of free cell suspension flow, there are some disturbances in cell movements and after image acquisition, the cells are overlapped while cell encapsulation.

In this chapter, I developed a system which addresses the three problems associated with increasing efficiency of live-cell collection. Image processing tool was used to identify the single cells automatically. Based on the algorithm, the targeted single cells positions were extracted and it automatically generated the photopolymerization pattern. Gelatin methacrylate (GelMA) was used as

the encapsulated hydrogel because it has fast degradation properties [42] and it allows for collection of live cells. Using the generated pattern, the hydrogels were polymerized that contain the desired targeted cell using multi light irradiations. In this system, the three data transfer methods were compared and filters the best processing time to achieve the maximum encapsulation rate.

2.2 Methods

2.2.1 Working flow of Single-Cell encapsulation

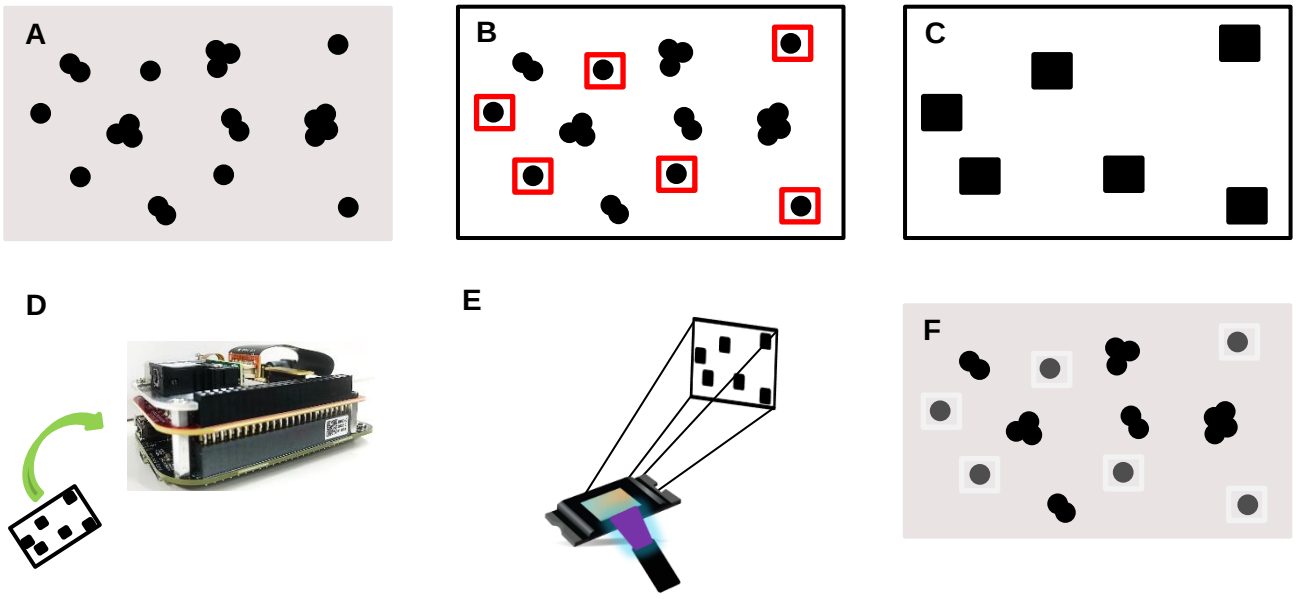

Figure 2.1 The working flow of the single-cell encapsulation system. (A)Image acquisition. (B) Identification of single cells. (C) Image processing of desired cells. (D) Automatic data transfer to BBB. (E) DMD reflects the transferred image. (F) Photopolymerization of gel around desired single cells.

Figure 2.1 shows the working flow of the single-cell encapsulation system. In the beginning of the experiment, the cell suspension (hydrogel that mixed cell suspension) was prepared and kept on the stage and the high resolution camera was used to capture the samples (Fig. 2.1(A)). From the captured image, the targeted single cells were identified (Fig. 2.1(B)), Single cells were marked by square boxes) which were automatically processed by using LabVIEW software. From that process, the photopolymerization image pattern (Fig. 2.1(C)) was formed. And this pattern was transferred to BeagleBone Black (BBB) (Fig. 2.1(D)). The BBB board was coupled with a DMD that read and projected the image (Fig. 2.1(E)). Then the beam shutter was opened, and it allowed the light source to DMD. The reflected light from DMD was irradiated on the sample which was placed on an inverted

microscope stage. Here, the photo-crosslink occurred on hydrogels around the desired single cells, and that the cells were encapsulated in the hydrogels (Fig. 2.1(F)).

2.2.2 Working Experimental setup

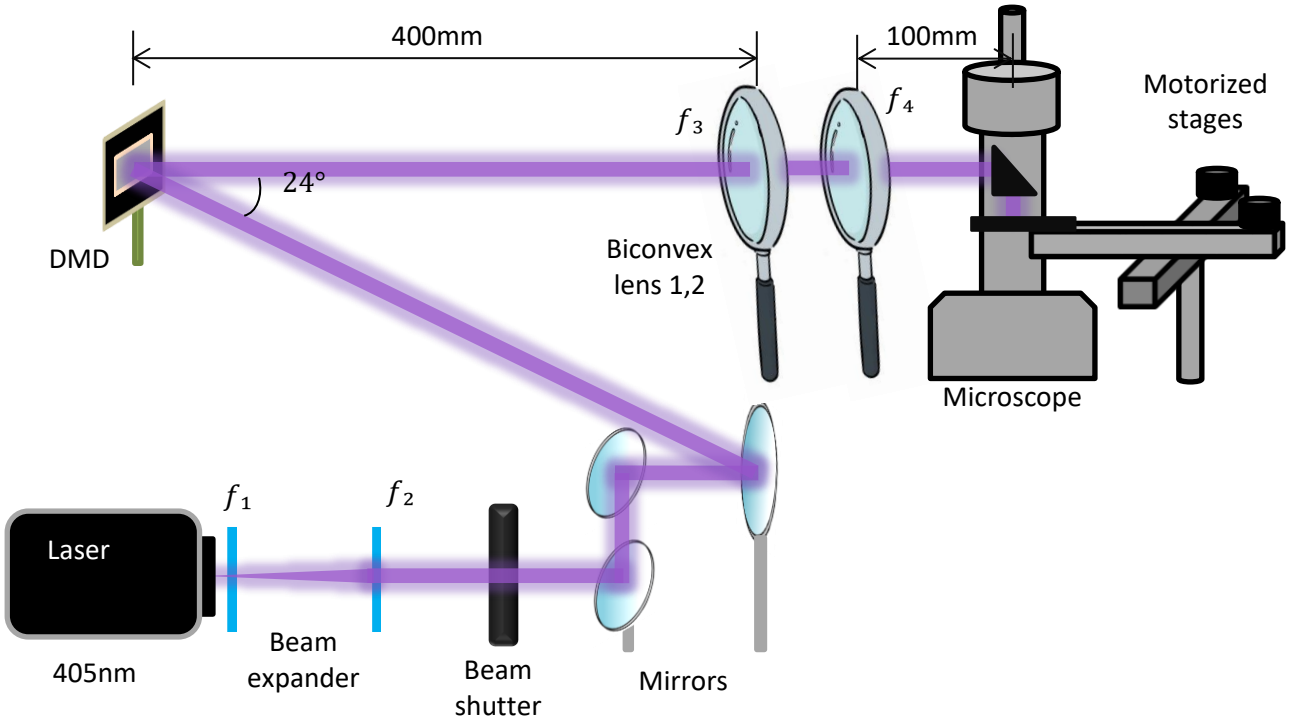

Figure 2.2 Experimental setup of the single-cell encapsulation system. In beam expander, concave lens have focal length of f_1 = -35 mm and convex lens have focal length of f_2 = 125 mm. Biconvex lens 1 and 2 have focal lengths of f_3 = 400 mm and f_4 = 100mm respectively.

To construct an automatic single-cell screening system, several components were used such as motorized stage, camera and optical system that includes DMD and source laser and arranged in proper displacement for stable and efficient operation. Figure 2.2 shows the experimental setup of the single-cell encapsulation system.

In the optical guidance system, an oscillatory wavelength of 405nm (OBIS laser (purple color), coherent) was used as a light source. In the initial stage, the diameter of the light source was 0.8 mm. By using Galilean beam expander, the laser diameter was expanded to minimize the energy density difference of photopolymerization pattern and uniform projection of light source in the DMD screen.

$$M_1 = \frac{-f_2}{f_1} \ldots\ldots\ldots (2.1)$$

Where, M_1 = Magnification of the Galilean system

f_1 = Focal length of lens 1 and is a negative value (input lens)

f_2 = Focal length of lens 2 (exit lens)

The spacing between the two lenses (t)

$$t = f_2 + f_1 \ldots\ldots\ldots (2.2)$$

For the beam expander, the combination of Thorlabs N-BK7 Plano-concave lens (focal length of -35 mm) and Thorlabs N-BK7 Plano-convex lens (focal length of 125 mm) was used and the final laser diameter was expanded to 2.86 and the distance between the two lenses was 90 mm based on the Equations (2.1) and (2.1).

After the beam expander, the Thorlabs SH1 beam shutter was used, and it was controlled by the Thorlabs SC10 shutter controller that allowed the light source passage. During the photopolymerization process, if the shutter was in open condition, it allows the light source to DMD for performing the irradiation process. If this shutter was in close condition, it doesn't allow the light source to DMD. Therefore, the irradiation process doesn't occur.

The mirrors were aligned for changing the light path and reflected onto the DMD screen. Here, the DMD (DLP 2000EVM, Texas Instrument) was used. In the DMD device, thousands of micromirrors were arranged and each micromirror was rotated or tilted ±10-12º individually based ON and OFF state. By tilting micromirrors, the image was formed. Here, the DMD was coupled with the BBB, which is used to transfer the data, and it allows computer programming.

$$M_2 = \frac{f_4}{f_3} \ldots\ldots\ldots (2.3)$$

Where, M_2 = magnification factor of the projector image on the sample

f_3 = Focal length of Biconvex lens 3

f_4 = Focal length of Biconvex lens 4

For the experimental purpose, the reflected light from the DMD was projected on the sample with the reduction magnification factor of ¼. Based on the Equation (2.3), the two Thorlabs N-BK7 Biconvex lenses with different focal lengths of f_3 = 400 mm and f_4 = 100mm were selected in between the DMD and the sample. The first Thorlabs N-BK7 Biconvex lens (f_1= 400 mm) was placed at a distance of 400 mm from the DMD screen and the Thorlabs N-BK7 Biconvex lens (f_2 =

100 mm) was placed at the distance of 100 mm from the sample/ stage. To direct the light source from the shutter to the objective lenses, the Thorlabs BB211-E02 mirrors were arranged. From this optical arrangement, the irradiation power of 148 mW/cm² was obtained. This irradiation power was used to polymerize the hydrogel, and the desired cells were captured on the gel.

For capturing the images, the inverted microscope (ECLIPSE Ti-U, Nikon) combined with a camera (DS-Qi1Mc, Monochrome Digital Camera, Nikon) was used and the sample images were taken at 30 ms exposure time. To automate the image capturing, the two single-axis stage L150 Originalmind CNC-controlled motorized stages were used. The personal computer was used to control all the electronic components that were presented in the system.

2.2.3 Photo polymerization pattern

To perform the photopolymerization process, the polymerization patterns were needed, and it can be created by the LabVIEW image-processing toolbox that contains a large number functional image-processing techniques. Below, the sequential procedures were listed for creating the photopolymerization pattern.

1) At first, an image was captured from the sample.
2) The captured image was converted into a grayscale.
3) To detect cell edges or boundaries, by adjusting the slope value of tone curve to removal of background.
4) To convert the grayscale image into binary images, the threshold value was applied.
5) Holes in the cellular regions were filled with white.
6) Removal of small objects such as debris.
7) Next, the merging of cells that were in proximity to each other with a proximity range of < 5 µm.
8) To remove larger particles, the particle filter was applied with the condition of objects with a volume > 127 µm.
9) For the experimental purpose, the desired cell morphologies were changed into squares and enlarged up to 50 µm.
10) Based on the DMD screen, the image resolution was converted into 640×360 pixels.
11) To extract the cell's information, a particle analysis function was used.
12) Finally, the targeted cell was black and the background image was white and the image was flipped vertically to align with the sample projection.

In this study, the NI vision assistant software was used to convert the sample image into the required photopolymerization pattern. In this software, the Balanced Histogram Threshold (BHT) approach was used. Generally, the image was divided into two main classes, one was background (0-144) and other was foreground (145-255). The optimization of the threshold can be achieved by balancing the foreground class value. If the brightness and contrast of the original bright-field images were varied from certain image conditions, again the system wants to train.

For the creating photopolymerization pattern, it was necessary to adjust the pixels of the converted images based on DMD and optical magnification. By using the following Eqs (2.4) and (2.5), the width w and height h of the photo polymerized pattern image was calculated.

$$w = \frac{p_w a}{m} \ldots\ldots\ldots (2.4)$$

$$h = \frac{p_h a}{m} \ldots\ldots\ldots (2.5)$$

Where p_w and p_h = Width and Height of the DMD pixels respectively,

$a =$ size of one pixel ($a = 7.56$ µm)

$m =$ magnification of the optics ($m = 4$)

For single cell encapsulation, a 50 µm × 50 µm was irradiated on the hydrogel and it was suitable for single cell dimension, and it was sufficient for cell movement inside the encapsulated hydrogel. To obtain the 50 µm × 50 µm, 26-27 pixels were approximated value for p_w and p_h.

In the photopolymerization process, it was very important to transfer the converted polymerized pattern to the BBB board. The transfer time is long, there will be difficulty in polymerizing the desired cells on the hydrogel due to the slight movement of cells and disturbance. To overcome these transferring issues, the three different techniques were used and found out the best technique to reduce the transfer time. In below, the techniques were listed.

1) Manual transfer using a USB drive.
2) SFTP and WinSCP with manual transfer.
3) SFTP and WinSCP with Microsoft PAD.

For easy transferring, SFTP was a network protocol for secure and it was allowed to transfer the data directly between two devices.

2.2.4 Preparation of photopolymerization sample

For the experimental processes, the concentration of 5 % w/v GelMA hydrogel was used. To prepare the hydrogel, add 2 mL of PBS in the centrifuge tube. Add 100 mg of GelMA (60% degree of substitution, gel strength of 90-110 g Bloom, Sigma Aldrich Co Ltd.) which has a photocurable resin oligomer in that centrifuge tube. Using a vortex mixer, mix the solution. The concentration of GelMA was 5% w/v in PBS. And then add 10 mg of LAP (Lithium Phenyl (2, 4, 6-thrmethey-benzoyl) phosphinate, Tokyo Chemical Industry Co Ltd.) in that centrifuge tube. Again, using a vortex mixer, mix the solution properly. Finally, the concentration was 0.5 % w/v LAP and 5 % w/v GelMA in PBS. To avoid contact with the outer environment, the tube was covered with aluminum foil and kept in a dark area for 3-4 hours.

At first, HeLa cells were cultured on the polystyrene petri dish. Drain the culture medium (MEM, 10 % of FBS + 1 % of Pen Strep, Gibco Ltd.) from the petri dish and then the cells were washed with 3 mL of PBS and drain it. After that add 3 mL of trypsin (0.25 % Trypsin EDTA (1X), Gibco Ltd.) on the petri dish and keep that petri dish in an incubator for 4 minutes. After incubating, add 3 mL of MEM (MEM, 10 % of FBS + 1 % of Pen Strep, Gibco Ltd.) on the petri dish and it deactivates the trypsin. The inhale and exhale were performed repeatedly to disperse the cells. In the centrifuge tube, transfer the mixed solution and centrifuged at 1500 rpm for 3 minutes. And then removed the supernatant from the tube and added the prepared GelMA gel into that centrifuge tube. Using a micropipette, inhale and exhale the solution to suspend the cell properly.

For making sample containers, the two different size glass substrates were used. Figure 2.3(A) Shows schematic diagram of sample substrate and Fig. 2.3(B) Shows the substrate holds cell suspension.

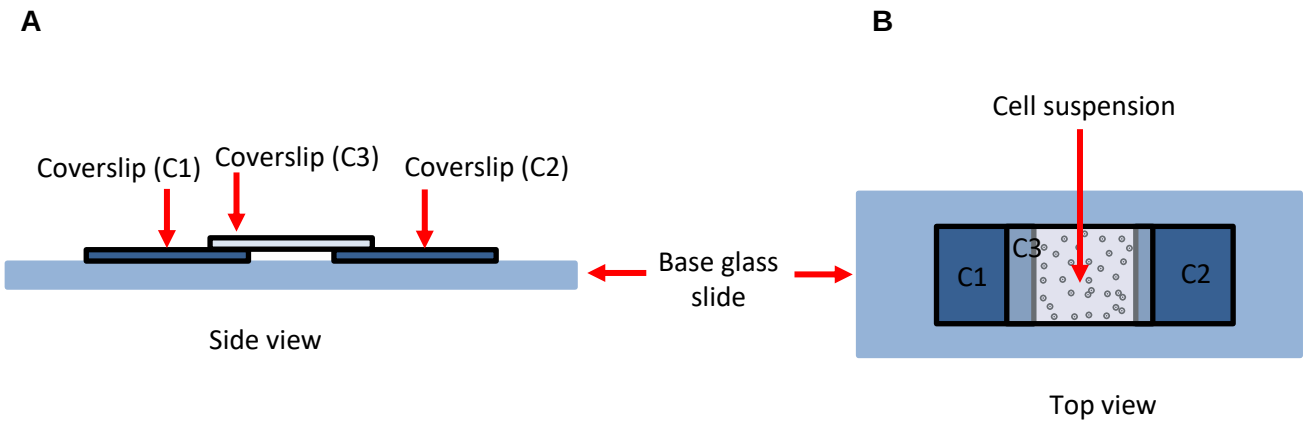

Figure 2.3 Schematic diagram of a sample substrate. (A)Side view of sample substrate. (B) Top view of sample substrate holds cell suspension.

A glass slide with a polished edge (26 mm × 76 mm with a thickness of 0.8 mm-1.0 mm, S1111, Matsunami Glass) was kept as a base. And then, place the two coverslips (C1 and C2) (18 mm × 18mm with thickness of 0.13 mm-0.17 mm, Matsunami Glass) at top of the base glass slide with some distance between two cover glass slips. Finally, place the coverslip (C3) at the top of C1 and C2 coverslips. And by arranging the glass slips, the slit was formed in between the base glass slide and coverslip (C3). The required amount of cell suspension was transferred to that slit and kept in the motorized stage to perform the photopolymerization process.

2.3 Results and Discussion

2.3.1 Image processing of photo polymerization pattern

Using NI vision assistant, the various algorithm was created and tested with micro-practical suspended in GelMA hydrogel. Here some of the image-processing algorithms were discussed below.

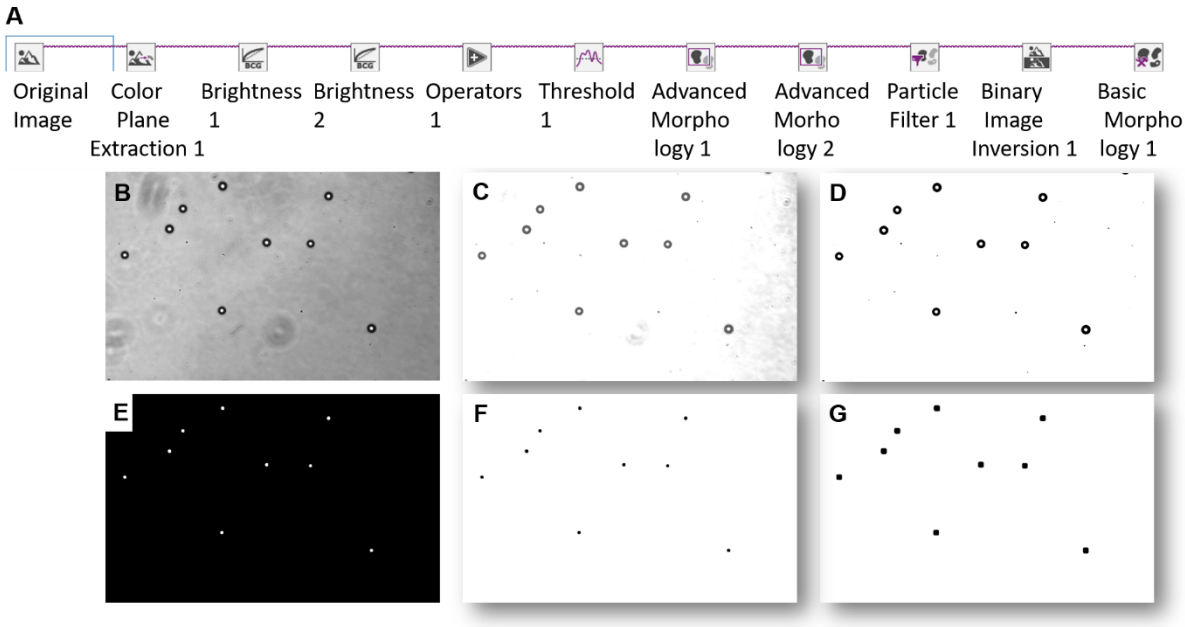

Figure 2.4 Image processing of photopolymerization pattern. (A) Flow of image processing algorithm in NI vision assistant. (B) The image was captured from a sample. (C) Object detection. (D) Image after threshold applied. (E) Removal of unwanted objects. (F) Invert the image background and object. (G) Convert the required photopolymerization pattern

Figure 2.4 shows the image processing of photopolymerization patterns. Figure 2.4(A) shows the flow process of the image algorithm in NI vision assistant software. The image (Fig 2.4(B)) was captured from the sample. Using the color plane extraction function, the captured image was used to convert the original image into a gray scale image. By adjusting the brightness of the image, making the objects more prominent while reducing the background noise and adding another cycle of brightness adjustment, the objects were clearer. The image (Fig 2.4(C)) shows the clear distinction between the objects and the background. By applying a threshold, the image was converted from grayscale image into a binary image, where the pixels were converted either black or white. In the image (Fig 2.4(D)), the object's pixels appeared in black, and the background's pixels appeared in white. The morphological operations were applied to remove the small unwanted objects and highlight the targeted objects. To improve uniform shape and size, the additional morphology

function was applied again (Fig 2.4(E)). After removing the unwanted object, the image background was inverted from black to white and the objects were inverted and vice versa using the binary inversion function (Fig 2.4(F)). Using basic morphology functions, the shape and size of the objects were changed according to experimental conditions. Finally, the required photopolymerization pattern (Fig 2.4(G)) was generated.

In this process, the color extraction, brightness adjustment, thresholding and morphology functions were used to refine the image. This image processing algorithm was able to detect the objects to convert an original image into a binary image. Based on these algorithms, the image was captured from a sample contains cell suspension hydrogel and uploaded into an image processing tool. The single cells were automatically detected and generated the required single-cell photopolymerization pattern.

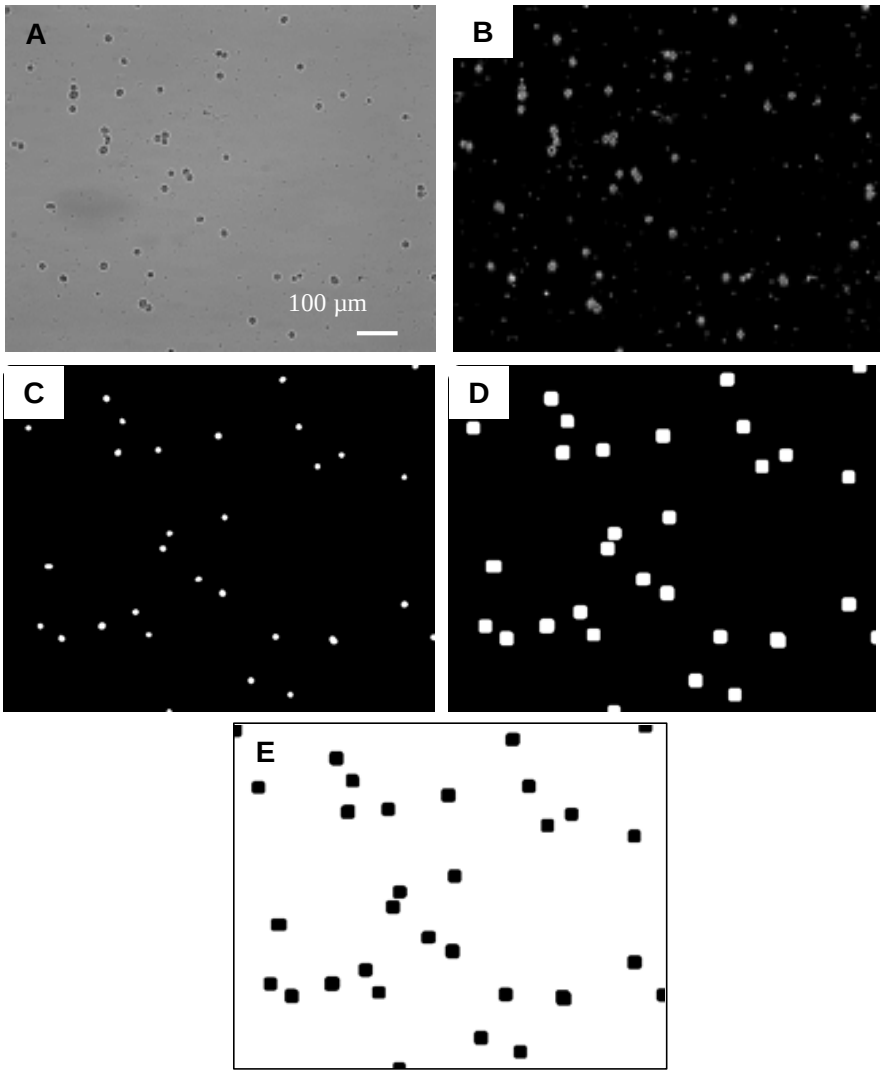

Figure 2.5 Results of image processing for single-cell encapsulation pattern. (A) Grayscale image. (B) Binary images of the captured image. (C) Removal of unwanted objects. (D) Conversion of circular objects to square and size enlargement (E) Required photopolymer

Figure 2.5 shows the image processing for the single-cell encapsulation pattern. The image (Fig. 2.5(A)) was captured from the cell sample. In that original image, the cell boundaries were detected by adjusting the tone curve of the captured image. After detecting the cell edges, it was converted into a binary image (Fig. 2.5(B)) for further process. In the binary image, the holes were filled which were presented in the cells. And then single cells were identified by their shapes and sizes. Using particle filter function, the unwanted cells and objects were removed and to maintain the targeted single cells (Fig. 2.5(C)). Here the targeted cells' morphologies were changed shape from sphere to square (Fig. 2.5D)) and increase the sizes of the shapes. The image was inverted, and the targeted

cells were changed from white to black color, like wish the background was changed from black to white color (Fig. 2.5(E)). The total image processing was done within 7.5 s.

To find out the performance of the single-cell detection of an image, the efficiency of image processing was calculated by relation between the tone curve angle and the detection of a single cell. The cell detection rate R_d was calculated by using Eq. (2.6).

$$R_d = \frac{N_d}{N_t} \ldots\ldots\ldots (2.6)$$

N_d = Number of detected single cells

N_t = Total number of single cells

To increase the cell detection rate was directly proportional to the tone curve angle. The cell detection rate was increased by increasing the tone curve angel. Figure 2.5 shows the images of addition of angle to a tone curve at 45º, 65º, 70º and 75º.

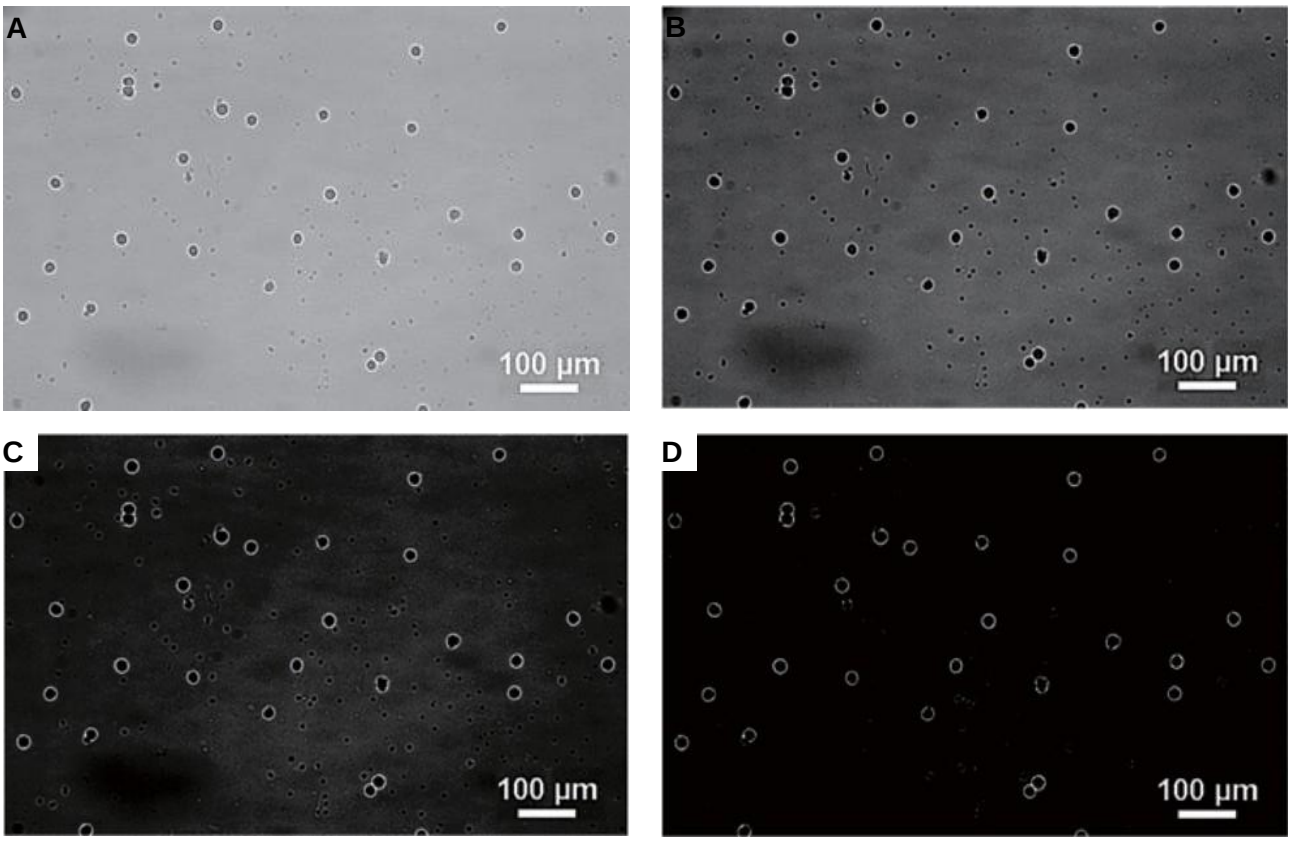

Figure 2.6 Results of addition of angle to a tone curve. Image with a tone curve at (A) 45º, (B) 65º, (C) 70º and (D) 75º slope.

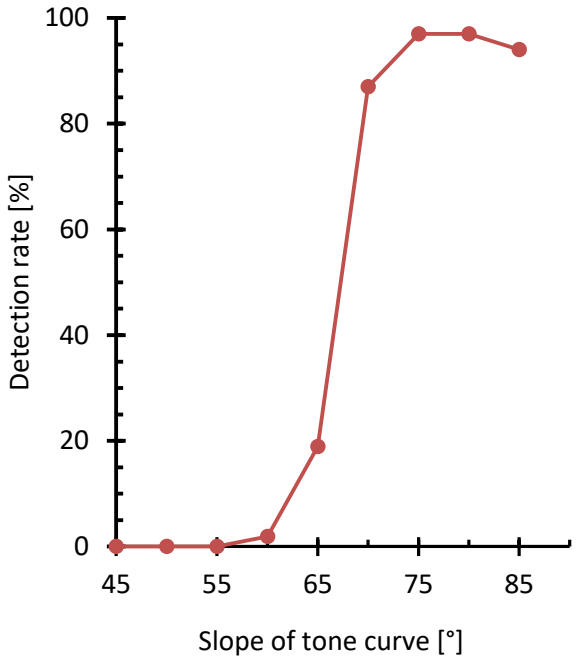

Figure 2.7 Effect of contrast addition.

Figure 2.7 shows the detection rate variously by changing the tone curve angel. The tone curve angle was up to 65º, the cell detection rate was less than 20%. With proper contrast adjustment in the image, the cell edges and removing the background were extracted and without proper contrast adjustment, the background remained the same and the detection rate decreased (Fig. 2.6(A)). There was a threshold jump between 65º (Fig. 2.6(B)) and 70º (Fig. 2.6(C)) and the moistest of the background pixels were converted to zero at 70º. At the tone curve angle of 75º (Fig. 2.6(D)) and 80º, the cell detection rate was reached its maximum of 97% and it remained saturate at 85º.

The tone curve angle was determined by the horizontal axis and vertical axis. The horizontal axis represents the brightness level of the input image, and the vertical axis represents the brightness level of the output image. If the brightness of the input and output image was the same, the tone curve angle was 45º that indicated by a straight line drawn from the bottom left to the top right. By changing the brightness and contrast of the image, the tone curve angle also changed.

2.3.2 Formation of photopolymerization pattern

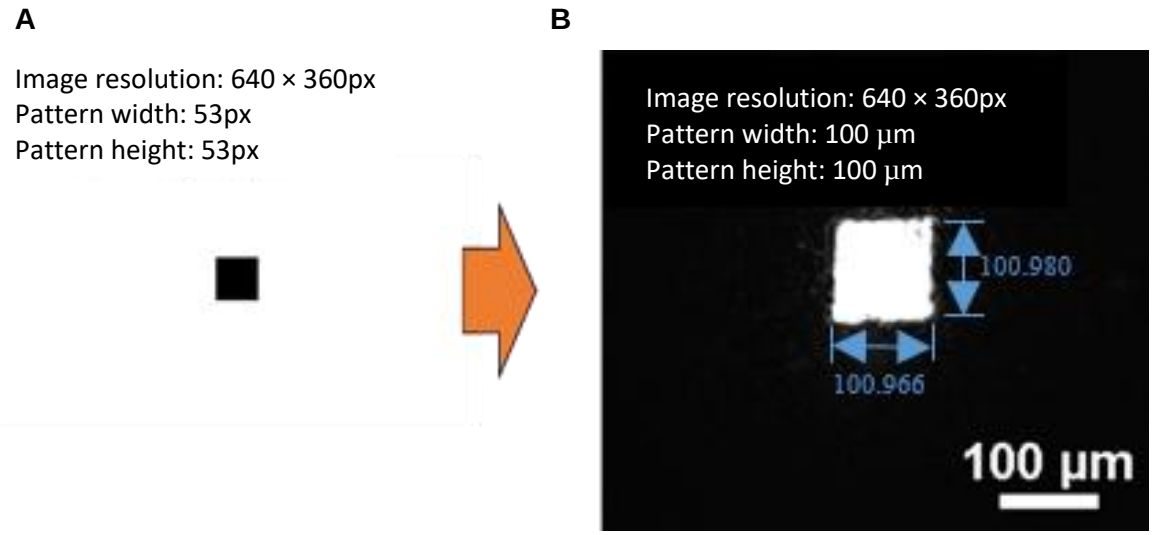

Figure 2.8 Formation of light pattern. (A) Polymerization pattern with a dimension of 53 × 53 pixels. (B) Microscopic view of projected photopolymerization pattern on the sample.

Figure 2.8 shows the formation of light patterns. Using Eqs (3) and (4), the 100 µm square box was formed, and it has 53 ×53 pixels (Fig. 2.8(A)). The polymerized pattern was observed with a microscope (Fig. 2.8(B)). The size of the formed irradiation pattern was 101 µm × 101µm and it was almost same as the creating photopolymerized pattern.

2.3.3 Encapsulation of single-cell on hydrogel

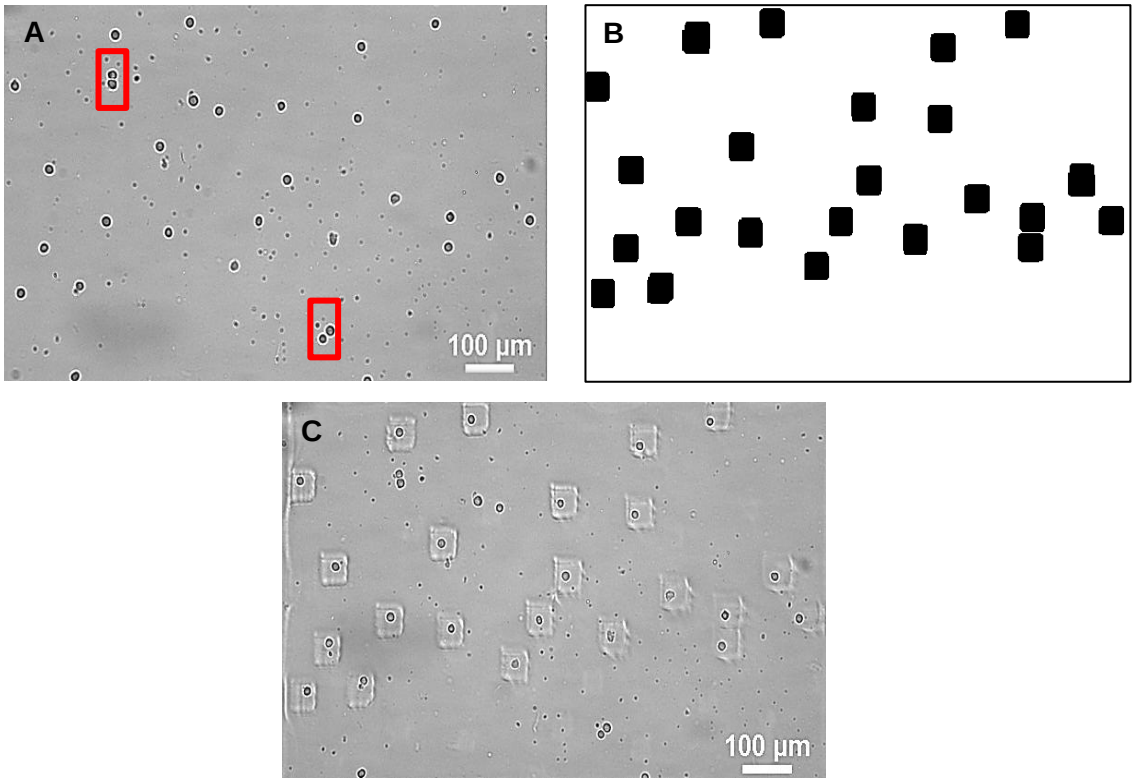

Figure 2.9 Photopolymerization process of GelMA at single cell. (A) Before photopolymerization. (B) Single-cell encapsulation pattern. (C) Cell encapsulated in around 50 µm square hydrogel.

Figure 2.9 shows the photopolymerization process of GelMA at a single cell position. An image was captured from the cell sample (Fig. 2.9(A)). From that image, the single cells were detected and the two or groups of cells were rejected. The total 29 number of cells was identified from that image. The single cells were indicated by a red circular shape. And the unwanted or group cells were indicated by red color box shape. Figure 2.9(B) shows the single-cell photopolymerization pattern. Based on the identification of single cells, the photopolymerization pattern was formed and the group cells were eliminated successfully using an image processing algorithm. In that pattern, 23 square boxes were formed with the dimension of 50 µm. Then the pattern was uploaded in BBB broad and the DMD projects the pattern. 405 nm light source was used and irradiation with the intensity of 110 mW/cm² for 13 seconds. The light energy was 1430 mJ/cm². Figure 2.9(C) shows the image of 50 µm square photopolymerized GelMA around the desired single cells. The total 23 squares polymerization was formed, and the cells were encapsulated in the hydrogel. And the group cells were not photopolymerized.

2.3.4 Alignment error of single cells in photo-curable hydrogel

In initial experiments, the data was transferred manually to DMD (DLP 3000EVM, Texas Instrument). During the process, the targeted single cells were not aligned with the photopolymerized hydrogel. To encapsulate the targeted single cells inside the photopolymerized hydrogel, the DMD in the experimental setup was upgraded from DMD (DLP 3000EVM, Texas Instrument) to DMD (DLP 2000EVM, Texas Instrument). When in the new transferring method, still some errors occurred. Using the PAD software, all the processes including data transfer were integrated and the total process was performed automatically. Here, the three data transfer methods are mentioned below.

- SFTP and WinSCP with PAD
- SFTP and WinSCP with manual
- USB flash drive

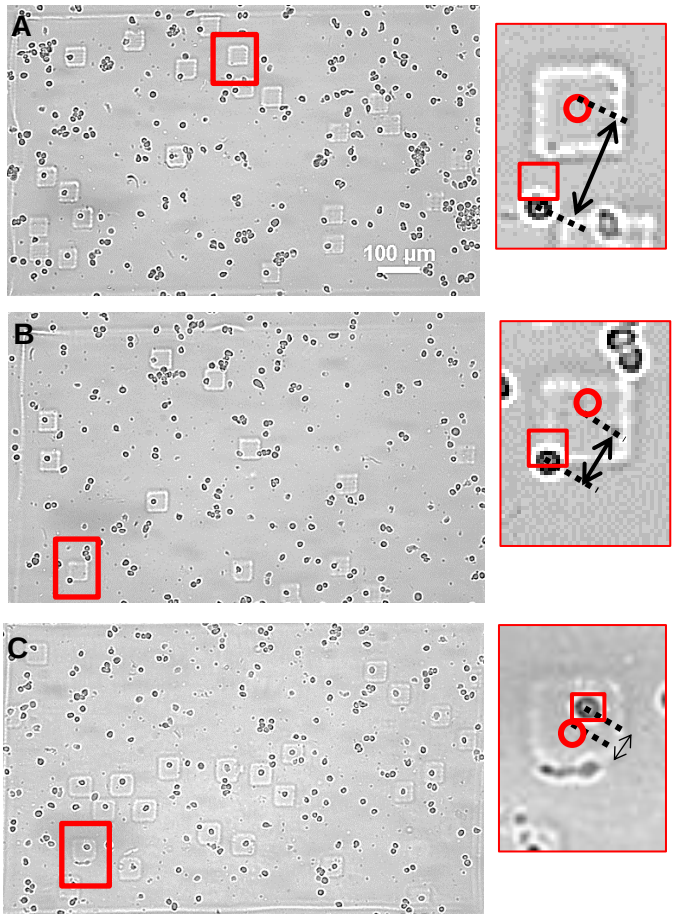

Figure 2.10 Alignment error of single cells in polymerized hydrogel (A) SFTP and WinSCP with PAD. (B) SFTP and WinSCP with manual input. (C) USB flash drive. (D), (E) and (F) Enlarge image of polymerized 50 µm square hydrogel from (A), (B) and (C) respectively.

Figure 2.10 shows the alignment error of single cells in polymerized hydrogel. In various transferring modes, the encapsulation rates were changed. In the case of SFTP and WinSCP with PAD (Fig. 2.10(A)), the total number of 25 polymerization square boxes on the sample were equal to the number of 25 square boxes in the polymerization pattern. Therefore, the encapsulation rate was 100 %. Figure 2.10(B)-2.10(C), the encapsulation rate of SFTP integrated with WinSCP and USB flash drives was 85 % (=11/13) and was 70 % (= 14/20), respectively. The enlarged views of single-cell photocurable hydrogel (Fig. 2.10(D), Fig. 2.10(E), and Fig. 2.10(F)) was indicated by red boxes. In those boxes, the circular shape indicates the original cell position of the desired cell at the image capturing time and the box shape indicates the position of the polymerized cell. Figure 2.10(C) shows some of the cells were encapsulated in the edge or outside of the irradiation pattern. Out of 20 cells, six cells were not encapsulated in the irradiation region while using the USB flash drive. The encapsulation rate was affected by increasing the data transferring process.

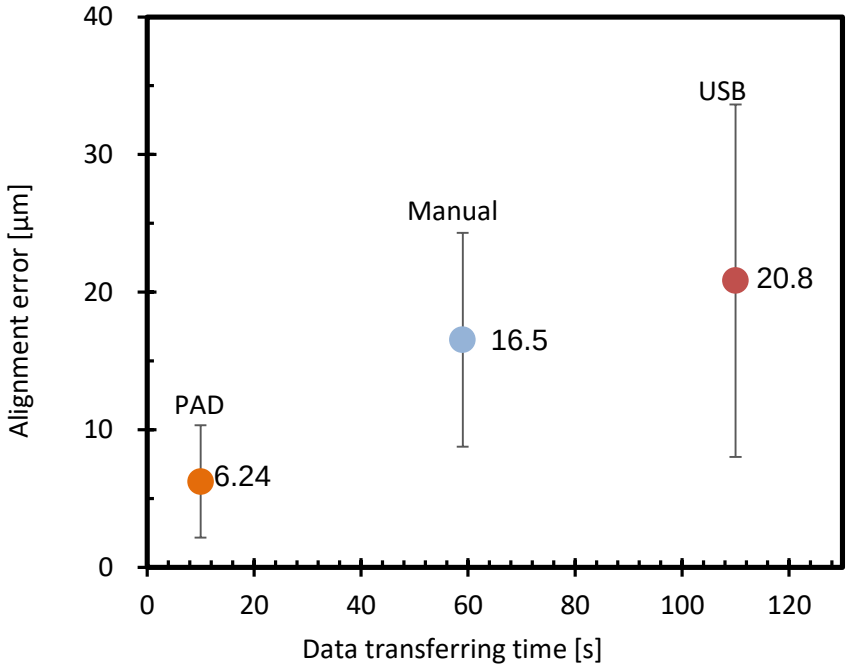

Figure 2.11 Alignment error using various data transfer method.

Figure 2.11 shows the alignment error concerning the transfer time of various data transfer methods. The alignment error was formulated by the distance between the original position of a single cell at image capturing time and the position of the cell in the polymerized hydrogels. While using PAD transfer methodology, the alignment error was minimal compared to other methods. In the PAD method, the manual interaction was eliminated, and it reduced the pattern transfer time. The

transferring and projecting of the images in the sample required 10 seconds. This ensured the alignment error of 6.24 µm. In the other two data transfer methods, manual interaction was required and so the alignment error of 16.5 µm and 20.8 µm were obtained by SFTP and WinSCP with manual and USB flash drive methods respectively.

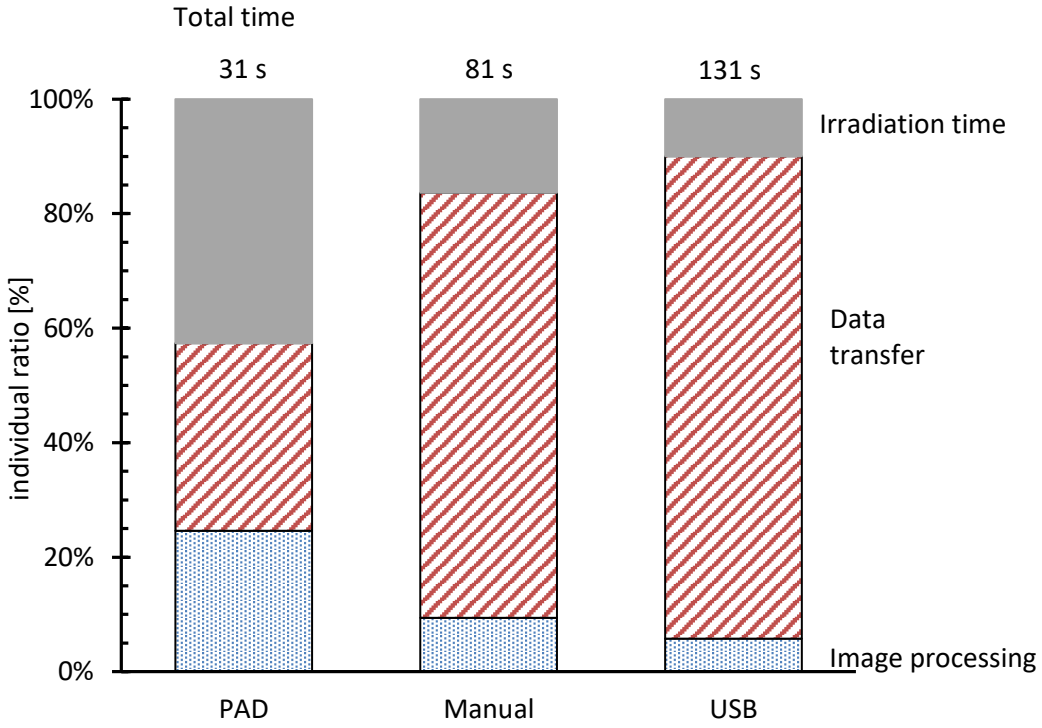

Figure 2.12 Total time of polymerization process using various transfer methods.

Figure 2.12 shows the total time of polymerized process with various transfer methods such as SFTP and WinSCP with PAD, SFTP and WinSCP with manual input and USB flash drive. Here the total time of the polymerized process was added by image processing time, data transfer time and irradiation time. In the PAD method, more than 50 % of total time was occupied by image processing and data transfer methods. In PAD data transfer method, 20.5 seconds was required for image processing and data transfer method out of total 31 seconds. In the manual method, the image processing and data transfer time took nearly 72 seconds, and the irradiation processes took only 8-10 seconds. But in the USB method, the image processing and data transfer took nearly 92 seconds, and the irradiation processes was obtained by 8-10 seconds. In the data transfer method, the PAD was superior method compared to the manual and USB drive. Because in the manual and USB methods,

the image processing and irradiation time was almost same, but the differentiation was data transfer time.

This system is DMD based approach and has a higher efficiency compare than a single probe [32 - 35]. To achieve the efficient live single-cell collection, the limitations from the previous studies were addressed below [38 - 40]. The identification of single-cell processes was automated and there was no need for manual interaction for identification of single-cell processes.

1) For live cell collection, the cells were polymerized and captured in GelMA hydrogel more suitable than PEGDA hydrogel [43].

2) This method reduced the total processing time of encapsulated single-cells and increased the cell encapsulation rate.

A substrate-free method was developed to increase the number of substrate types. This method maintains the advantages of the DMD based approach and the free-floating single cells were encapsulated.

2.4 Conclusion

In this chapter, the construction of an automated single-cell encapsulation with integral optical and DMD systems was developed. By using an image processing tool, the single cells were identified and converted into the required photopolymerized pattern. The HeLa suspension cells were captured in the GelMA hydrogel by multi-light irradiation. In this process, the 50 µm square boxes were used to encapsulate the single HeLa cells. Here, I addressed the major advantage of this system.

The transfer of photocuring pattern to the DMD device by manual method was eliminated from using various data transfer methods of the encapsulation process, and the alignment error of suspended single cells was observed after the photopolymerization process. By reducing the time in transferring the photopolymerization pattern to the DMD device, the alignment error was minimized. This kind of approaches increased the efficiency of the system.

Chapter 3 Behavior of cells encapsulated in GelMA

3.1 Introduction

Hydrogel is widely used in tissue engineering because of their specific physical properties (such as mechanical properties, straightness of the gel and pore size), biocompatibility (like cell proliferation, tissue construct formation) and different composition [44, 45]. In the last few years, lots of hydrogels combinations have been established by natural or synthetic material [46, 47] and crosslinking the hydrogel by using various techniques based on their application [48]. The hydrogel materials are absorbed the oxygen, nutrients, and other water-soluble metabolites. Due to its properties, it is used as drug or protein carriers, contact lens material and medium for cell encapsulation techniques because of their high volume of water content, flexible materials and biocompatibility with cells [49]. The hydrogels scaffolds maintain their shape and it is helpful for cell growth, proliferation, extracellular environment and functional expression [50].

In general, hydrogels are polymers material, so the Ultraviolet light (UV light) is used to polymerize and it's induced free radical polymerization reactions that means chemical reaction occurred on the hydrogel [51]. The chemical reaction process is classified by four processes, such as chain initiation, chain growth, chain termination and chain transfer [50].

Polyethylene glycol is a synthetic polymer material and it has high mechanical properties and maintains its scaffold shape [52]. Polyethylene glycol can decrease clearance, deceleration of enzymatic degradation, and offer efficient immune system shielding [53]. PEGDA hydrogels are irradiated with UV-light, then the photoinitiator particle absorb the light source and create the free radicals. These free radicals respond with the acrylate groups on the ends of PEG chains and forming molecular bonds between the chains. This leads in the formation of 3D cross-linked polymers which offers the PEGDA hydrogel its mechanical strength and shape. The main disadvantage of PEGDA is poor biodegradability and nowadays researchers are doing a lot of research in degradation things (degradation time of PEGDA scaffolds) for some particular applications [41, 54].

Gelatin methacryloyl (GelMA) is a natural polymer material and it has been used in tissue engineering and is more useful on 3D printers. The gelatin is a prime component of GelMA hydrogel and gelatin has been widely used due to its good biocompatibility [55]. GelMA hydrogel is a hydrophilic polymer and it has been irradiated with UV light. During this process, the chemically modified GelMA with methacryloyl side group undergoes rapid polymerization by cross-linking of

the methacryloyl backbone and it is used for cell encapsulation and 3D printing application [56]. While using PEGDA and GelMA hydrogels in the photopolymerization process, the photo initiators are used as a catalyst.

In cell encapsulation application, the polymerized hydrogel shape wants to be degraded for live cell collection and longtime observation. The GelMA hydrogel is more suitable for biocompatible material degradation in cells as well as enzymes [44, 57, 58]. In recent decades, the GelMA hydrogel based micromodules [59] and microsphere [60, 61] proved the cell's encapsulation in polymerized regions has high long term viability. In applications like high efficiency drug delivery experiments, to investigate stem cell variation and also in fabrication of heterogeneous tissue prototypes, the cells were arranged in some sequential pattern and encapsulated in GelMA hydrogel by inducing UV-light [62 - 64]. In GelMA hydrogel can be degraded using enzymes like [57] and collagenase [58, 59]. In previous chapter 2, the automation single-cell encapsulation system has developed and investigated the formation of single-cell polymerization pattern and how it’s formed on the hydrogel and observed the differentiation in various pattern transfer methods. But the behavior of cells in encapsulated regions were not mentioned.

In this chapter, the studies in cell proliferation, biodegradation, and cell motility of encapsulated cells in polymerized GelMA hydrogel were conducted. The collection of both suspended and adherent encapsulated cells from GelMA hydrogel were performed. The collection of cells was successfully carried out by using time-control trypsin addition.

3.2 Methods

3.2.1 Preparation of bioink and cell suspension

To prepare the bioink, transfer 2 mL of PBS (phosphate buffered saline, Gibco Ltd, pH 7.4, 1X) in the centrifuge tube. Add 100 mg of GelMA (gel strength of 90-110g of Bloom, 60% of degree of substitution, Sigma Aldrich.), in the centrifuge tube and mix the solution using vortex mixer. The concentration of the GelMA solution was 5 % W/v. and then, add 10 mg of Lithium phenyl (2, 4, 6-trimethey-benzoyl) phosphinate (LAP, Tokyo Kasei Kogyo Co., Ltd) and mix with the solution of 5 % concentration GelMA. The final concentration of LAP was 0.5 % w/v in PBS. To control the exposure with outer environment, Wrap the centrifuge tube with aluminum foil and kept in a dark environment for 3-4 hours.

In culture medium (MEM, 10 % of FBS + 1 % of Pen Strep, Gibco Ltd.), HeLa cells (RCB0007, RIKEN BRC) were cultured on the polystyrene petri dish. From the culture dish, the medium was removed and washed with 3 ml of PBS and again drained. Then transfer 3 ml of trypsin (0.25 % Trypsin EDTA (1X), Gibco Ltd.) on the petri dish and incubate for 4 minutes in an incubator. Mix 3 ml of MEM to the trypsinized cells solution and transfer the mixed solution in a centrifuge tube. At 1500 RPM, perform centrifuges for 3 minutes and remove supernatant from the tube. Finally the cells were suspended with prepared bioink.

At bottom, place the glass slide of 26 mm × 76 mm with thickness 0.8 mm-1.0 mm (S1111, Matsunami Glass) was kept. At the top of the bottom slide, kept two coverslips (18 mm × 18mm with thickness of 0.13 mm-0.17 mm, Matsunami Glass) with some spacing between two. Kept a coverslip with grid lines (GC1300, 13 mm diameter of thickness 0.16 mm-0.19 mm, Matsunami Co., Ltd.). Based on this arrangement, the space was created.

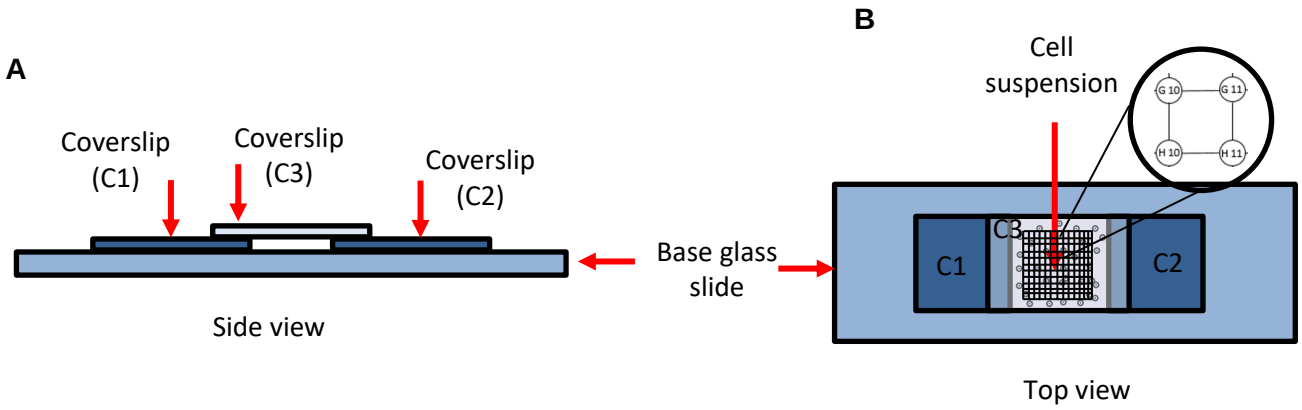

Figure 3.1 Schematic diagram of a sample plate. (A) Side view of sample substrate. (B) Top view of sample substrate holds cell suspension.

3.2.2 Experimental setup

In the previous section 2.2.1, the construction of an automatic single-cell screening was described. Here, I briefly described the working of the experimental setup.An OBIS laser (purple color) with an oscillatory wavelength 405 nm was used as a light source. For the polymerization pattern, the four-square boxes of each box dimension 98 µm were arranged in equal distance with the neighboring boxes. And this pattern was uploaded in DMD. For cell encapsulation, the cells suspension GelMA hydrogel was exposed with the light source at 100-300 mW/cm² for an integrated light intensity of 600-2000 mJ/cm². Based on this parameter, the irradiation time for the process varies from 2 seconds to 8 seconds. The total experimental process was carried out at the temperature of 23º C.

3.2.3 Observation of cell encapsulation in GelMA for long period observation

For observation of cells encapsulated, HeLa cells were polymerized at 1000 mJ/cm^2 of 10 seconds and encapsulated in GelMA hydrogel. After that, the cells were washed with PBS and kept the sample in a 50 mm petri dish filled with the MEM (MEM with 10 % of FBS + 1 % of Pen Strep, Gibco Ltd.). To observe encapsulated cells every day, the petri dish was kept in an incubator at environmental condition of 37ºc and 5 % CO_2. In the observation of encapsulated cells, the cell proliferation, biodegradation of the gel, cell motility and cell viability were analyzed. In this analysis, the photopolymerization of GelMA hydrogel area without and with cells were monitored for 5 days.

3.2.4 Observation of cell viability

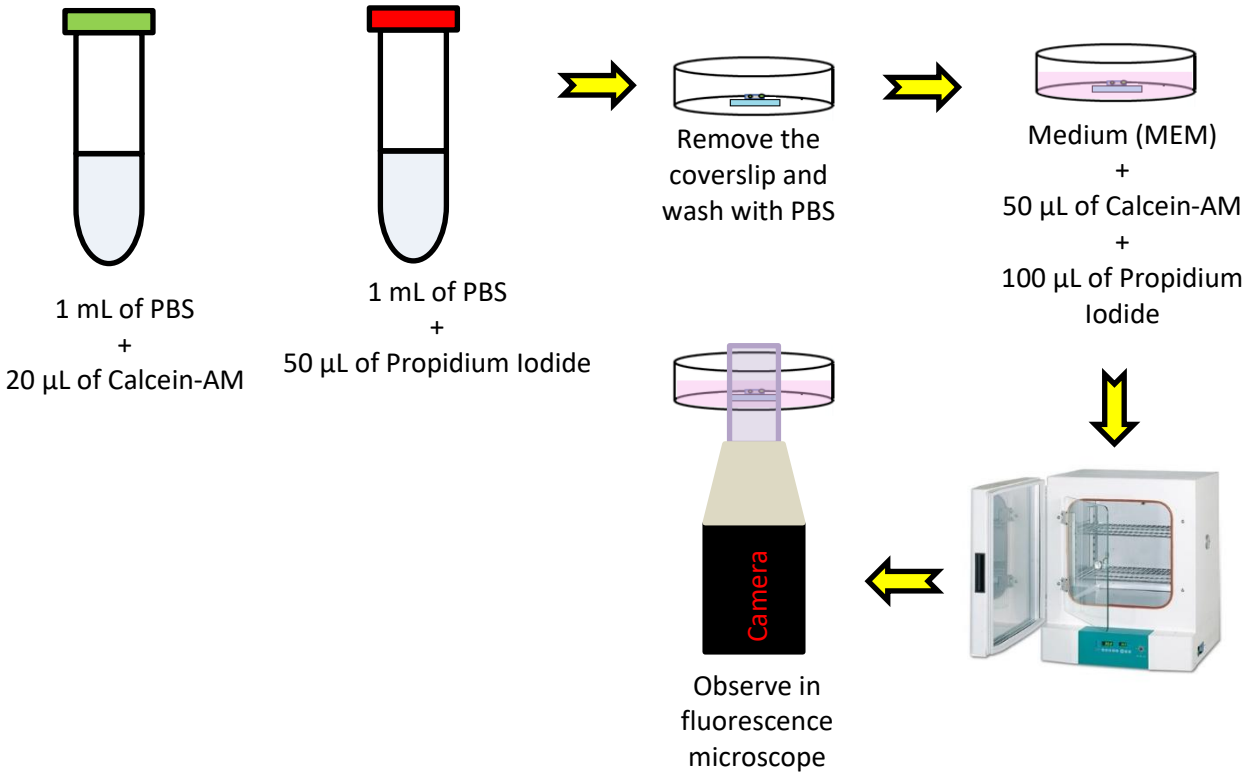

Figure 3.2 Procedure of cell viability.

To conduct the cell viability experiment, Calcein AM and Propidium Iodide (PI) were used as a fluorescent agent. Add 20 µL of Calcein-AM and 50 µL of Propidium Iodide with 1 mL of PBS solution in the separate centrifuge tube respectively. After photopolymerization, the samples were washed with PBS and kept in a 50 mm Falcon petri dish that filled with MEM solution. And then, transfer 50 µL of Calcein-AM and 100 µL of Propidium iodide from the concentrate solution tube. To initiate the staining process with gel, place the petri dish in the incubator for 35 minutes at the environmental condition of 37ºc and 5 % CO_2. After 35 minutes, the dish was placed under a microscope (Eclipse Ti-U, Nikon) coupled with camera (Nikon, DS-Qi1Mc) fitted with fluorescent filters (B2A: 150 ms, C-FL-C TRITC: 150 ms). In observation, green color fluorescence was shown the live cells and red color fluorescence was shown the dead cells. By using the below equation, the efficiency of cell viability rate was calculated by Eq. (3.1).

$$cell\ viability = \frac{N_{Live}}{(N_{Live}+N_{Dead})} \ldots\ldots\ldots (3.1)$$

N_{Live} = The number of live cells

N_{Dead} = The number of dead lives

3.2.5 Collection of unwanted cells and cured cells in polymerized GelMA hydrogel

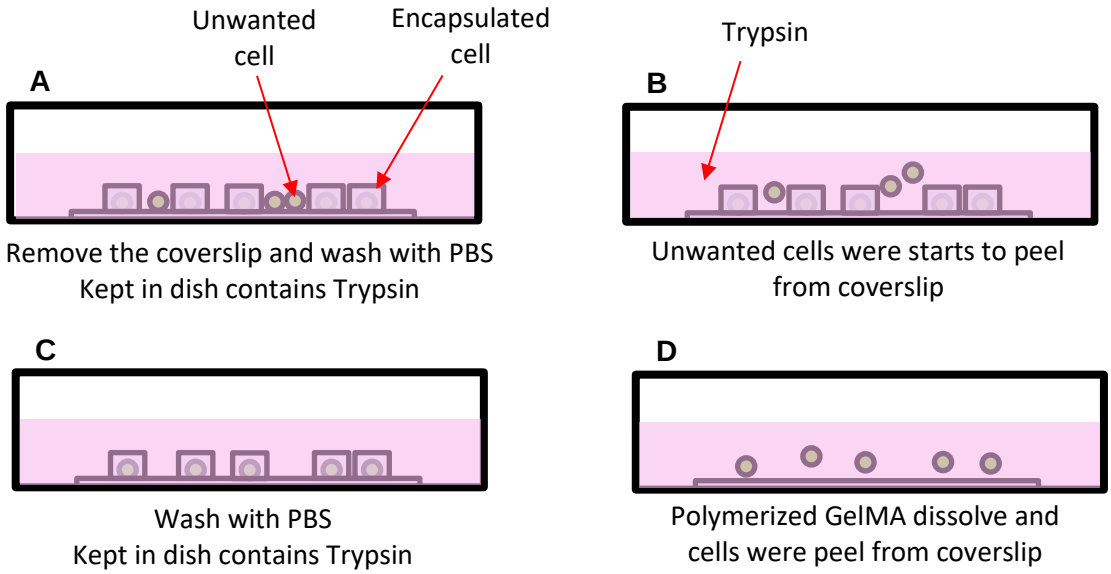

Figure 3.3 Setup for collection of uncured and cured cells. (A-B) Removal of uncured cells from the sample. (C-D) Removal of cured cells from the sample.

To recover unwanted cells and cured cells in the polymerized GelMA hydrogel, the trypsin (0.25 % Trypsin EDTA (1X), Gibco Co Ltd.) was used and the main control parameter for conducting the process was time. The time is directly proportional to the cells collection rate in both cured and uncured cells.

Figure 3.3(A)-3.3(B) shows the schematic diagram of recovery of unwanted cells in polymerized hydrogel. After photopolymerization, the top coverslip was removed and washed with PBS. Next the coverslip was transferred to a 50 mm Falcon petri dish and filled with Trypsin (Fig. 3.3(A)). Figure 3.3(B) shows the unwanted cells were starts to peel from the coverslip after some minutes. Finally, after some times, the unwanted cells were completely removed from the polymerized hydrogel. Figure 3.3(C)-3.3(D) shows the schematic diagram of recovery of cured cells in polymerized hydrogel. To remove the cured cells from the sample, the sample was washed and treated with trypsin. And the encapsulated cells were released by dissolving polymerized gel in the trypsin solution. Using an inverted microscope coupled with a camera, the process was observed.

3.3 Results and Discussion

3.3.1 Behavior of photo polymerization GelMA

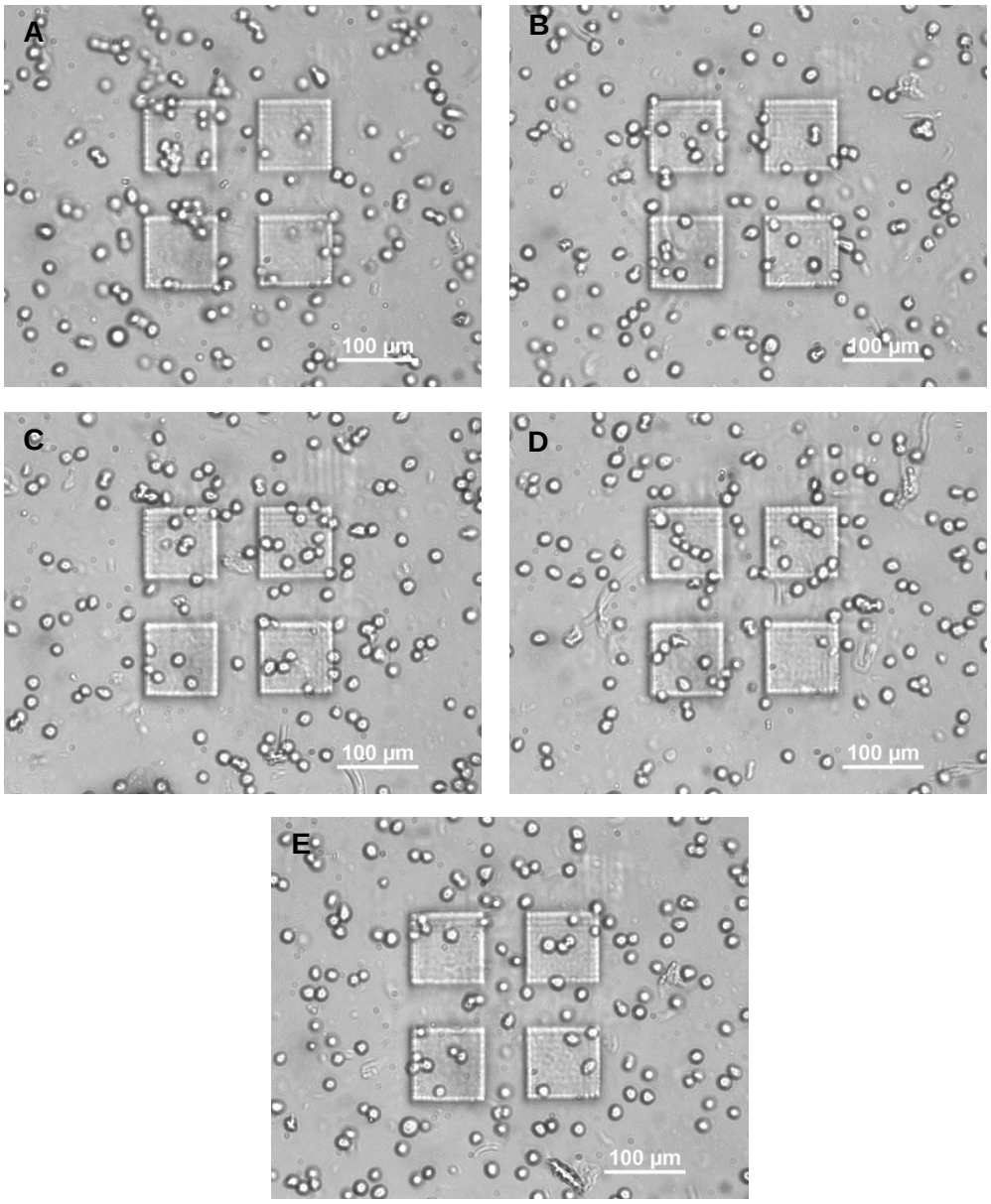

Figure 3.4 Microscopic images of cured gel at 5 % w/v GelMA hydrogel. (A) 1070, (B) 1280, (C) 1490, (D) 1700 (E) 1920 mJ/cm^2.

Figure 3.4 shows the microscopic images of polymerized GelMA of concentration of 5 % w/v. The prepared cell suspension was transferred into the sample and placed under the inverted microscope. The general photocuring pattern was uploaded to DMD and the laser was irradiated on the sample. In this polymerization process, the exposure time that means the light irradiation time reacted with the sample is directly proportional to the light integral. Figure 3.1(A)-3.1(E) exposed to

view the polymerized pattern on the GelMA hydrogel which was irradiated at the exposure time of 8 to 4 seconds with varying the light integral value from 1070 mJ/cm² to 1920 mJ/cm². At 5 % w/v concentration of GelMA hydrogel, the polymerized hydrogel areas were transparent even after the polymerization process happened. The cells which were encapsulated in the polymerized region were visible. This can help the encapsulated cells to retain their movements and the visibility because of a thin layer of hydrogel.

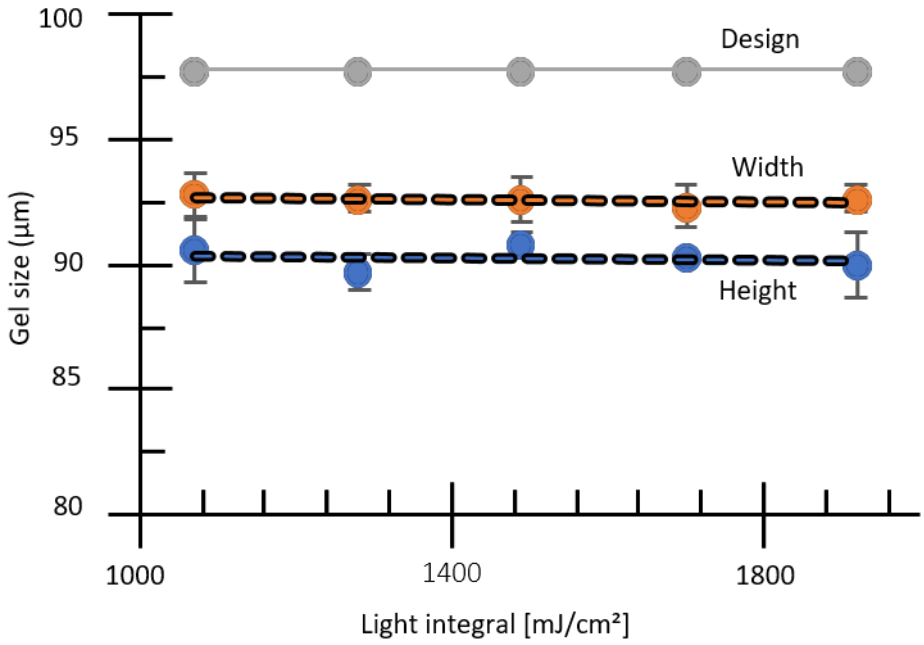

Figure 3.5 Dimension of cured hydrogel at different light integral.

Figure 3.5 shows height and width of the polymerized hydrogel at different light integral values. In the graph, the X-axis plotted the light integral value of the light source, and the y-axis plotted the size of the polymerized gel. From that graph, the hydrogel sizes were changed with respect to the light integral. In different light integral, the size of the polymerized regions was almost same of the polymerized pattern dimensions that means the sizes of photo-crosslink were changed 92-94 µm near to the dimension of original pattern of 98 µm.

In the general case of hydrogel-based encapsulation approaches, the polymerization region is one of the important factors because the distance between two neighboring patterns wants some distances. If the distance is less, there may be chances of interaction between the formations of the photocured pattern. The boundary of the pattern wants to be important, that means the formed photocured region is the same as the original design of the polymerization pattern. From the above graph the polymerization region was almost the original size with different light integral values.

3.3.2 Cell viability of encapsulated cells in GelMA hydrogel

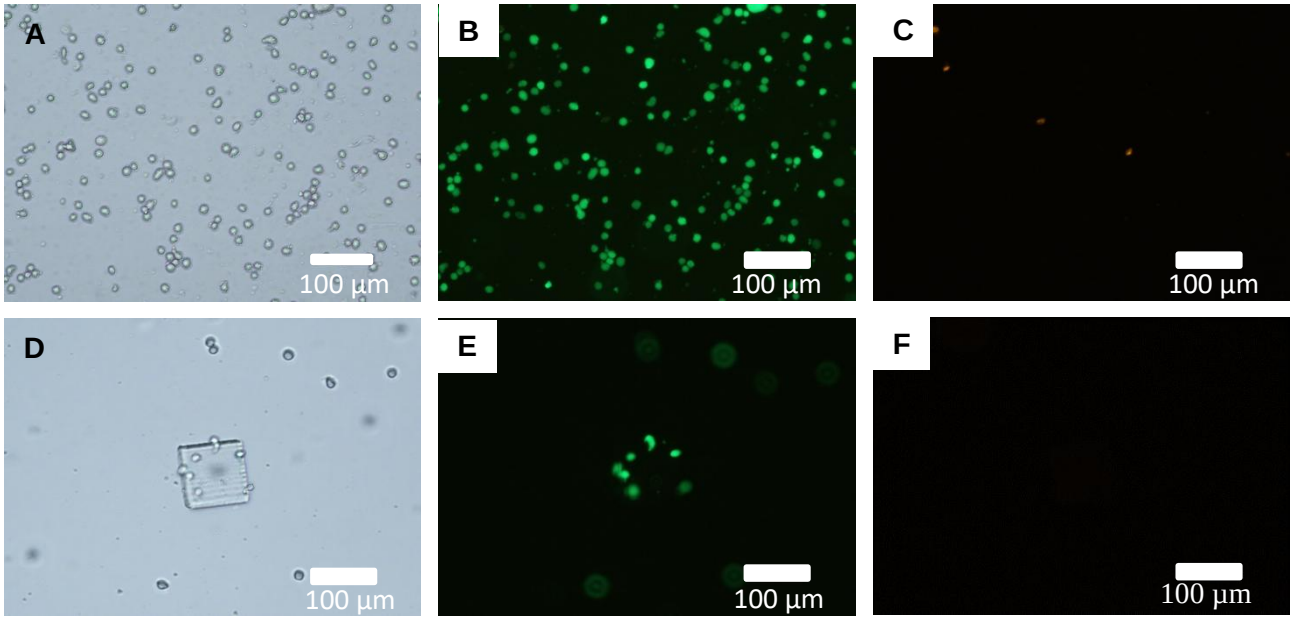

Figure 3.6 Microscopic images of HeLa stained with Calcein-AM and PI. (A-C) Negative control of hydrogel. (D-F) 5 % w/v of GelMA cured gel at 1200 mJ/cm². (A, D) bright field images. (B-E) Green fluorescent images. (C, F) Red fluorescent images.

To perform the cell viability, the hydrogel with cells suspension was polymerized at 1200 mJ/cm². Using the sub-section 3.2.4 procedure, the staining liquids were added and observed in the fluorescence microscope. Figure 3.6(A-C) shows the negative control experiment without conducting the polymerization process. Figure 3.6(B) shows the cells stained with Calcein-AM in green fluorescence which indicates viable cells. Figure 3.6(C) shows the cells stained with PI in red fluorescence which indicates dead cells. From the observation, the efficiency of cell viable in negative control experiments was 98 %. Figure 3.6(D) shows the bright field images of 5 % w/v GelMA hydrogel that were polymerized at 1200 mJ/cm². Figure 3.6(E) shows the viable cells that were encapsulated in the polymerized gel. Figure 3.6(F) looks black, that means there are no dead cells detected from that image. The efficiency of cell viable at 5 % w/v of polymerize gel was 96 %.

3.3.3 Cell proliferation of polymerized GelMA

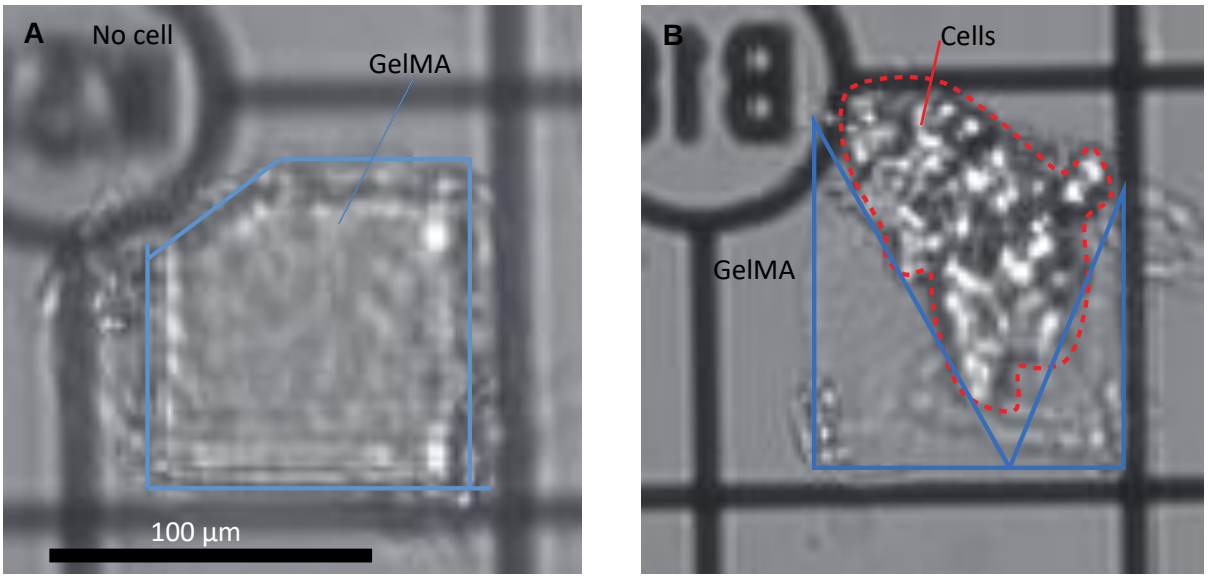

Figure 3.7 GelMA degradation and cell proliferation of 5 % w/v of GelMA. (A) Microscopic image of polymerized gel without a cell. (B) Microscopic image of polymerized gel with gel.

Figure 3.7 shows the biodegradation and cell proliferation of 5 % w/v GelMA polymerized hydrogel without and with cells after 5 days. Here the experiment was performed by irradiating the light source of 405 nm at the light intensity of 150 mW/cm² for 8 seconds. The light integral value was 1200 mJ/cm². Figure 3.7(A) shows the gel degradation without a cell after 5 days. The blue color polygonal shape indicates the polymerized gel area. The polymerized cell-free gel had a slight decrease in its original area (100 µm × 100 µm), it was not a larger deformation. Figure 3.7(B) shows the gel degradation with cells after 5 days. The red color polygonal shape indicates the gel with cells that were present inside the photopolymerized hydrogel and the blue shape indicates the degraded gel area after 5 days. Here the cells were still present inside the photopolymerized hydrogel even after 5 days of observation. The degradation of gel with the presence of cell was significantly high compared to the degradation of gel without cell. The degradation of gel with the cell was significantly high compared to the original size (100 µm × 100 µm).

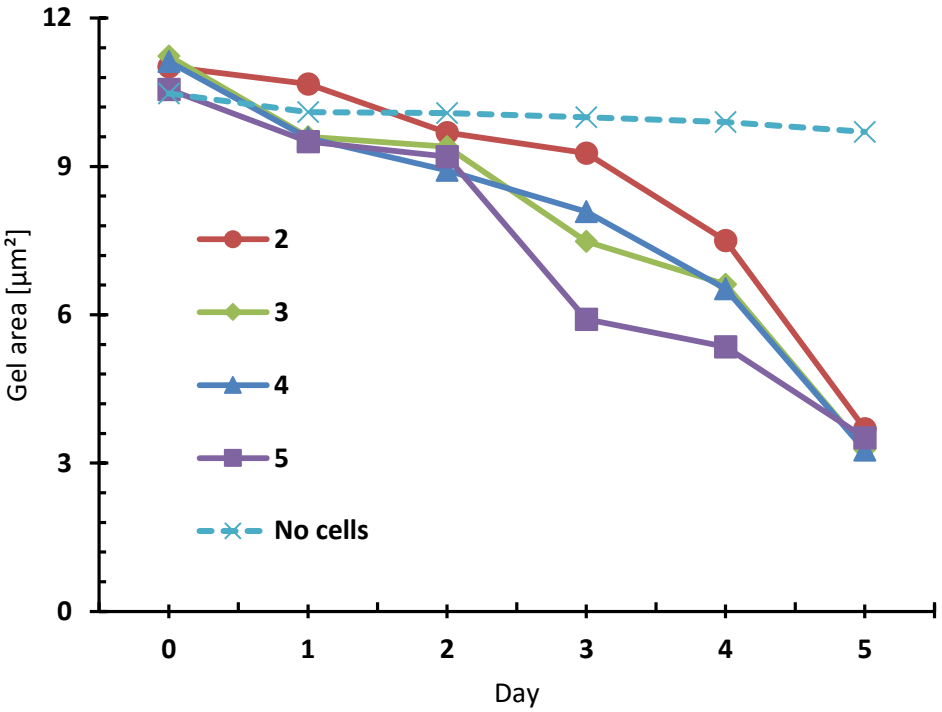

Figure 3.8 Degradation of gel area without/with cells.

Figure 3.8 shows the change in the gel area without and with cells. The X-axis provides the number of days and the Y-axis provides the polymerized gel area. For the light irradiation process, 100 μm × 100 μm square pattern was used. The dotted line represents the biodegradability of polymerized gel without a cell, and it shows the degradability rate was almost same and from day 0 to day 5. The others solid colors lines indicated biodegradability of gel with cell respectively with count of cells. In that observation, the degradation rate with cell was decreased slightly up to day 3 and there was dramatic decrease, and the gel area was $3.4 \pm 0.2 \times 10^3$ μm². That means, the cell-mediated was starts to degrade after some hours after the irradiation process. But in the case of cell-free gel, the degradation area at 5 day was 10×10^3 μm² approximately and it was the same as the original irradiation pattern dimension.

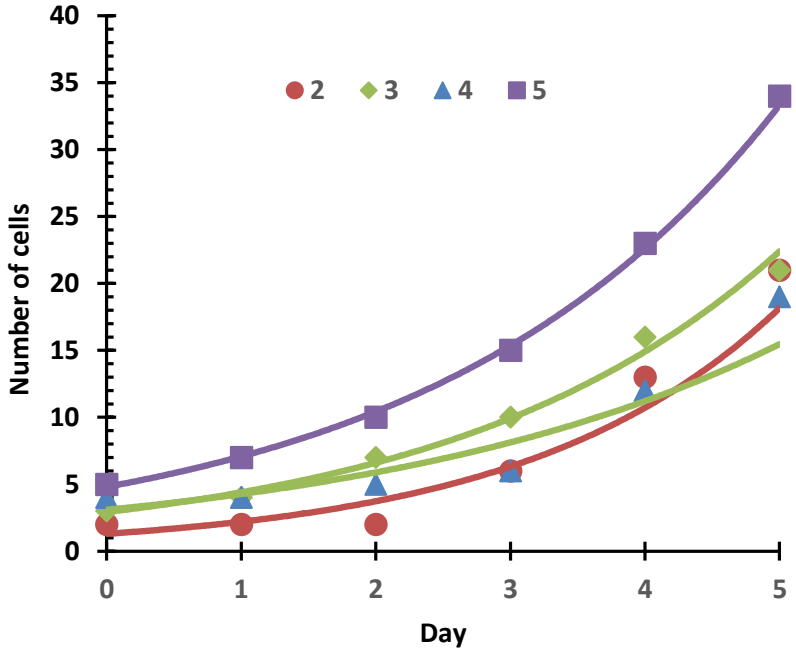

Figure 3.9 Cell proliferation of encapsulated cells.

Figure 3.9 shows the cell proliferation from day 0 to day 5 in the 5 % w/v of polymerized gel. The X-axis represents the number of days, and the Y-axis represents the cell counts. Here the cell proliferation was observed in the 100 µm × 100 µm square irradiated area that contains HeLa cells. The 2-5 series of lines shows the initial count of cells encapsulated in the polymerized region at day 0. On Day 5, the cell count increased by day by day. In that observation, the initial cell count in gel was 2 on Day 0 and the cell count increased approximately 16 on Day 5. And these exponential growth curves expressed the normal cell proliferation patterns.

3.3.4 Mobility of cells encapsulated in GelMA

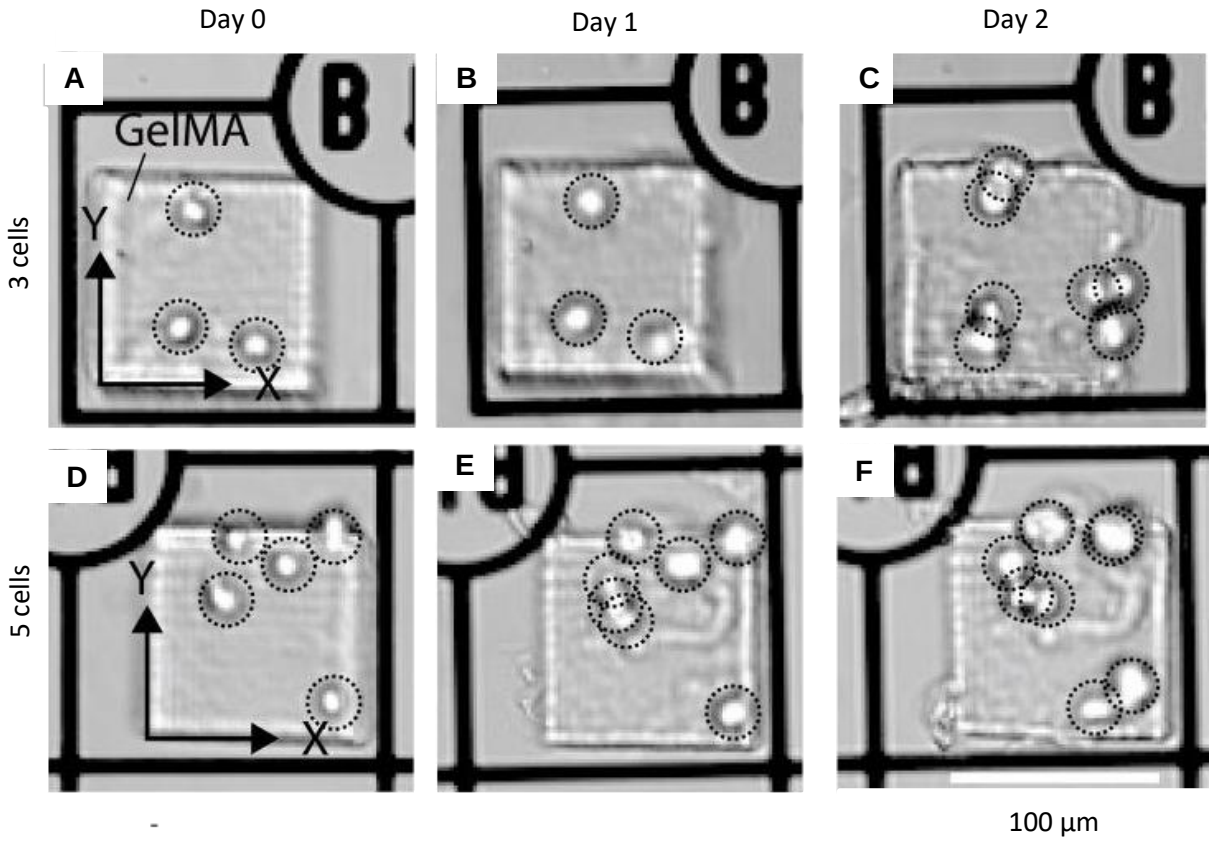

Figure 3.10 Time-lapse images of HeLa cells encapsulated in the GelMA hydrogel from Day 0 to Day2. (A-C) Observation of three cells on Day 0-2. (D-F) Observation of five cells on Day 0-2.

Figure 3.10(A-C) represents the time-lapse images of cells count of 2 HeLa cells encapsulated in a GelMA hydrogel from Day 0 to Day 3 respectively. Here the experiment was performed by irradiating the light source of 405 nm at the light intensity of 150 mW/cm² or 8 seconds. The light integral value was 1200 mJ/cm². The observation at Day 0, the initial cell count was 2 and at Day 1, the cell count was and there was a slight mobility observed. But on Day 3, the cell count was increased, and the cell mobility was also changed from its original position. And this mobility was indicated by the dotted black circle. Fig. 3.10(D-F) shows the same mobility of cells, but the cell count was 5 HeLa cells. From Day 2, the GelMA hydrogel starts to deform, and it leads to some biodegradation by the cells.

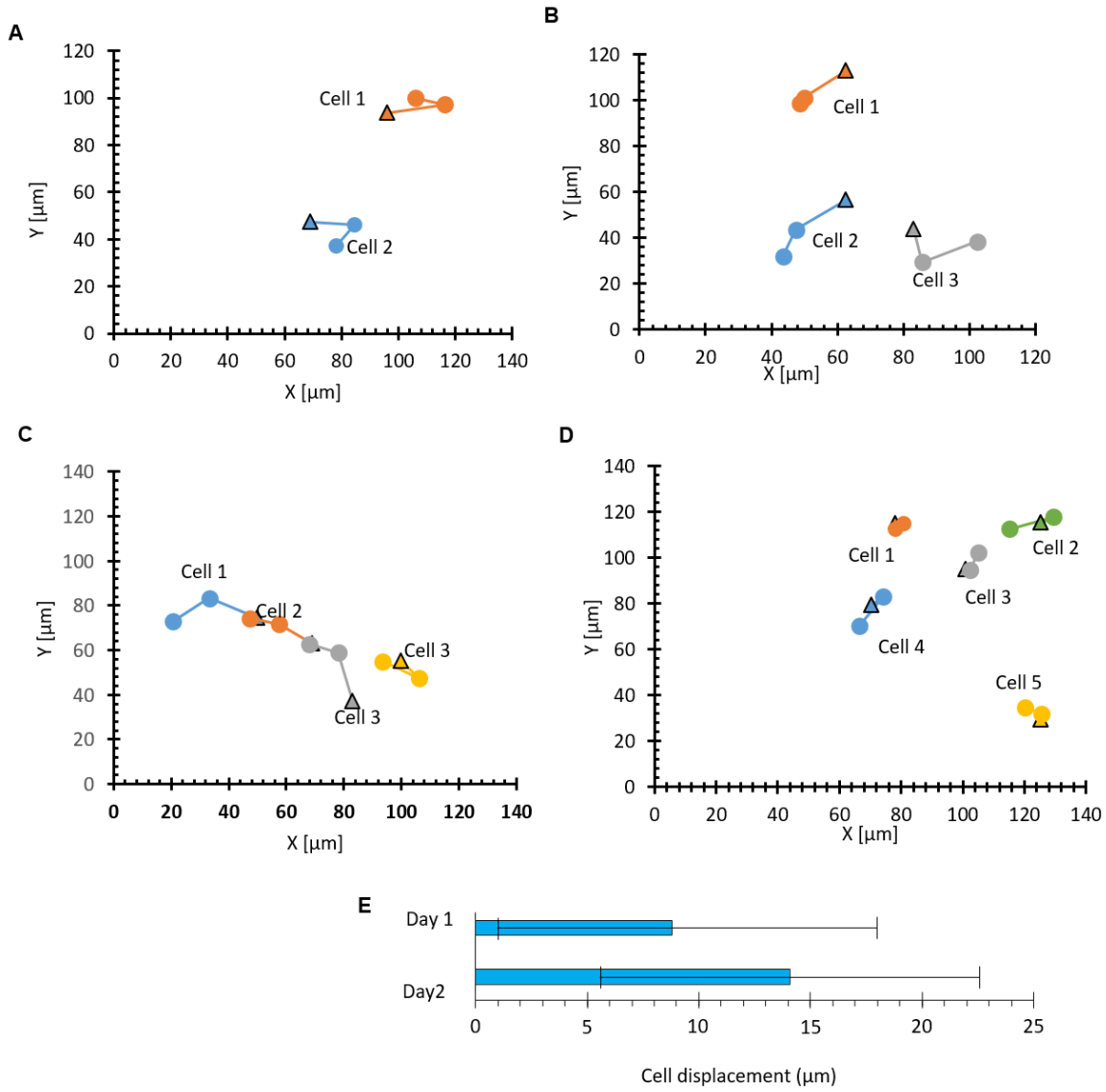

Figure 3.11 Mobility analysis of HeLa cells encapsulated in GelMA hydrogel.

Figure 3.11 shows mobility of HeLa cells encapsulated in GelMA hydrogel for 2 days. The X-axis and Y-axis represent the coordinates of the polymerization pattern that was used in the irradiation process. Figure 3.11(A-D) sections present the trajectories of cells with the initial counting from 2 to 5 respectively. In Fig. 3.11(A), the cell count was 2 and the mobility was traced and plotted. Figure 3.11(E) presents the cell displacement measurement from its origin (that means the position of cells at hydrogel after 0 min of irradiation process). In that observation, the cell displacement was 12.2 ±7.6 µm on Day 1 and on Day 2, the average displacement was 16.1 ± 9.6 µm. The cells were confined within the polymerized hydrogel. It proved the GelMA hydrogel stiffness, and it was the main cause in the reduction of cell movement or displacement inside the gel after the irradiation process occurred.

3.3.5 Recovery of unwanted cells in polymerized GelMA hydrogel

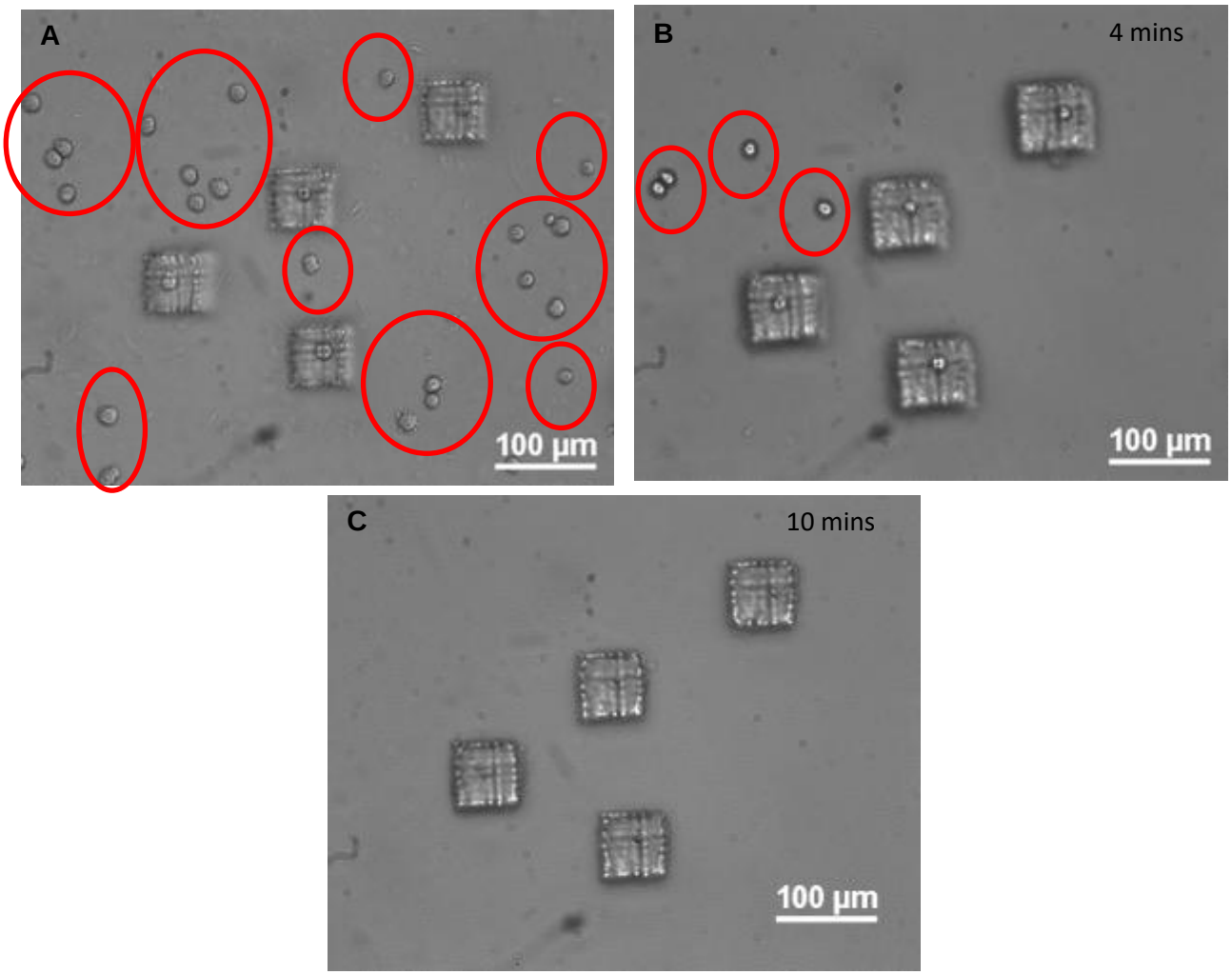

Figure 3.12 Microscopic view of cells encapsulated in GelMA photocured at 800 mJ/cm². (A) Immediately after irradiation (B) After 4 minutes (C) After 10 minutes of addition of trypsin. The red circles indicate the unwanted cells.

Here the unwanted cells were removed from the sample by using trypsin solution. The polymerization pattern was irradiated on the 5 % w/v GelMA hydrogel at 800 mJ/cm² for 6 seconds. And then the top coverslip was removed and placed at 50 mm Petri dish and enough trypsin was added. Figure 3.12(A) presents the microscopic view of irradiated cells encapsulated hydrogel that merged with trypsin solution at 0 minutes after the irradiation process. In that figure, some of the uncured cells were present in the hydrogel. Figure 3.12(B) shows the microscopic view of irradiated cell encapsulation after submerging them in 4 minutes. In this process, the unwanted cells started to peel from the sample. There were few cells present in the sample. After 10 minutes, the remaining uncured cells were recovered from the sample (Fig. 3.15(C)) and it shows the polymerized pattern remained present on the sample.

3.3.6 Collection of cured cells in polymerized GelMA hydrogel

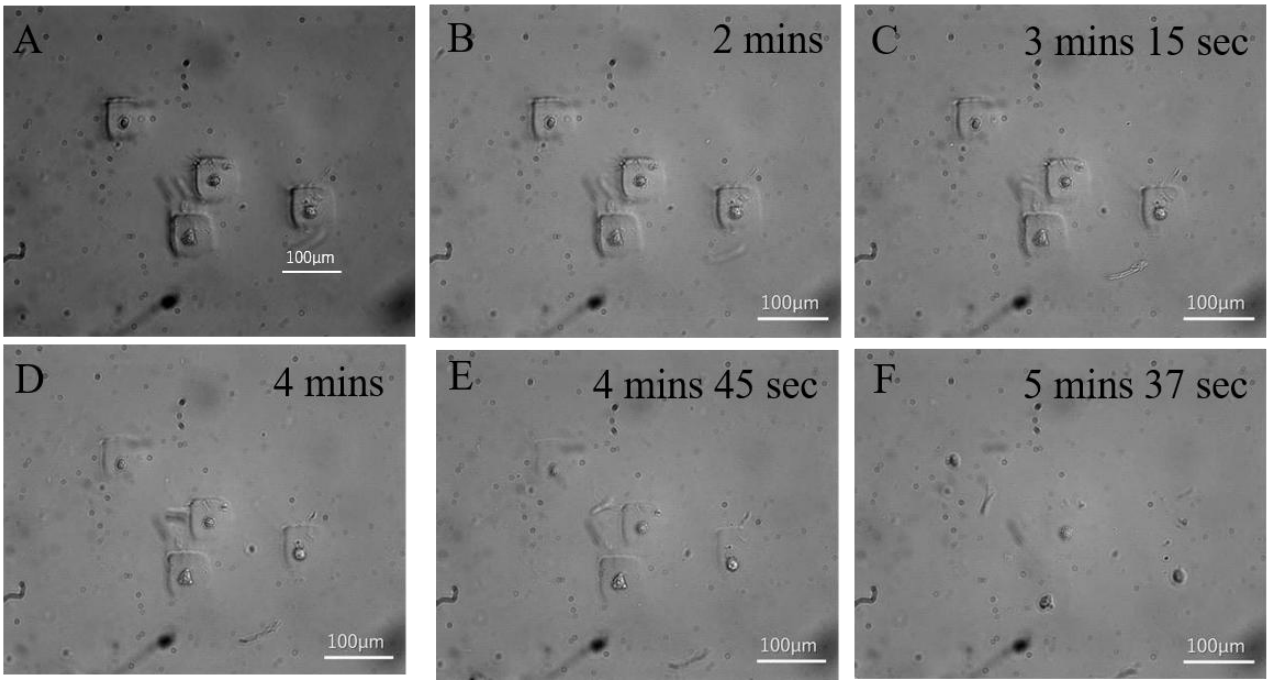

Figure 3.13 Degradation and collection of polymerized cells encapsulated in GelMA at 600 mJ/cm².Immediately after cured gel. (B) At 2 min 30 s, (C) At 3 min 15 s, (D) At 4 min, (E) At 4 min 45 s, (F) At 5 min 37 s after addition of trypsin. The red dished circle indicates the photopolymerized hydrogel that encapsulate the HeLa cells.

Here the cell suspension hydrogel was irradiated at 600 mJ/cm² for 4 seconds and the top coverslip was removed and washed with PBS to remove the uncured or unwanted cells from the sample. And then the sample was transferred in a 50 mm petri dish and filled with sufficient trypsin solution. Figure 3.13(A) shows the microscopic view of the irradiate pattern on the sample after polymerization. The sample was observed in a microscope up to the irradiate pattern dissolved in trypsin solution. Figure 3.13(B)-3.13(F) represents the dissolution of an irradiated pattern in the solution at a time interval of 2 minutes 30 seconds, 3 minutes 15 seconds, 4 minutes, 4 minutes 45 seconds and 5 minutes 37 minutes respectively. In this time interval period, the irradiation patterns slowly dissolved in the dish and it was indicated by a dotted red circle. At 600 mJ/cm² co ndition, the total of 5 minutes 37 seconds required to dissolve the irradiate pattern in the trypsin solution and the cells were released from the GelMA hydrogel after 5 minutes 37 seconds of recovery treatment.

Only in 150 mW/cm² irradiance, the GelMA degradation was achieved in 5 minutes 37 seconds. The experiments was conducted based on to find out the GelMA degradation in trypsin at various light integral values with differences in irradiation energy and time.

For that experiments, the irradiation value with various light integral value was mentioned below table 3.1

Table 3.1 Experimental parameters of hydrogel degradation

Intensity (mW/cm^2)	Light integral value (mJ/cm^2)	Photopolymerization time (sec)
100	500 / 1000 / 1500	5 / 10 / 15
240	1200 / 2400 / 3600	5 / 10 / 15
340	1700 / 3400 / 5100	5 / 10 / 15

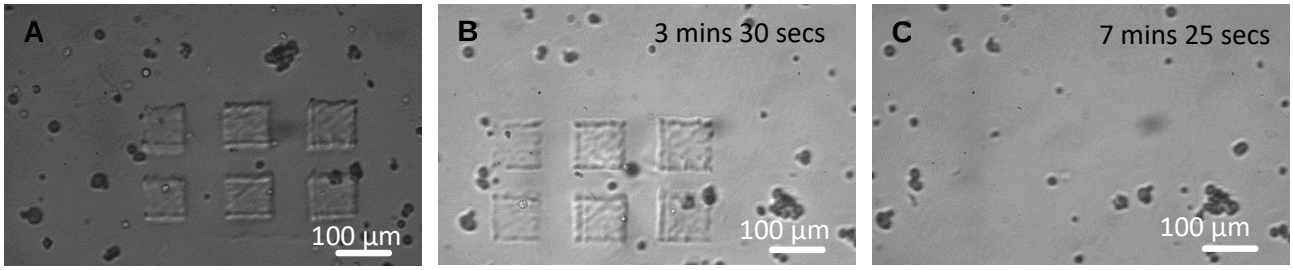

Figure 3.14 Degradation and collection of polymerized cells encapsulated in GelMA at 1000 mJ/cm^2.Immediately after cured gel. (B) At 3 mins 30 s, (C) At 7 mins 25 s after addition of trypsin. The red circle indicates the photopolymerized hydrogel

Fig 3.14(A) shows the microscopic view of the irradiate pattern on the sample at 1000 mJ/cm^2 in duration of 10 seconds. The sample was observed in a microscope up to the irradiate pattern dissolved in trypsin solution. Figure 3.14(B)-3.14(C) represents the dissolution of an irradiated pattern in the solution at a time interval of 3 minutes 30 seconds and 7 minutes 25 minutes respectively. In this time interval period, the irradiation patterns slowly dissolved in the dish, and it was indicated by a red circle.

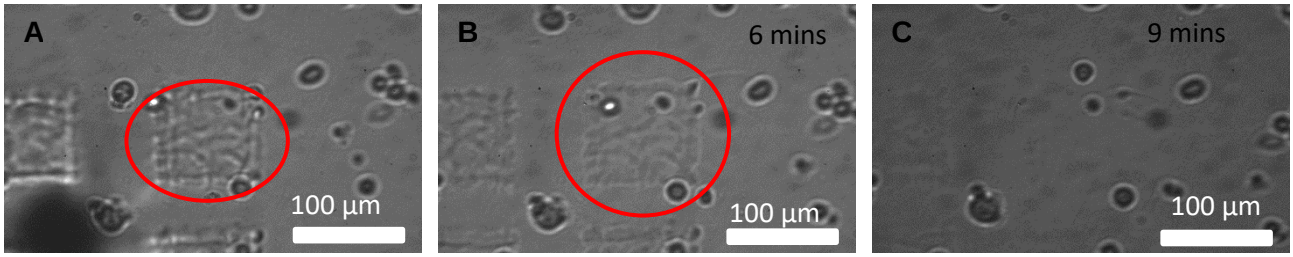

Figure 3.15 Degradation and collection of polymerized cells encapsulated in GelMA at 1500 mJ/cm².Immediately after cured gel. (B) At 6 mins, (C) At 9 mins after addition of trypsin. The red circle indicates the photopolymerized hydrogel

Fig 3.15(A) shows the microscopic view of the irradiate pattern on the sample at 1500 mJ/cm² in duration of 15 seconds. The sample was observed in a microscope up to the irradiate pattern dissolved in trypsin solution. Figure 3.15(B)-3.15(C) represents the dissolution of an irradiated pattern in the solution at a time interval of 6 minutes and 9 minutes. In this time interval period, the irradiation patterns slowly dissolved in the dish and it was indicated by a red circle.

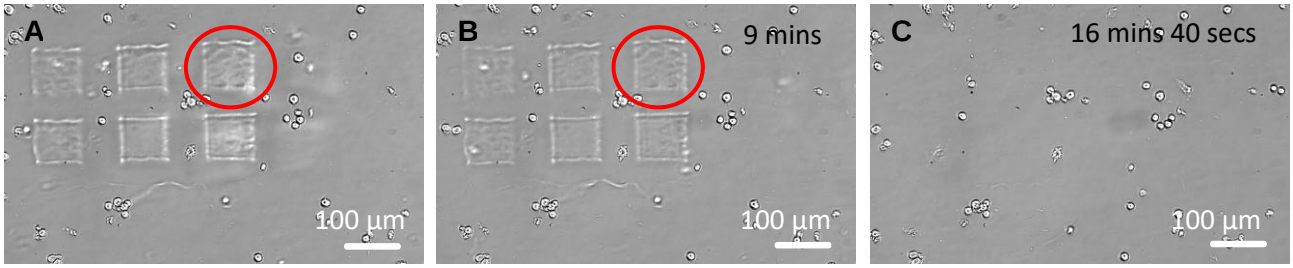

Figure 3.16 Degradation and collection of polymerized cells encapsulated in GelMA at 2400 mJ/cm².Immediately after cured gel. (B) At 9 mins, (C) At 16 mins 40 secs after addition of trypsin. The red circle indicates the photopolymerized hydrogel

Fig 3.16(A) shows the microscopic view of the irradiate pattern on the sample at 2400 mJ/cm² in duration of 10 seconds. The sample was observed in a microscope up to the irradiate pattern dissolved in trypsin solution. Figure 3.16(B)-3.16(C) represents the dissolution of an irradiated pattern in the solution at a time interval of 9 minutes and 16 minutes 40 seconds. In this time interval period, the irradiation patterns slowly dissolved in the dish and it was indicated by a red circle.

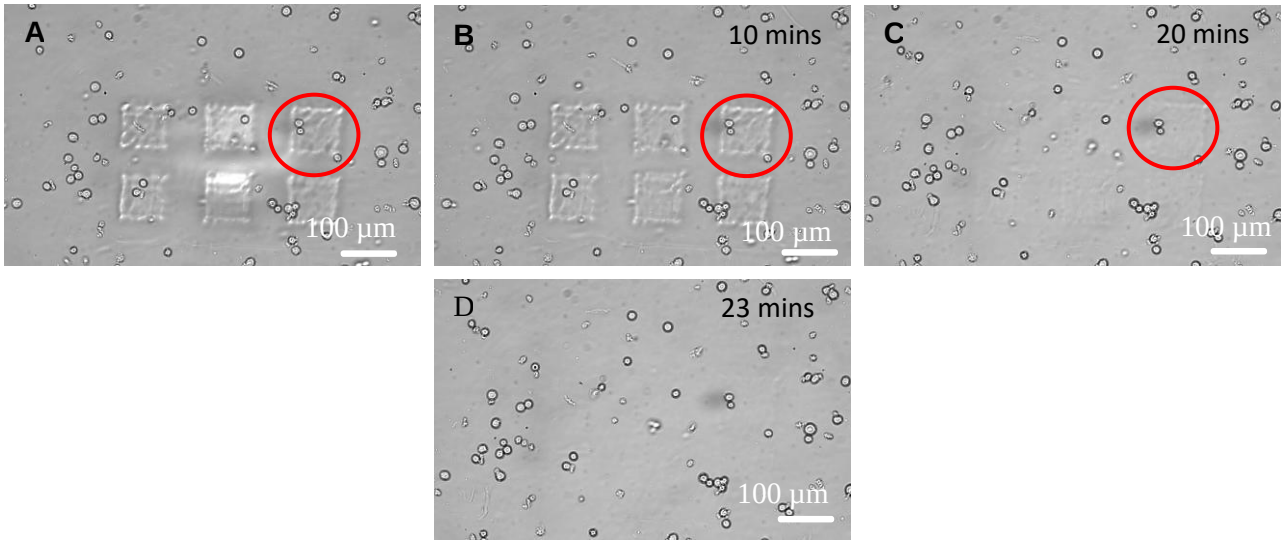

Figure 3.17 Degradation and collection of polymerized cells encapsulated in GelMA at 3600 mJ/cm².Immediately after cured gel. (B) At 10 mins, (C) At 20 mins, (D) 23 mins after addition of trypsin. The red circle indicates the photopolymerized hydrogel

Fig 3.17(A) shows the microscopic view of the irradiate pattern on the sample at 3600 mJ/cm² in duration of 15 seconds. The sample was observed in a microscope up to the irradiate pattern dissolved in trypsin solution. Figure 3.16(B)-3.16(D) represents the dissolution of an irradiated pattern in the solution at a time interval of 10 minutes, 20 minutes and 23 minutes. In this time interval period, the irradiation patterns slowly dissolved in the dish, and it was indicated by a red circle.

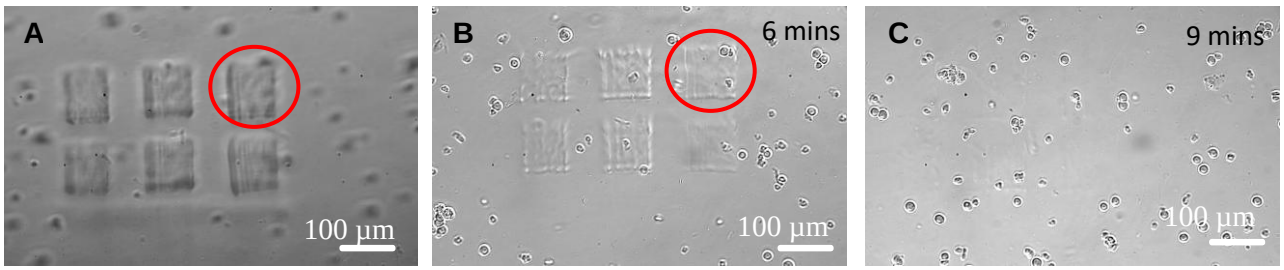

Figure 3.18 Degradation and collection of polymerized cells encapsulated in GelMA at 1700 mJ/cm².Immediately after cured gel. (B) At 6 mins, (C) At 9 mins after addition of trypsin. The red circle indicates the photopolymerized hydrogel

Fig 3.18(A) shows the microscopic view of the irradiate pattern on the sample at 1700 mJ/cm² in duration of 5 seconds. The sample was observed in a microscope up to the irradiate pattern dissolved in trypsin solution. Figure 3.18(B)-3.18(C) represents the dissolution of an irradiated pattern in the solution at a time interval of 6 minutes and 9 minutes. In this time interval period, the irradiation patterns slowly dissolved in the dish and it was indicated by a red circle.

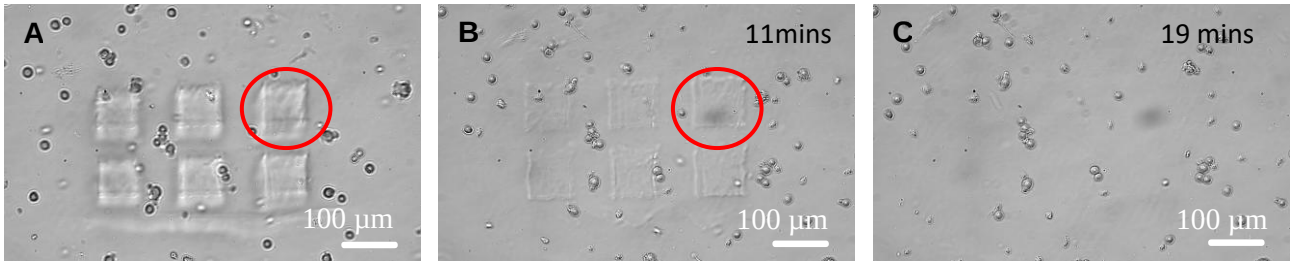

Figure 3.19 Degradation and collection of polymerized cells encapsulated in GelMA at 3400 mJ/cm².Immediately after cured gel. (B) At 11 mins, (C) At 19 mins after addition of trypsin. The red circle indicates the photopolymerized hydrogel

Fig 3.19(A) shows the microscopic view of the irradiate pattern on the sample at 3400 mJ/cm² in duration of 10 seconds. The sample was observed in a microscope up to the irradiate pattern dissolved in trypsin solution. Figure 3.19(B)-3.19(C) represents the dissolution of an irradiated pattern in the solution at a time interval of 11 minutes and 19 minutes. In this time interval period, the irradiation patterns slowly dissolved in the dish and it was indicated by a red circle.

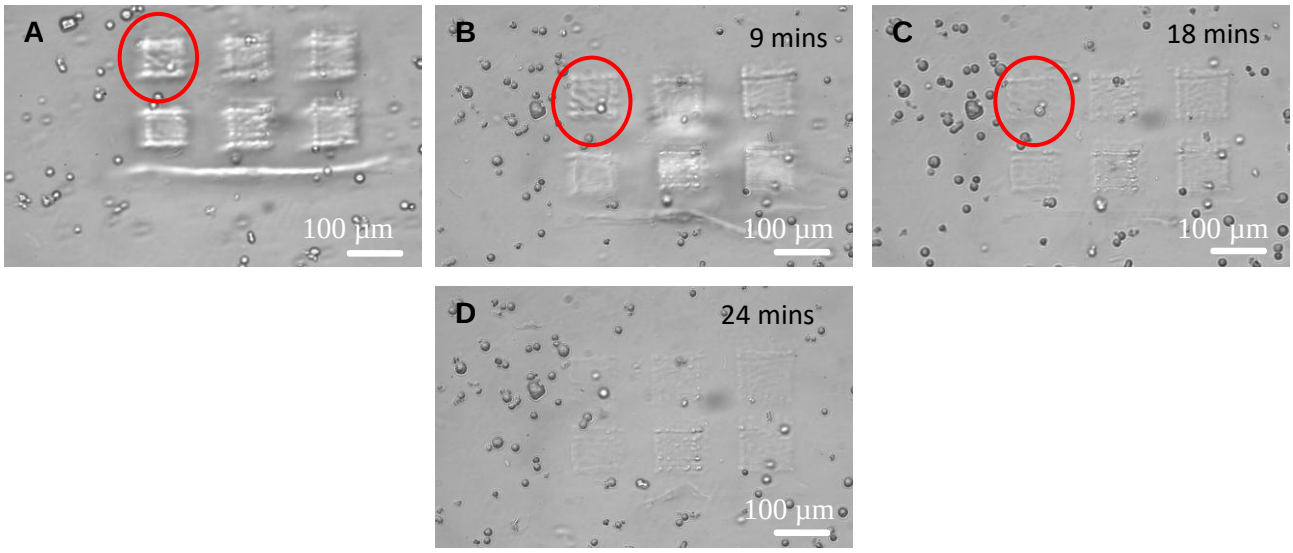

Figure 3.20 Degradation and collection of polymerized cells encapsulated in GelMA at 5100 mJ/cm².Immediately after cured gel. (B) At 9 mins, (C) At 18 mins and (D) 24 mins after addition of trypsin. The red circle indicates the photopolymerized hydrogel

Fig 3.20(A) shows the microscopic view of the irradiate pattern on the sample at 3400 mJ/cm² in duration of 10 seconds. The sample was observed in a microscope up to the irradiate pattern dissolved in trypsin solution. Figure 3.20(B)-3.20(D) represents the dissolution of an irradiated pattern in the solution at a time interval of 9 minutes, 18 minutes and 24 minutes. In this time interval period, the irradiation patterns slowly dissolved in the dish, and it was indicated by a red circle. Even

after 24 minutes, some of the polymerized GelMA patterns were not fully dissolve in trypsin. Due to the uniformity in formation of pattern, the degradation rate was changed in one polymerized pattern to another pattern.

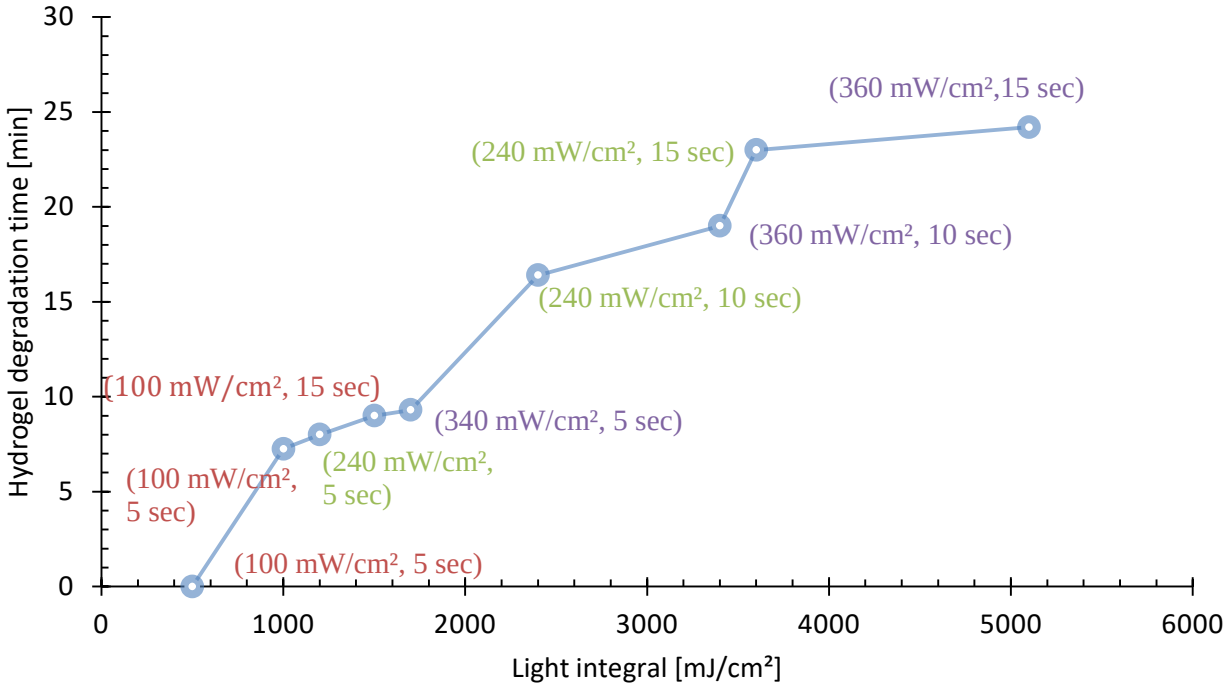

Figure 3.21 Degradation of polymerized GelMA hydrogel at various light integral value

Figure 3.21 shows the degradation of polymerized GelMA hydrogel at various light integral values. At 500 mJ/cm², the photopolymerization pattern was not formed on the sample because of the lower integral value, and the hydrogel degradation was considered 0 minutes. Here the polymerized hydrogel degradation time was increased by the light integral value. Up to 1800 mJ/cm² light integral value, the degradation time of hydrogel was within 10 minutes. But in 5100 mJ/cm², the degradation time was reached up to 24 minutes. The combination of longer exposure time and higher light intensity, the light integral value was higher. The polymerization was strong which led to increased GelMA resistance to enzymatic degradation. To optimize the degradation time and light energy, the formation of a polymerized pattern was controlled that can be useful in hydrogel degradation based on application.

This study chose GelMA over PEGDA due to its superior degradability with trypsin, as the degradation of PEGDA is more difficult[38], [40], [68]. PEGDA hydrogels primarily degrade via hydrolysis of the ester bonds, with degradation occurring rapidly at an acidic or alkaline PH. This

property of PEGDA has made it changeling to collect the live cells. In contrast, GelMA hydrogels degraded more readily than the PEGDA hydrogels under mild enzymatic conditions. The hydrolytic degradation of PEGDA is a slow process compared to the enzymatic degradation of GelMA. This approach takes advantage of the different properties inside and outside the GelMA hydrogels for targeted cell collection. The results confirm that prolonged expose to light increase the dissolution time of GelMA hydrogels, which is consistent with the previous reports on the proteolytic degradation of GelMA hydrogels[65], [66]

3.4 Conclusion

In chapter 3, this study proves the cell encapsulation in GelMA is better compared with PEGDA hydrogel. The experiments were conducted in different integrated light intensity of 1000 mJ/cm²-2000 mJ/cm², the dimensions of polymerized pattern on the hydrogel, viability of polymerized cells encapsulated and its behavior over the period was studied. From these studies, the collection of cells in 5 % w/v polymerized GelMA hydrogel were superior within 2 days and the polymerization patterns were stable and it started to degrade after 2 days. Using the property of biodegradation of GelMA hydrogel, the cell proliferation was good even up to 5 days. The cells encapsulated in the polymerized hydrogel region remained inside due to its property and the average displacement of cells encapsulated in polymerized gel was less than 20 µm from the original position after the irradiation process.

The two kinds of experiments were performed to recover the uncured and cured cells from the sample. The first method demonstrated the recovery of uncured cells from the top coverslip at experimental condition of 800 mJ/cm² and it was treated with trypsin medium. In this process, most of the uncured cells were peeled from the sample after 4 minutes. After 10 minutes, the encapsulated cells remained in the sample and the total uncured or unwanted cells were completely peeled off from the sample. In the other approach, the encapsulated cells in gel were recovered. In this method, the cell suspension was irradiated at 600 mJ/cm² and remove the top coverslip. And then it was washed with PBS to remove the unwanted cells and treated with trypsin. The cured cells were collected after 4 minutes 37 seconds. The experiments were conducted at various light integral values. From these experiments, 100 mW/cm² and 10 seconds, the dissolution time is 7 minutes 25 seconds and 340 mW/cm² and 15 seconds, the dissolution time extends to 24 minutes 20 seconds. For effective GelMA photopolymerization and extending its resistance to trypsin dissolution, the higher light intensity and

longer exposure time was necessary. To efficient cell recovery method, the integration of automated irradiation setup and cell detection method were used.

Chapter 4 Single-cell encapsulation using LCD screen based printer and behavior of cells encapsulated in GelMA.

4.1 Introduction

In generally, there are two types of UV-induced polymerization processes used. One is a DMD based light cured [69] and the other is a liquid crystal display (LCD) light cured [70]. However, in both methods, the wavelength is almost similar and both systems are able to process the optical patterns while performing photopolymerization. The main limitation of the DMD based photopolymerization process is to irradiate the small region per cycle. For example, the area of 1.2 mm × 0.9 mm was photocured per single shot. But in the LCD based photocuring setup, the larger area is covered in a single shot. The light intensity of LCD based photocuring is low compared to the DMD based photocuring [69], [71]. For the photopolymerization process, the light intensity is an important parameter for curing the hydrogel. In the LCD based photocuring setup, the amount of initiator or the exposure time was increased to cure the hydrogel.

In the LCD based photopolymerization process, the liquid crystal display is used as an imaging system. When applying electric charges to the liquid crystal, it will change the molecular arrangement and allow light passing through the LCD screen. In recent days, the resolution is very high. While switching the electric field, the small number of crystal molecules can't rearrange, and it leads to weak light leakage. The precision of LCD based polymerization systems is lesser to DMD based systems [72].

In this chapter, the LCD based photopolymerization setup is developed. The Phrozen Sonic mini 8KS LCD printer is remodified and the photopolymerization parameters are set up. Here, the formation of cell encapsulation and the behavior of encapsulated cells are observed. This study introduces a significantly enhanced approach utilizing an LCD screen of a 3D printer for efficient and user-friendly single-cell encapsulation within hydrogels.

4.2 Methods

4.2.1 Working flow of single-cell encapsulation using LCD based system

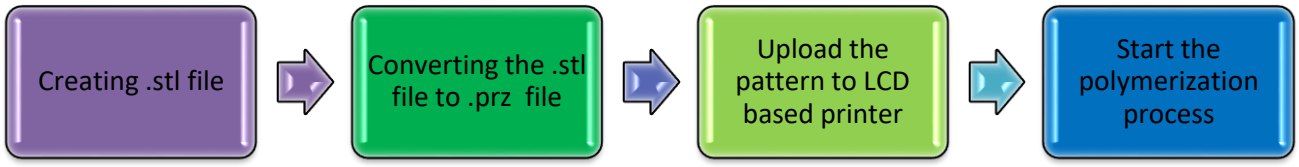

Figure 4.1 Working flow of single-cell encapsulation using LCD based system.

Figure 4.1 illustrates the working flow of a single-cell encapsulation system using an LCD screen-based 3D printer. At first, the photopolymerization pattern was created by using CAD software and the pattern file format was .stl file. In this experiment, the 3D printer requires the specific file format. For that required format, the .stl file was uploaded into the specific software and saved as .prz file format. The .prz file contains the information of pattern position on the LCD screen and the photopolymerization process time. After converting it into .prz file, the file was uploaded to the 3D printer via USB flash drive. And then the process was started by commanding the start function.

4.2.2 Working experimental setup

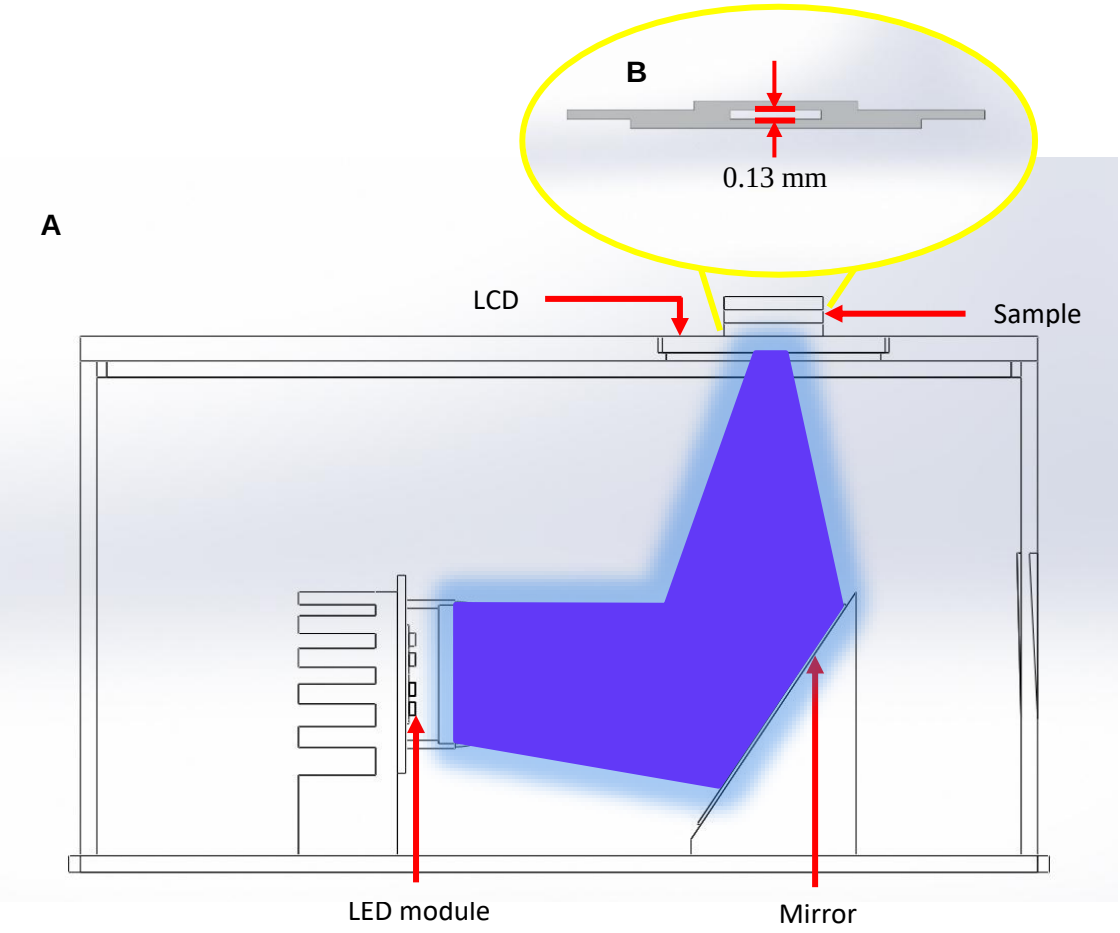

Figure 4.2 Single-cell encapsulation of LCD screen based 3D printer.

Figure 4.2 illustrates the re-modify version of single-cell encapsulation of LCD screen based sonic mini 8 K 3D printer. This printer has a 7.1-inch mono LCD screen with larger functional area and it has ultra-high resolution of 22 µm that means 1152 pixel per inch (ppi) and the linear projection LED module has improved light uniformity. This printer has a specific microcontroller, and it's operated by Phrozen OS. To form the pattern on the LCD screen, the CHITUBOX software was used to create the required code format (.prz file format). The data was transferred by USB flash drive only. For the cell encapsulation system, the motorized stage (Z-axis) was removed for easy operation. Otherwise, the offset value for the Z-axis wants to provide at the time of pattern formation. A LED module was used as a light source. And then the sample was directly placed on the top of the LCD screen.

In working of cell encapsulation, the polymerization pattern was uploaded and the LED module emits the light source. The wavelength of the UV-LED light source was 405nm. The mirror was used

to reflect the light and hit the bottom side of the LCD screen. The polymerized pattern was formed on the LCD screen based on the code and the light source was passed through the LCD formed pattern. Here the light intensity of the system was 2.5 mW/cm².

The wavelength of the irradiation light plays an important role in affecting the photopolymerization characteristics of GelMA such as absorption and depth of penetration, cross-link efficiency and spatial resolution. In the case of depth of penetration, the longer wavelength light source was used for deep penetration compared to the shorter wavelength.

4.2.3 Creation of photopolymerization pattern

For performing the polymerization process, the polymerized pattern required .prz file format. At first, the required pattern model was designed in 3D CAD software and saved as a .stl file format (Fig 4.3(A)). And then the .stl file was uploaded in the CHITUBOX software. In the software, the pattern was sliced and provided the required parameters such as layer thickness and polymerization time. After providing the required data, the file was saved as .prz file format (Fig 4.3(B)).

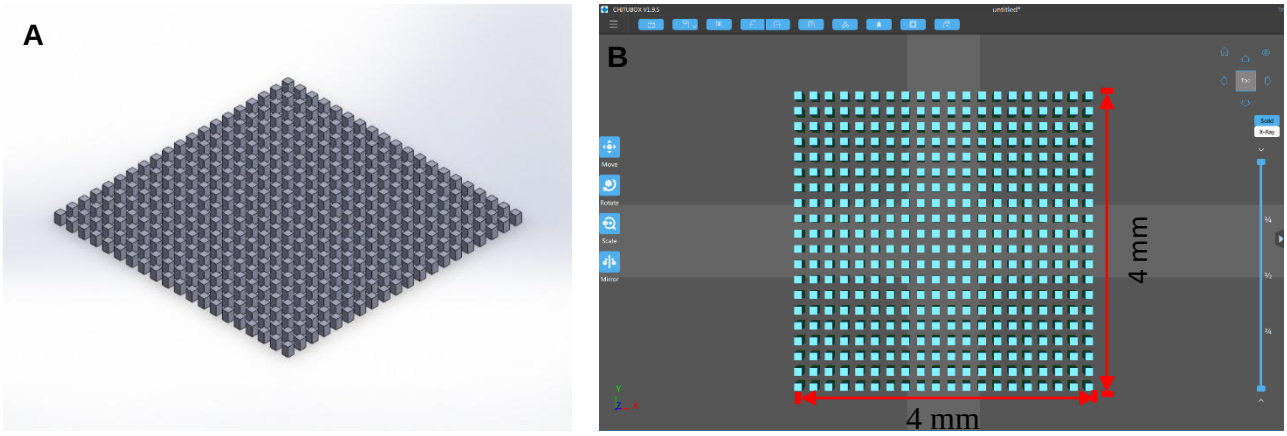

Figure 4.3 Creation of polymerization pattern. (A) .stl file of 4 × 4 mm pattern with each box of 100 × 100 µm size. (B) Top view of polymerization pattern on the LCD screen in the software and converted into .prz file format.

4.2.4 Materials

In the centrifuge tube, add 2 ml of PBS and add 100 mg of GelMA (60% degree of substitution, gel strength of 90-110 g Bloom, Sigma Aldrich Co Ltd.) which has a photocurable resin oligomer in that centrifuge tube. Using a vortex mixer, mix the solution. The concentration of GelMA was 5% w/v in PBS. Add 10 mg of LAP (Lithium Phenyl (2, 4, 6-thrmethey-benzoyl) phosphinate, Tokyo

Chemical Industry Co Ltd.) in that centrifuge tube. Again, using a vortex mixer, mix the solution properly. Finally, the concentration was 0.5 % w/v LAP and 5 % w/v GelMA in PBS. To avoid contact with the outer environment, the tube was covered with aluminum foil and kept in a dark area for 3-4 hours.

In culture medium (MEM, 10 % of FBS + 1 % of Pen Strep, Gibco Ltd.), HeLa cells (RCB0007, RIKEN BRC) were cultured on the polystyrene petri dish. From the culture dish, the medium was removed and washed with 3 ml of PBS and again drained. Then transfer 3 ml of trypsin (0.25 % Trypsin EDTA (1X), Gibco Ltd.) on the petri dish and incubate for 4 minutes in an incubator. Mix 3 ml of MEM to the trypsinized cells solution and transfer the mixed solution in a centrifuge tube. At 1500 rpm, perform centrifuges for 3 minutes and remove supernatant from the tube. Finally the cells were suspended with Prepared GelMA hydrogel.

In this experiment, the base coverslip was coated with PDMS and it prevented the gel adhesion while removing the top coverslip after the polymerization process.

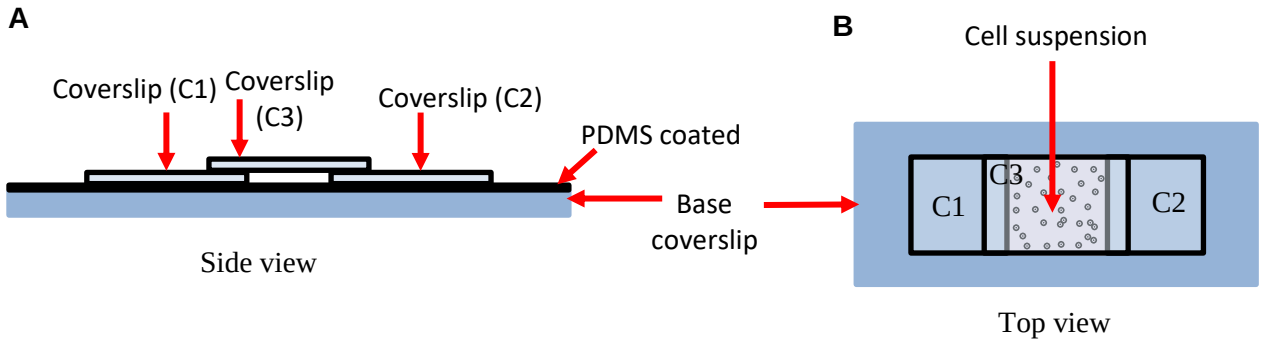

Figure 4.4 Schematic diagram of a specimen. (A)Side view of sample substrate. (B) Top view of sample substrate holds cell suspension.

Figure 4.4 shows the schematic diagram of a specimen. Take the base circular coverslip with dimension of 90 mm and the thickness of 0.145 mm and coated with PDMS. The coating process was carried out by 5 sec slope of 500 rpm, increased 60 sec slope of 4500 rpm and decreased to 10 sec slope of 500 rpm. Kept the coated base coverslip on the hot plate at 80º c for 2 hours. And then place the two coverslips (C1 and C2) (18 mm × 18mm with thickness of 0.13 mm-0.17 mm, Matsunami Glass) at top of the base glass slide with some distance between two cover glass slips. Finally place the coverslip (C3) at the top of C1 and C2 coverslips. And by arranging the glass slips (Fig 4.4(A)), the slit was formed in between the base glass slide and coverslip (C3). The required amount of cell

suspension was transferred to that slit (Fig 4.4(B)) and kept in the motorized stage to perform the photopolymerization process.

4.3 Result and discussion

4.3.1 Formation of photopolymerization pattern on LCD screen

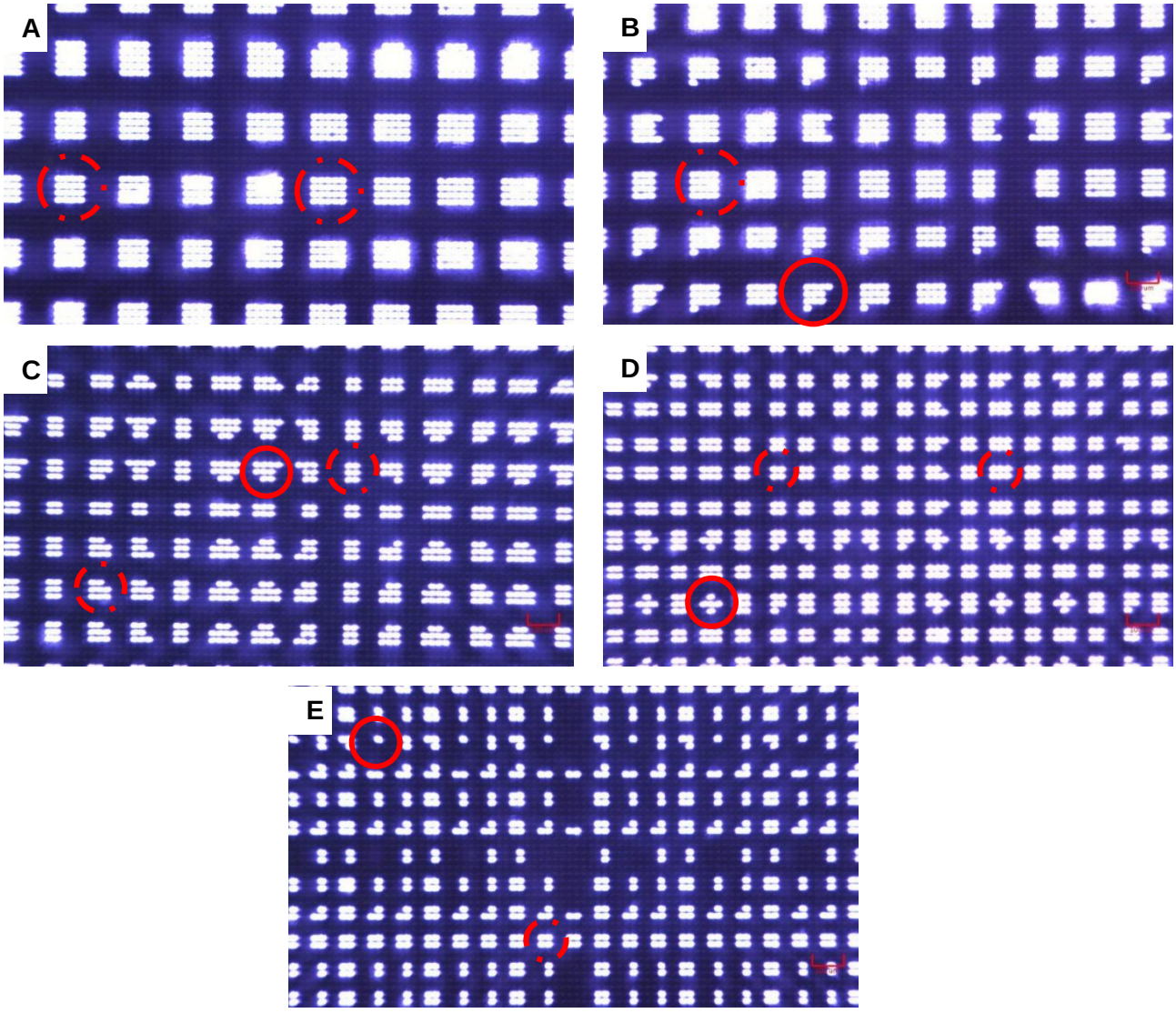

Figure 4.5 Polymerization pattern formation on LCD screen. Each box dimension of (A) 100 µm (B) 88 µm (C) 66 µm (D) 50 µm (E) 44 µm.

Figure 4.5 shows the formation of a photopolymerization pattern on the LCD screen. When polymerized the hydrogel by using common photopolymerization pattern, the height was almost same in all the boxes, but the width was changed. If the photopolymer pattern has 10 columns, some column has less width in the boxes, and some has high in the boxes. For understanding the width difference

in the columns, the photopolymerized was display on the LCD screen and observed by the microscope. In the Fig. 4.5(A), each box dimension of the photopolymerization pattern was 100 µm and the distance between the neighboring boxes were the same as 100 µm. The dotted circle represents the pixels of each pattern square box. In some of the columns, the boxes have five pixels in row and the other columns have only four pixels in that row. In the Fig. 4.5(B), each box dimension of polymerized pattern 88 µm and the formation of pattern in some columns has four pixels and others has three pixels. The solid circle represents the irregular formation of polymerization pattern boxes. Figure 4.5(C)-4.5(D) shows the same condition occurred. Here the pixels in some columns were changed and the irregular boxes were formed. But in the pattern 44 µm (Fig. 4.5(E)), the irregular boxes were formed and the one of the row and column boxes were not formed almost.

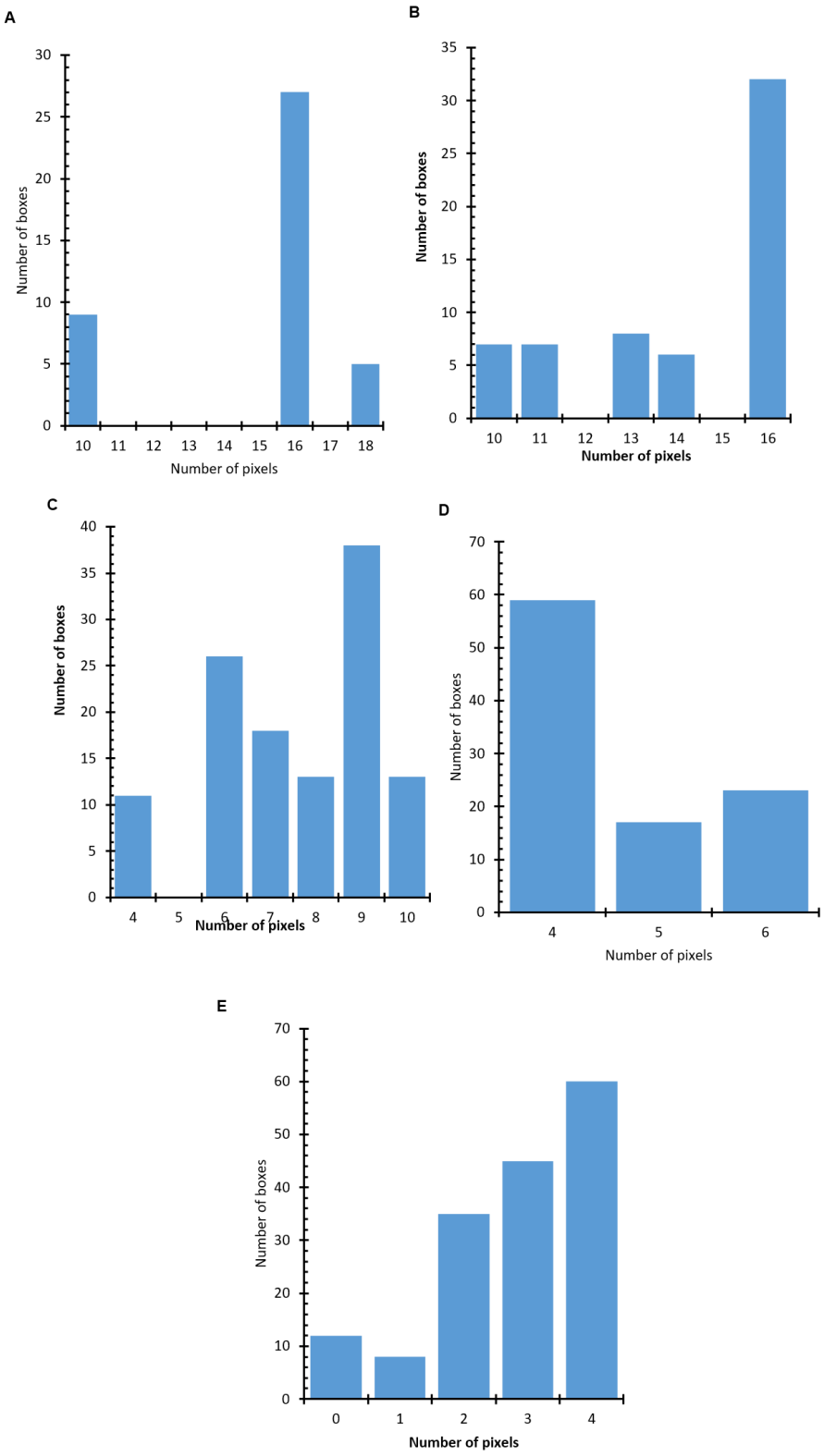

Figure 4.6 Histogram of number of pixels of each box in a pattern. (A) 100 µm (B) 88 µm (C) 66 µm (D) 50 µm and (E) 44 µm.

Figure 4.6 shows the histogram of the number of pixels of each box in a photopolymerization pattern. The X-axis represents the number of pixels in each box in the polymerization pattern and the Y-axis represents the number of boxes formed on the LCD screen. To generate photopolymerization patterns of 88 µm, 66 µm, and 44 µm on the sample using an LCD screen, the specific number of pixels for each pattern based on the corresponding pixel size in micrometers based on the magnification and resolution of the setup. For 88 µm, 66 µm and 44 µm patterns, the pattern should be represented by 16, 9 and 4 pixels per box on the LCD screen respectively. In the case of 100 µm and 50 µm pattern, the pattern should be represented by approximately 20 and 5 pixels per box. In the 50 µm pattern, the formation of pixels in the width of the boxes were not the same and it was changing by changing the alternative column. In general, the diameter of HeLa cells was 20-40 µm. for cell encapsulation, the 50 µm pattern is sufficient but the pixels were missing on the LCD screen. Meanwhile in the 100 µm pattern formation in the LCD, the missing of pixels were low compared to all other patterns and the dimensions of the photopolymerization pattern was almost same compared to original design that was discussed in upcoming section. The main reason for malfunction of pixels forming on the LCD was caused because of electrical issues. Due to these issues, the certain pixels were to fail or not receive the proper signal and it leads to dark or discolored spots on the LCD screen.

4.3.2 Formation of photopolymerization pattern on GelMA hydrogel

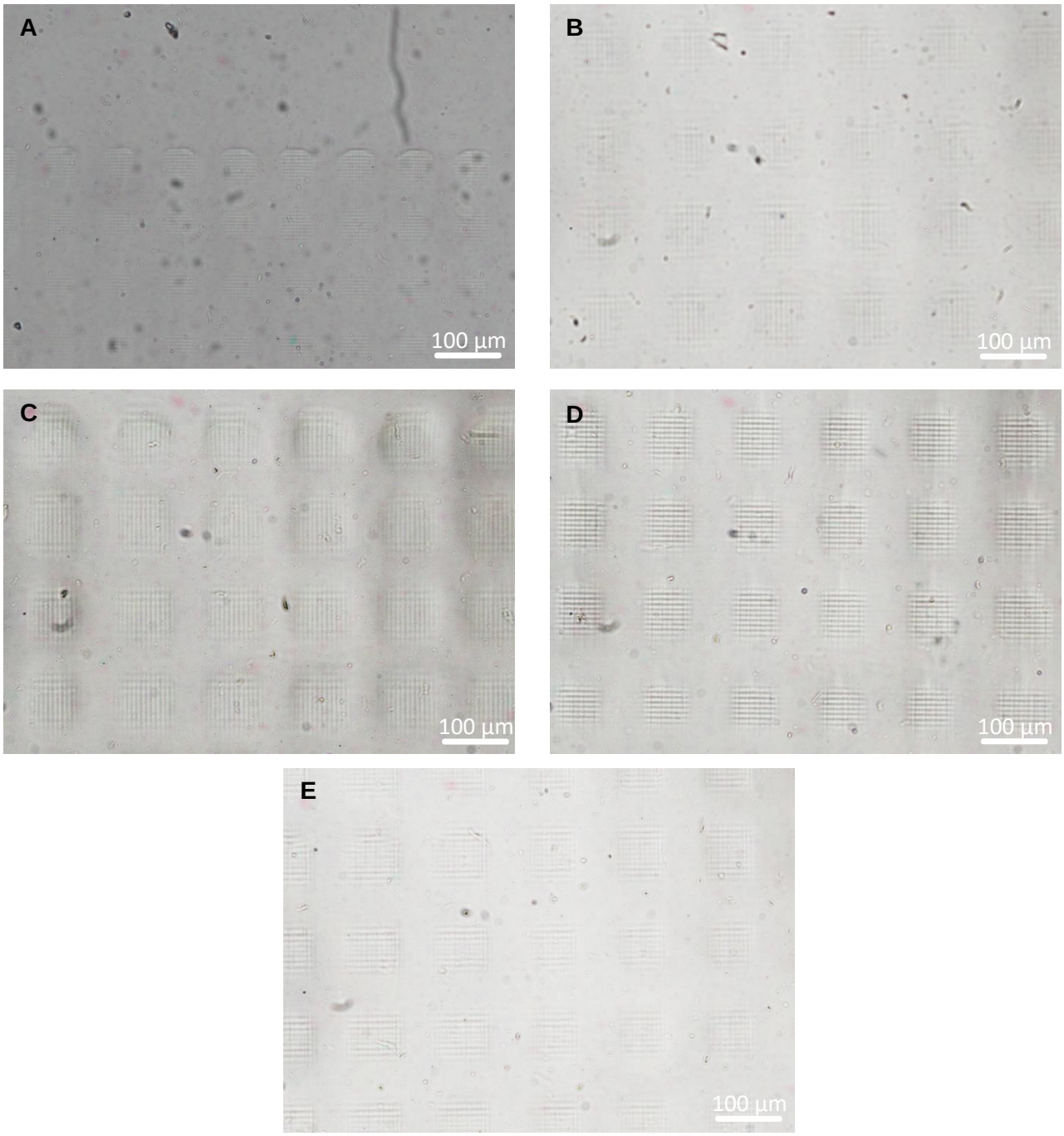

Figure 4.7 Microscopic images of photopolymerization pattern on GelMA hydrogel. (A) 200 s, (B) 250 s, (C) 300 s, (D) 350 s and (E) 400s.

Figure 4.7 shows the microscopic images of polymerized GelMA of concentration of 5 % w/v. The prepared polymerized gel was transferred into the sample and placed on top of the LCD based printer. The converted .prz file was uploaded to the printer and the LED module was emitted on the sample. In this polymerization process, the exposure time that means the light irradiation time reacted

with the sample is directly proportional to the light integral. Figure 4.7(A)-4.7(E) exposed to view the polymerized pattern on the GelMA hydrogel which was polymerized at the exposure time of 200 to 400 seconds with varying the light integral value from 500 mJ/cm² to 1000 mJ/cm². At 5 % w/v concentration of GelMA hydrogel, the polymerized hydrogel areas were transparent even after the polymerization process happened. Also, the cells which were encapsulated in the polymerized region were visible.

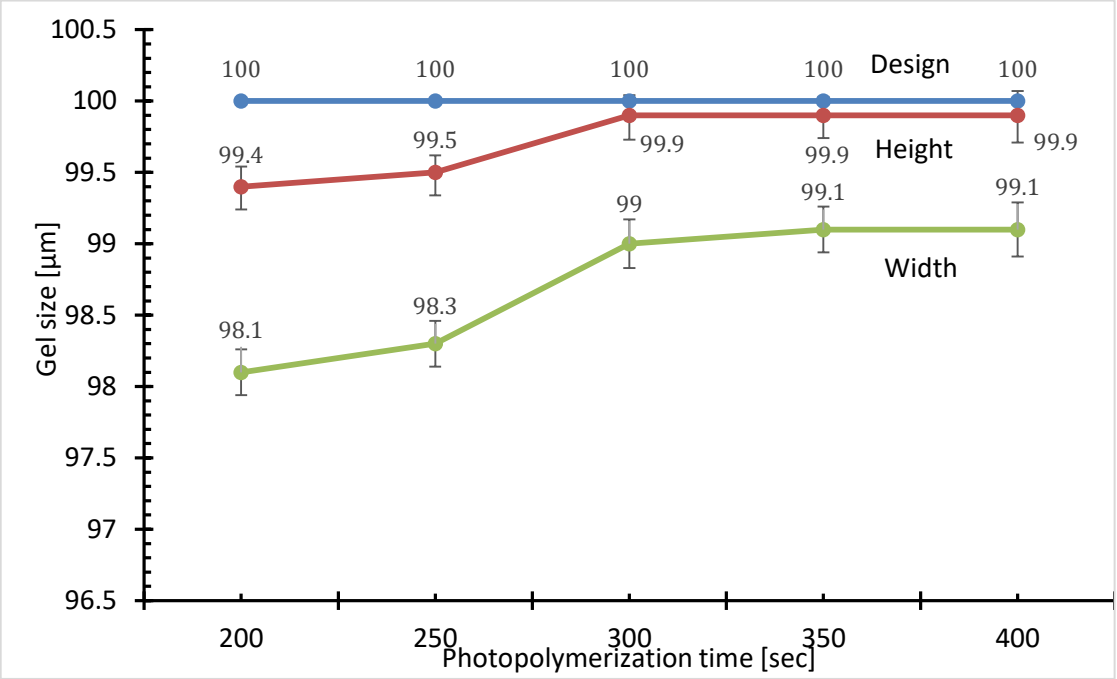

Figure 4.8 Dimension of polymerized boxes at different light integral.

Figure 4.8 shows the height and width of polymerized pattern boxes on the GelMA hydrogel at different light integral value. The X-axis represents the light integral values, and the Y-axis represents the polymerized hydrogel size. In various photopolymerization timing, the formation of photopolymerization pattern height of the each individual box was measured approximately 99.4 – 99.9 µm and the formation of photopolymerization pattern width of the each individual box was measured approximately 98.1 – 99.1 µm. In 300, 350 and 400 seconds, the width and height of the polymerized gel were almost same. But in the other irradiation time, the dimensions were different because of the patterned pixels distribution on the LCD screen.

4.3.3 Cells encapsulation in polymerized hydrogel

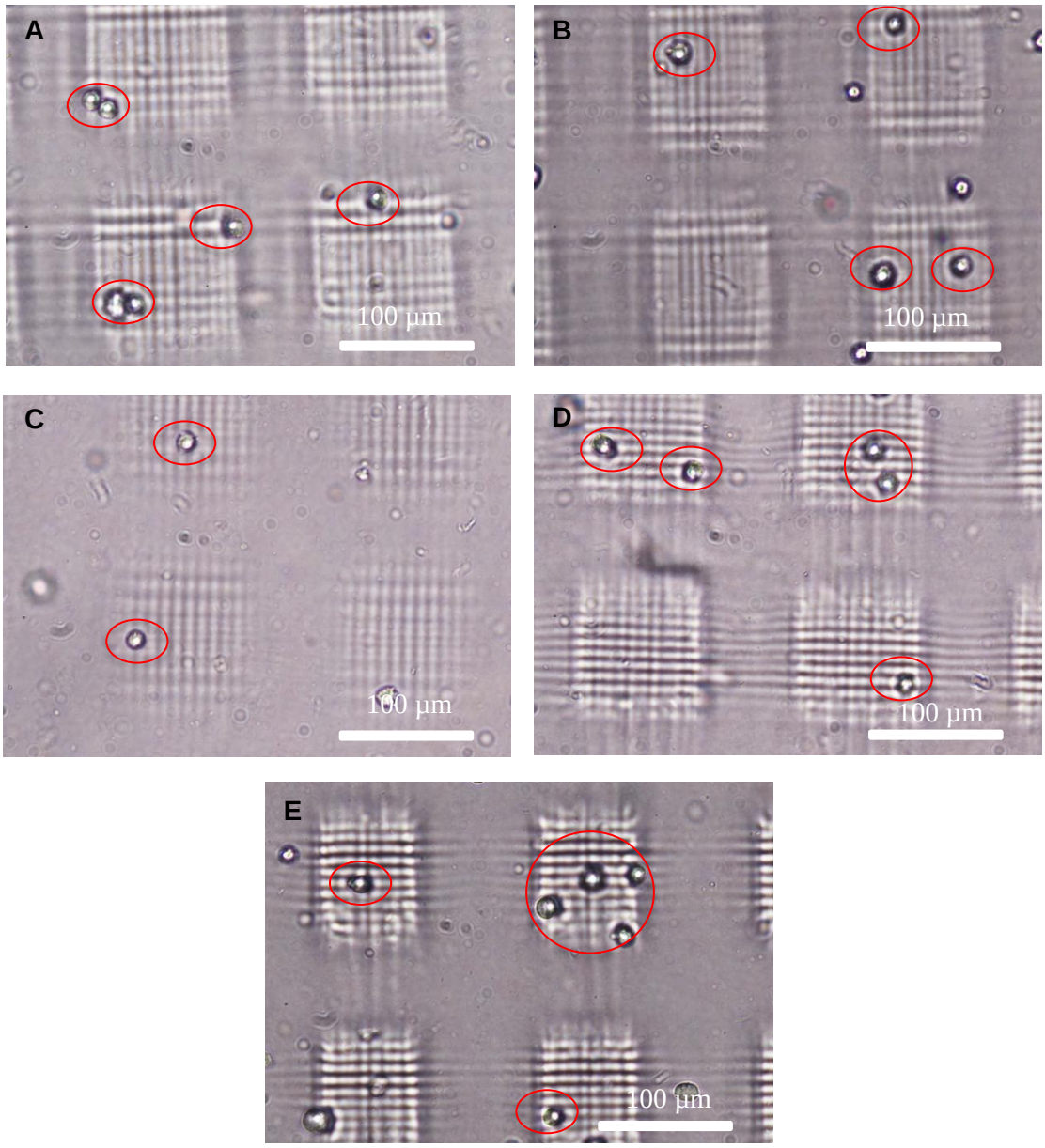

Figure 4.9 Microscopic images of cells encapsulated on GelMA hydrogel. (A) 200 s, (B) 250 s, (c) 300 s, (D) 350s and (E) 400 s.

Figure 4.9 shows the microscopic images of cells encapsulated in polymerized GelMA of concentration of 5 % w/v. The prepared polymerized gel with HeLa cells were transferred into the sample and placed on top of the LCD based printer. The converted .prz file was uploaded to the printer and the LED module was emitted on the sample. In this polymerization process, the exposure time that means the light irradiation time reacted with the sample is directly proportional to the light integral. Figure 4.9(A)-4.9(E) exposed to view the cell encapsulated in polymerized pattern on the

GelMA hydrogel which was polymerized at the exposure time of 200 to 400 seconds with varying the light integral value from 500 mJ/cm² to 1000 mJ/cm².

At 5 % w/v concentration of GelMA hydrogel, the polymerized hydrogel areas were transparent even after the polymerization process happened. In the polymerized pattern region, the cells were captured inside the GelMA hydrogel. This can help the encapsulated cells to retain their movements and the visibility because of a thin layer of hydrogel. The red circular indicates the encapsulation of HeLa cells in the GelMA hydrogel.

4.3.4 Cell viability of encapsulated cells in GelMA hydrogel

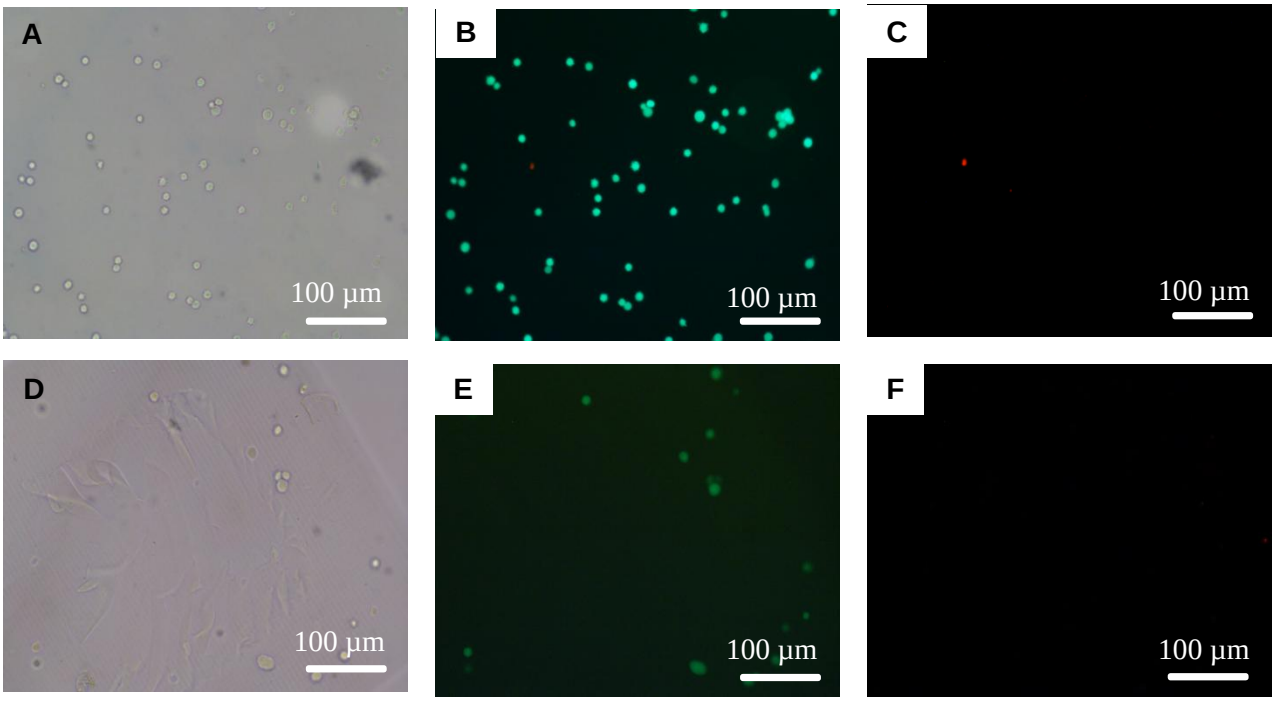

Figure 4.10 Microscopic images of HeLa stained with Calcein-AM and PI. (A-C) Negative control of hydrogel. (D-F) 5 % w/v of GelMA cured gel at 600 mJ/cm². (A, D) bright field images. (B-E) Green fluorescent images. (C, F) Red fluorescent images

To perform the cell viability, the hydrogel with cells suspension was polymerized at 600 mJ/cm². Using the sub-section 3.2.4 procedure, the staining liquids were added and observed in the fluorescence microscope. Figure 4.10(A-C) shows the negative control experiment without conducting the polymerization process. Figure 4.10(B) shows the cells stained with Calcein-AM in green fluorescence which indicates viable cells. Figure 4.10(C) shows the cells stained with PI in red fluorescence which indicates dead cells. From the observation, the efficiency of cell viable in negative

control experiments was 98 %. Figure 4.10(D) shows the bright field images of 5 % w/v GelMA hydrogel that were polymerized at 1200 mJ/cm². Figure 4.10(E) shows the viable cells that were encapsulated in the polymerized gel. Figure 4.10(F) looks black, that means there are no dead cells detected from that image. The efficiency of cell viable at 5 % w/v of polymerize gel was 97 %.

4.3.5 Cell proliferation of encapsulated cell

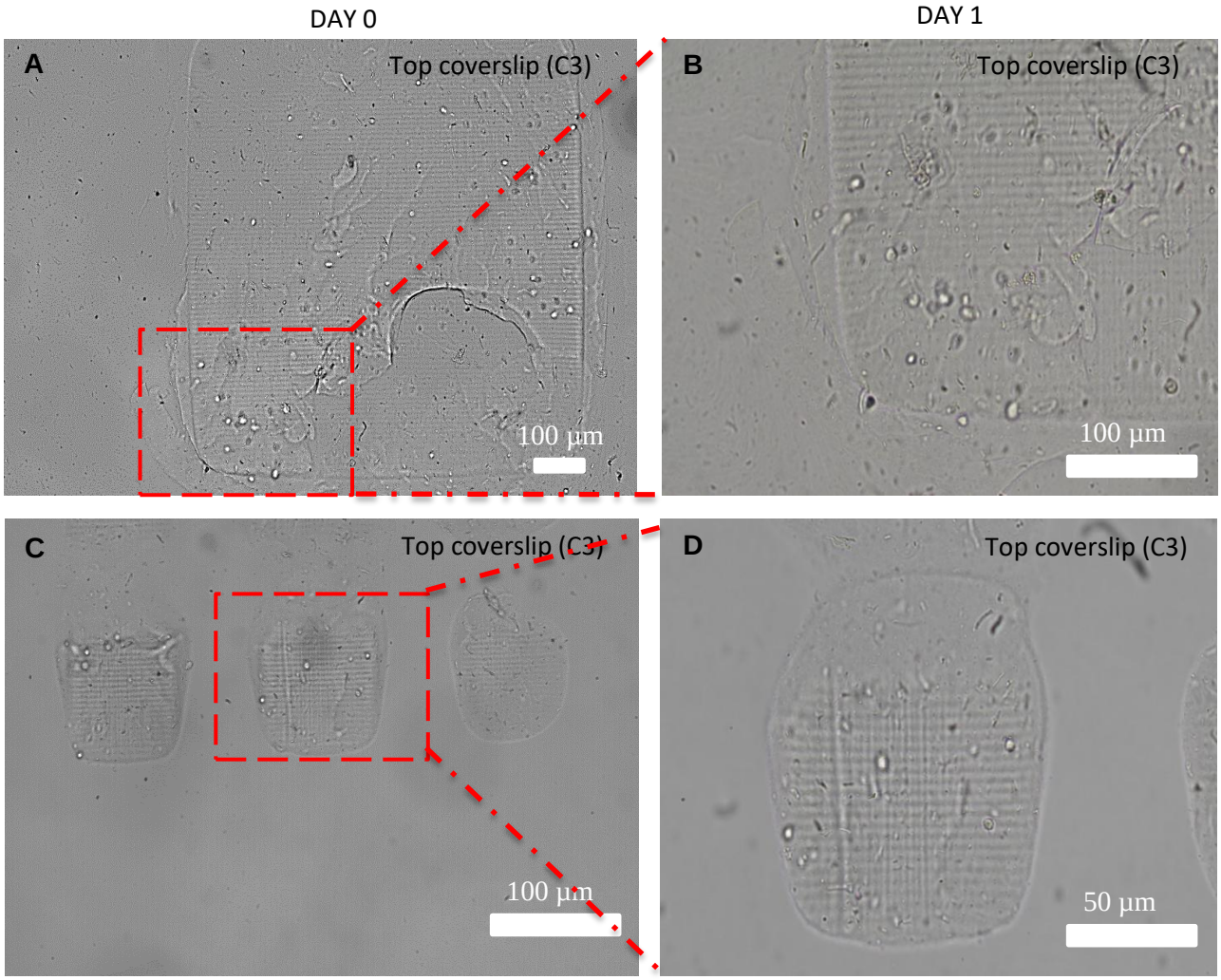

Figure 4.11 Microscopic image of cured gel at 5 % w/v GelMA. (A-B) Observation of encapsulated cells in 1 mm×1 mm polymerization pattern on Day 0-1. (C-D) Observation of encapsulated cells in 100 µm ×100 µm polymerization pattern on Day 0-1

Figure 4.11 shows the microscopic images of cured gel at 5% w/v GelMA. Here, the cell suspension was irradiated at 500 mJ/cm² in duration of 200 sec. After the photopolymerization process, the top coverslip was removed and washed with PBS. For observation, the washed top coverslip was kept in a Petri dish and filled with medium. Figure 4.11(A) shows the 1 mm×1 mm

photopolymerized pattern where the cells were encapsulated in GelMA on day 0. Figure 4.11(B) shows the magnification view of the red dotted box in fig 4.11(A), observed on day1. Figure 4.11(C) shows the 100 µm×100 µm photopolymerized pattern where the cells were encapsulated in GelMA on day 0. Figure 4.11(D) shows the magnification view of the red dotted box in fig 4.11(C), observed on day 1. In fig 4.11(B) and 4.11(D), it can be observed that the encapsulated cells did not proliferate by day 1 and it remained in the same condition as data 0. In these experiments, the long-term observation was carried by using the top coverslip from the sample. In general principle in the LCD system, the light source passes from base coverslip to top coverslip during the polymerization process. The most of the cells were present in bottom coverslip and the few cells were present in top coverslip. The cells which present in the top cover don't adhere to the coverslip. The cell proliferation doesn't occur.

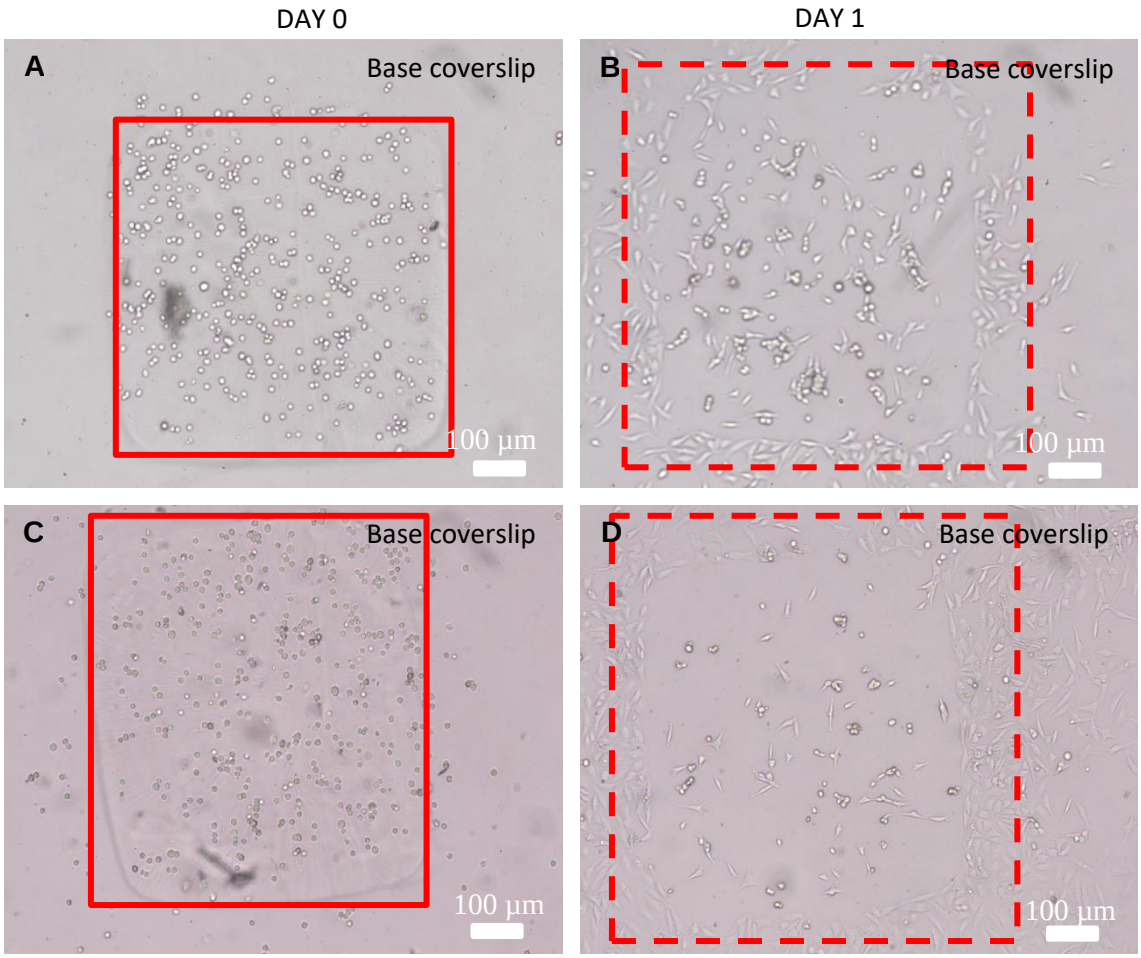

Figure 4.12 Microscopic image of cured gel at 5 % w/v GelMA. (A-B) Observation of encapsulated cells in 1×1 mm polymerization pattern on Day 0-1. (C-D) Observation of encapsulated cells in 1×1 mm polymerization pattern on Day 0-1

Figure 4.12 shows the microscopic images of cured gel at 5% w/v GelMA. Here, the cell suspension was irradiated at 250 mJ/cm² in duration of 100 sec. After the photopolymerization process, the top coverslip was removed and washed with PBS. For observation, the washed bottom coverslip was kept in a Petri dish and filled with medium. Figure 4.12(A) shows the 1 mm×1 mm photopolymerized pattern where the cells were encapsulated in GelMA on day 0 and the red solid box indicates the formation of polymerization pattern on the sample. Figure 4.12(B) shows the 1 mm×1 mm photopolymerized pattern where the cells were encapsulated in GelMA on day 1 and the red dotted box indicates the traces of polymerization pattern. Figure 4.12(C) shows the 1 mm×1 mm photopolymerized pattern where the cells were encapsulated in GelMA on day 0. Figure 4.12(D) shows the 1 mm×1 mm photopolymerized pattern where the cells were encapsulated in GelMA on day 1 and the red dotted box indicates the traces of polymerization pattern. In these experiments, the bottom coverslip was taken and observed. From the observation, the cells were adherent to the coverslip and the cell proliferation occurs. Even the cells were adherent at the surrounding area of the polymerized pattern. The visibility of polymerized gel on day 1 was unclear compared to the results with the DMD approach. In the LCD approach, the light integral value was low, and the crosslink of hydrogel was not sufficient for control of the encapsulated cells.

For long-term observation, the experiments were also conducted at 650 mJ/cm² in duration of 250 seconds. In this experiment, the bottom coverslip was taken for observation and the cells didn't proliferate. In conclusion, further optimization was required for long-term observation of encapsulated cells in the LCD-based system.

4.3.6 Removal of Unwanted cells in polymerized hydrogel

Unwanted cells were released from the sample by using trypsin solution. The polymerization pattern was irradiated on the 5 % w/v GelMA hydrogel at 800 mJ/cm². And then the top coverslip was removed and placed at 50 mm Petri dish and added enough trypsin. Figure 4.13(A) presents the microscopic view of irradiated cells encapsulated hydrogel that merged with trypsin solution at 0 minutes after the irradiation process. In that figure, some of the uncured cells were present in the hydrogel and the red dished circle indicates the unwanted cells. Figure 4.13(B) shows the microscopic view of irradiated cell encapsulation after submerging for 10 minutes.

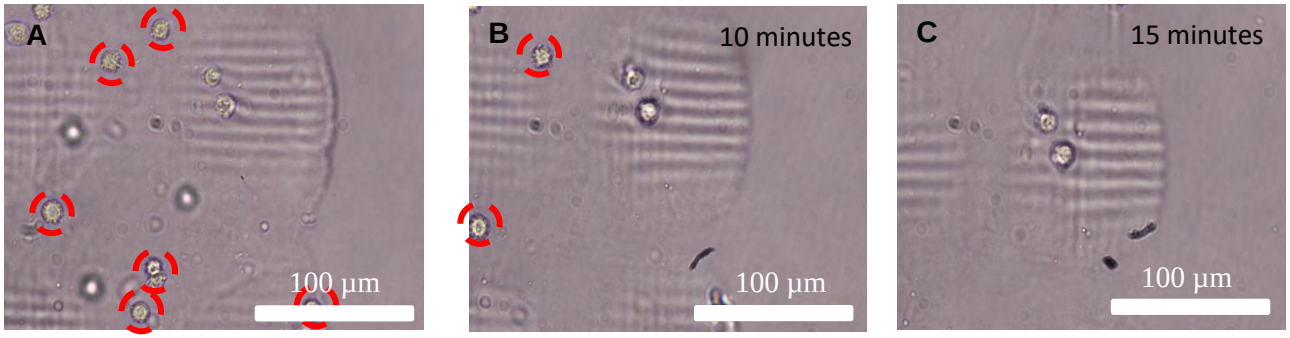

Figure 4.13 Collection of unwanted cells in GelMA photocured at 800 mJ/cm² by trypsin treatment. (A) Immediately after polymerization (B) 10 minute (C) 15 minutes.

In this process, the four uncured cells from a total of six cells started to release from the sample and there were few cells present on the sample. After 15 minutes, the remaining uncured cells were recovered from the sample (Fig. 4.13(C)) and it shows the polymerized pattern remained present on the sample.

4.3.7 Collection of cured cells in polymerized GelMA hydrogel

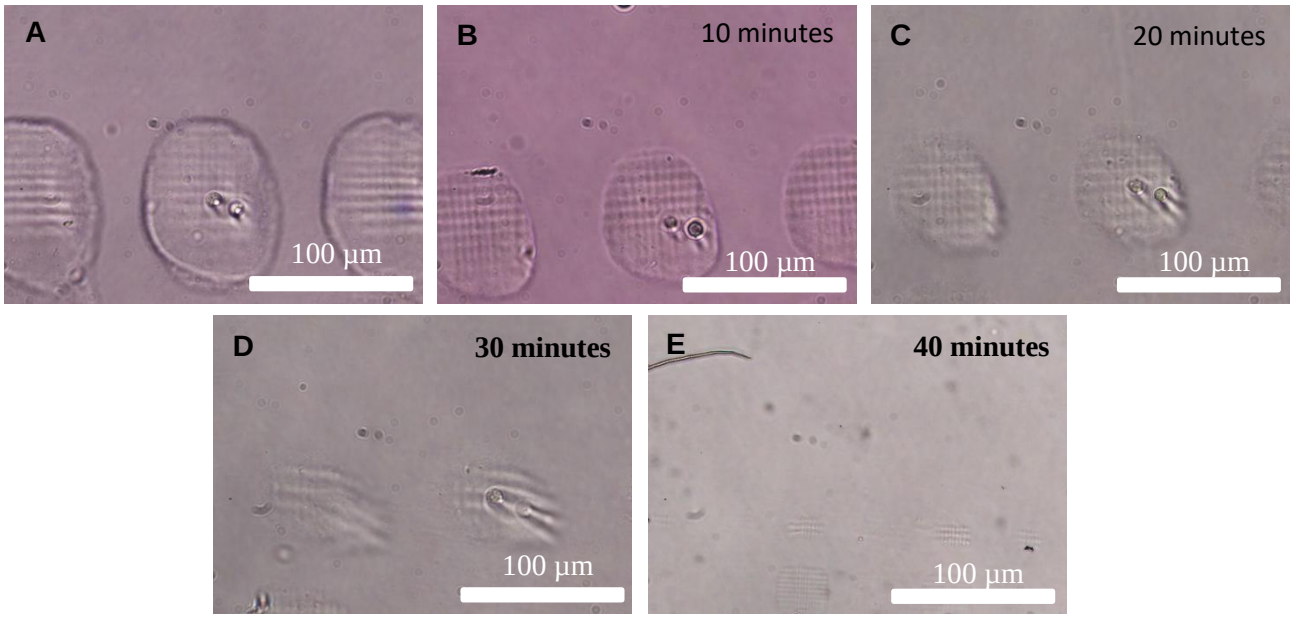

Figure 4.14 Degradation of GelMA photocured hydrogel at 600 mJ/cm² in trypsin (A) Immediately after polymerization (B) 10 minute (C) 20 minutes (D) 30 minutes and (E) 40 minutes.

Here the cell suspension hydrogel was irradiated at 600 mJ/cm² and removed the top coverslip and washed with PBS to remove the uncured or unwanted cells from the sample. And then the sample was transferred in a 50 mm petri dish and filled with sufficient trypsin solution. Figure 4.14(A) shows the microscopic view of irradiate pattern on the sample after polymerization. The sample was observed in microscope up to the irradiate pattern dissolve in trypsin solution. Figure 4.14(B)-4.14(E)

represents the dissolution of an irradiated pattern in the solution at a time interval of 10 minutes, 20 minutes, 30 minutes and 40 minutes respectively. In this time interval period, the irradiation patterns slowly dissolved in the dish. At 600 mJ/cm² condition, the total of 40 minutes required to dissolve the irradiate pattern in the trypsin solution and the cells were released from the GelMA hydrogel after 40 minutes of recovery treatment.

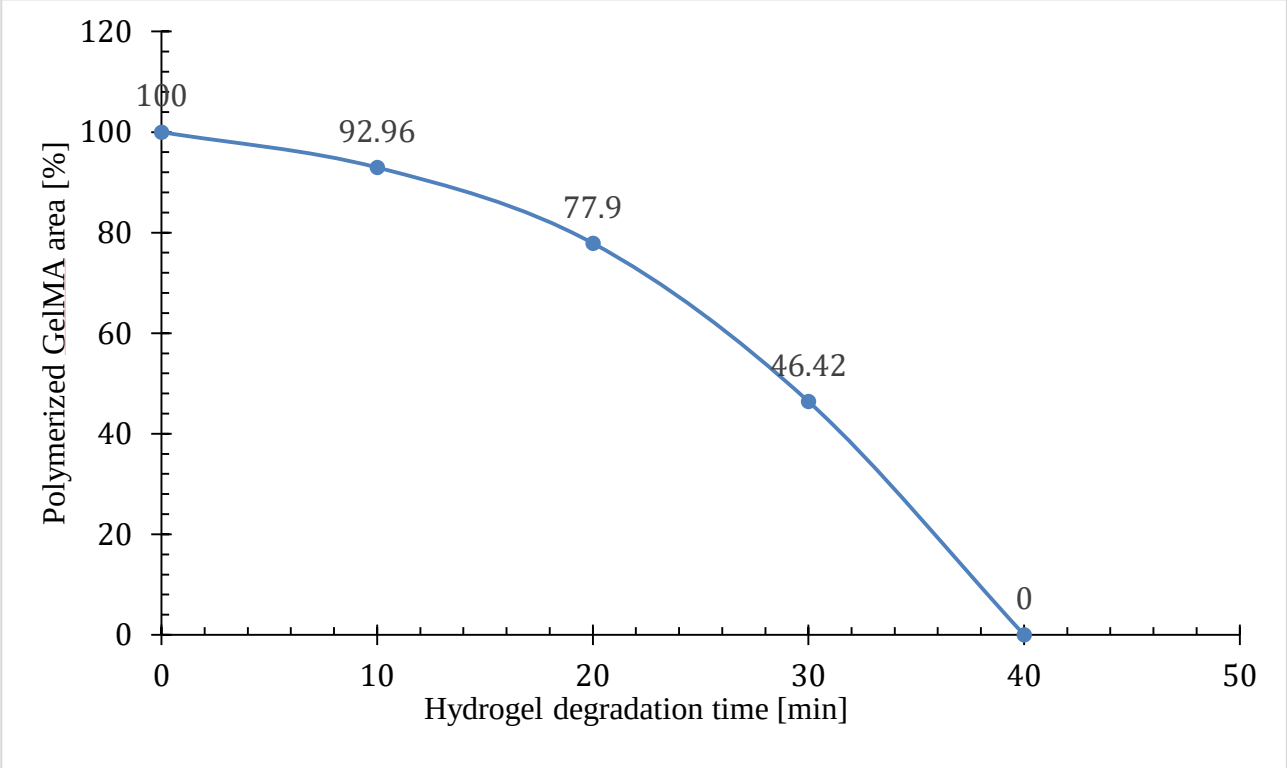

Figure 4.15 Change of size of GelMA hydrogel degradation in a trypsin solution

Figure 4.15 shows change of size of 5 w/v% polymerized GelMA degradation in trypsin solution. Here, the X-axis represents the hydrogel degradation time, and the Y-axis represents the polymerized hydrogel area. Here, the hydrogel was irradiated at 600 mJ/cm² using 100 µm × 100 µm pattern size. After submerge the sample in trypsin, the sample was observed in the time interval of 10 minutes, 20 minutes, 30 minutes and 40 minutes and the area of polymerized pattern was degraded averagely 92.96 %, 77.9 %, 46.42 % and 0 respectively. As the time was increased, the polymerized hydrogel was decreased due to trypsin solution.

In the LCD based photopolymerization method, both the removal of unpolymerized cells and degradation of GelMA photocured hydrogel required more time compared to the DMD based setup. In the case of removal of unpolymerized cells, the DMD based system required 10 minutes and the LCD based 3D printer system required 15 minutes. It shows that the DMD system was better control in polymerization process. The removal of unpolymerized cells from the sample was lesser timing compared to the LCD system.

While in the degradation of photocured hydrogel, the LCD based system needed 40 minutes, but the DMD based system required only 5 minutes 37 seconds. It concludes that DMD system was more suitable to degradation because there was difference in crosslinking density or uniformity by the both DMD and LCD based system.

4.4 Conclusion

In this chapter, the LCD screen-based 3D printer was remodified and used for polymerization function. In that system, the different dimension patterns were created in the 3D software and it was converted into required .prz file format using CHITUBOX where the polymerization parameters such as exposure time, thickness of the pattern and position and orientation of the pattern that wants to display on the LCD screen. In experiments, the patterns were exposed at the time of 200 seconds to 400 seconds with the light integral of 500 mJ/cm^2 to 1000 mJ/cm^2. In all light integral, the dimensions were approximately same as the original dimensions of the polymerized pattern. In these experimental conditions, the HeLa cells were captured in sample range of 4 × 4 mm in a single exposure. Also, the cell encapsulated viability experiments were conducted and the cell viability efficiency of 5% concentration GelMA was 97%. Initially in the long-term observation, the cells were not proliferated. After alter process in observation, the cells were proliferated and still the process wants to optimize to achieve better output. While conducting the removal of uncured cells, 15 minutes required to peel off uncured cell from cover slip. The total time of 40 minutes is required to dissolve the polymerized GelMA hydrogel into the trypsin solution.

Chapter 5 Conclusions

5.1 Conclusion

This study explored a method of live single-cell screening based on cell encapsulation using irradiation of pattern light. To enhance the cell encapsulation efficiency, the image-based cell sorting techniques was incorporated. By using the IBCS method, the single cells were automatically detected with the help of image processing tools or software. The single cells detection was basically performed by detection the single cells information from the sample images. With combination of IBCS and polymerization of hydrogel, I developed a system to encapsulate the single cells in the hydrogel with the help of image processing tool. In this system, both the DMD based approach, and the LCD screen-based approach was used to irradiate the photopolymer hydrogel.

Based on the experimental results and analysis, the following conclusions can be highlighted:

- Developed a novel live single-cell screening method using high-resolution imaging and photopolymerization in a DMD-based system.
- Optimized polymerization conditions: 5% GelMA concentration, specific light integral of 800-1200 (mJ/cm^2), and trypsin for cell collection. Addressed alignment errors through various data transfer techniques.
- Demonstrated GelMA hydrogel's superior suitability over PEGDA for long-term cell encapsulation and observation.
- Implemented an LCD-based approach, eliminating the need for complicated optics and enabling wider region photopolymerization.
- Compared system parameters: DMD system (160 mW/cm^2) achieved faster encapsulation, while LCD system (2.5 mW/cm^2 required longer time but allowed wider area processing.

Cancer is a common example of a disease where cellular heterogeneity plays a critical role. Tumors are habitually of a diverse population of cells with different genetic and phenotypic characteristics. Single-cell screening was able to identify these differences and the selection of targeted subpopulations of cells. Also, it was able to identify the potential drug targets by investigating how single cells responded to. This can lead to the innovation of new drug development that can't be achieved in bulk cell analyses. The single-cell screening can support personalized

treatment plans. During the treatment time, the patient's single cells were monitored and it's able to make some adjustments to the therapeutic strategy as needed.

As a result, single-cell screening was a powerful technique that improved the knowledge in cellular heterogeneity, developing a new approach in precise and effective cancer research, drug development and personalized medicine.

5.2 Future work

This research has laid the groundwork for advanced single-cell screening techniques, but there are several avenues for further development and expansion of the technology. In the DMD-based approach, future work will focus on encapsulating multiple cell types simultaneously. For instance, we plan to use HeLa cells stained with Calcein-AM and HEK 293 cells stained with Hoechst, incubating them separately before suspending both in hydrogel for transfer to the sample plate. By observing these samples under a fluorescent microscope with different filters, we can merge the images to identify single cells of both types. This information will be used to create a photopolymerization pattern where square shapes represent HeLa single cells and circular shapes represent HEK293 cells, allowing for simultaneous encapsulation of two distinct cell types.

For the LCD-based approach, while we have successfully demonstrated pattern formation and cell encapsulation, future work will focus on generating single-cell photopolymerization patterns and performing polymerization operations to encapsulate individual cells. This process will involve capturing sample images, processing them to extract single-cell information, and using this data to generate 3D box solid structures. These structures will then be converted into the file format required by the LCD screen printer microprocessor.

Additionally, we will conduct comprehensive studies on the behavior of encapsulated cells in both systems, aiming to determine and optimize the efficiency of our single-cell encapsulation techniques. This research will provide valuable insights into cell viability, proliferation, and functionality within the hydrogel environment, potentially opening new avenues for applications in drug screening, personalized medicine, and tissue engineering.

By pursuing these research directions, we aim to enhance the capabilities and applications of our single-cell screening technology, pushing the boundaries of what's possible in cellular analysis and manipulation.

Reference

[1] V. Fitzgerald and P. Leonard, “Single cell screening approaches for antibody discovery,” *Methods*, vol. 116, pp. 34–42, Mar. 2017, doi: 10.1016/j.ymeth.2016.11.006.

[2] N. Bossel Ben-Moshe *et al.*, “Predicting bacterial infection outcomes using single cell RNA-sequencing analysis of human immune cells,” *Nat. Commun.*, vol. 10, no. 1, p. 3266, Jul. 2019, doi: 10.1038/s41467-019-11257-y.

[3] C. Krieg *et al.*, “High-dimensional single-cell analysis predicts response to anti-PD-1 immunotherapy,” *Nat. Med.*, vol. 24, no. 2, pp. 144–153, Feb. 2018, doi: 10.1038/nm.4466.

[4] C. Trapnell, “Defining cell types and states with single-cell genomics,” *Genome Res.*, vol. 25, no. 10, pp. 1491–1498, Oct. 2015, doi: 10.1101/gr.190595.115.

[5] M. B. Elowitz, A. J. Levine, E. D. Siggia, and P. S. Swain, “Stochastic Gene Expression in a Single Cell,” *Science*, vol. 297, no. 5584, pp. 1183–1186, Aug. 2002, doi: 10.1126/science.1070919.

[6] C. Angermueller *et al.*, “Parallel single-cell sequencing links transcriptional and epigenetic heterogeneity,” *Nat. Methods*, vol. 13, no. 3, pp. 229–232, Mar. 2016, doi: 10.1038/nmeth.3728.

[7] S. J. Clark *et al.*, “scNMT-seq enables joint profiling of chromatin accessibility DNA methylation and transcription in single cells,” *Nat. Commun.*, vol. 9, no. 1, p. 781, Feb. 2018, doi: 10.1038/s41467-018-03149-4.

[8] A. P. Gasch *et al.*, “Genomic Expression Programs in the Response of Yeast Cells to Environmental Changes,” *Mol. Biol. Cell*, vol. 11, no. 12, pp. 4241–4257, Dec. 2000, doi: 10.1091/mbc.11.12.4241.

[9] C. Trapnell *et al.*, “The dynamics and regulators of cell fate decisions are revealed by pseudotemporal ordering of single cells,” *Nat. Biotechnol.*, vol. 32, no. 4, pp. 381–386, Apr. 2014, doi: 10.1038/nbt.2859.

[10] A. A. Kolodziejczyk, J. K. Kim, V. Svensson, J. C. Marioni, and S. A. Teichmann, “The Technology and Biology of Single-Cell RNA Sequencing,” *Mol. Cell*, vol. 58, no. 4, pp. 610–620, May 2015, doi: 10.1016/j.molcel.2015.04.005.

[11] J. Y. Kim, Y.-G. Kim, and G. M. Lee, “CHO cells in biotechnology for production of recombinant proteins: current state and further potential,” *Appl. Microbiol. Biotechnol.*, vol. 93, no. 3, pp. 917–930, Feb. 2012, doi: 10.1007/s00253-011-3758-5.

[12] S. Fischer, R. Handrick, and K. Otte, “The art of CHO cell engineering: A comprehensive retrospect and future perspectives,” *Biotechnol. Adv.*, vol. 33, no. 8, pp. 1878–1896, Dec. 2015, doi: 10.1016/j.biotechadv.2015.10.015.

[13] T. Omasa, M. Onitsuka, and W.-D. Kim, “Cell Engineering and Cultivation of Chinese Hamster Ovary (CHO) Cells,” *Curr. Pharm. Biotechnol.*, vol. 11, no. 3, pp. 233–240, Apr. 2010, doi: 10.2174/138920110791111960.

[14] F. Borriello, F. Granata, G. Varricchi, A. Genovese, M. Triggiani, and G. Marone, “Immunopharmacological modulation of mast cells,” *Curr. Opin. Pharmacol.*, vol. 17, pp. 45–57, Aug. 2014, doi: 10.1016/j.coph.2014.07.002.

[15] F. M. Wurm, “Production of recombinant protein therapeutics in cultivated mammalian cells,” *Nat. Biotechnol.*, vol. 22, no. 11, pp. 1393–1398, Nov. 2004, doi: 10.1038/nbt1026.

[16] P. D. Hsu, E. S. Lander, and F. Zhang, “Development and Applications of CRISPR-Cas9 for Genome Engineering,” *Cell*, vol. 157, no. 6, pp. 1262–1278, Jun. 2014, doi: 10.1016/j.cell.2014.05.010.

[17] S. J. Altschuler and L. F. Wu, “Cellular Heterogeneity: Do Differences Make a Difference?,” *Cell*, vol. 141, no. 4, pp. 559–563, May 2010, doi: 10.1016/j.cell.2010.04.033.

[18] A. A. Cohen *et al.*, “Dynamic Proteomics of Individual Cancer Cells in Response to a Drug,” *Science*, vol. 322, no. 5907, pp. 1511–1516, Dec. 2008, doi: 10.1126/science.1160165.

[19] S. R. Jackson *et al.*, “Applications of Hairpin DNA-Functionalized Gold Nanoparticles for Imaging mRNA in Living Cells,” in *Methods in Enzymology*, vol. 572, Elsevier, 2016, pp. 87–103. doi: 10.1016/bs.mie.2016.03.019.

[20] R. S. Santos, N. Guimarães, P. Madureira, and N. F. Azevedo, “Optimization of a peptide nucleic acid fluorescence in situ hybridization (PNA-FISH) method for the detection of bacteria and disclosure of a formamide effect,” *J. Biotechnol.*, vol. 187, pp. 16–24, Oct. 2014, doi: 10.1016/j.jbiotec.2014.06.023.

[21] T. Stuart and R. Satija, “Integrative single-cell analysis,” *Nat. Rev. Genet.*, vol. 20, no. 5, pp. 257–272, May 2019, doi: 10.1038/s41576-019-0093-7.

[22] P. Hu, W. Zhang, H. Xin, and G. Deng, “Single Cell Isolation and Analysis,” *Front. Cell Dev. Biol.*, vol. 4, Oct. 2016, doi: 10.3389/fcell.2016.00116.

[23] Ashok Kumar, Igor Yu Galaev, and Bo Mattiasson, *Cell Separation: Fundamentals, Analytical and Preparative Methods*, 106 vols. Springer, 2007.

[24] P. Shinde *et al.*, “Current Trends of Microfluidic Single-Cell Technologies,” *Int. J. Mol. Sci.*, vol. 19, no. 10, p. 3143, Oct. 2018, doi: 10.3390/ijms19103143.

[25] K. M. McKinnon, “Flow Cytometry: An Overview,” *Curr. Protoc. Immunol.*, vol. 120, no. 1, Jan. 2018, doi: 10.1002/cpim.40.

[26] A. Gross, J. Schoendube, S. Zimmermann, M. Steeb, R. Zengerle, and P. Koltay, “Technologies for Single-Cell Isolation,” *Int. J. Mol. Sci.*, vol. 16, no. 8, pp. 16897–16919, Jul. 2015, doi: 10.3390/ijms160816897.

[27] K. R. Schulz, E. A. Danna, P. O. Krutzik, and G. P. Nolan, “Single-Cell Phospho-Protein Analysis by Flow Cytometry,” *Curr. Protoc. Immunol.*, vol. 96, no. 1, Feb. 2012, doi: 10.1002/0471142735.im0817s96.

[28] S. Miltenyi, W. Müller, W. Weichel, and A. Radbruch, “High gradient magnetic cell separation with MACS,” *Cytometry*, vol. 11, no. 2, pp. 231–238, Jan. 1990, doi: 10.1002/cyto.990110203.

[29] G. M. Whitesides, “The origins and the future of microfluidics,” *Nature*, vol. 442, no. 7101, pp. 368–373, Jul. 2006, doi: 10.1038/nature05058.

[30] C. A. LaBelle, A. Massaro, B. Cortés-Llanos, C. E. Sims, and N. L. Allbritton, “Image-Based Live Cell Sorting,” *Trends Biotechnol.*, vol. 39, no. 6, pp. 613–623, Jun. 2021, doi: 10.1016/j.tibtech.2020.10.006.

[31] G. Orive *et al.*, “History, challenges and perspectives of cell microencapsulation,” *Trends Biotechnol.*, vol. 22, no. 2, pp. 87–92, Feb. 2004, doi: 10.1016/j.tibtech.2003.11.004.

[32] B. Cortés-Llanos, Y. Wang, C. E. Sims, and N. L. Allbritton, “A technology of a different sort: microraft arrays,” *Lab. Chip*, vol. 21, no. 17, pp. 3204–3218, 2021, doi: 10.1039/D1LC00506E.

[33] J. Jin *et al.*, “Robotic data acquisition with deep learning enables cell image–based prediction of transcriptomic phenotypes,” *Proc. Natl. Acad. Sci.*, vol. 120, no. 1, p. e2210283120, Jan. 2023, doi: 10.1073/pnas.2210283120.

[34] M. Nagai, K. Kato, K. Oohara, and T. Shibata, “Pick-and-Place Operation of Single Cell Using Optical and Electrical Measurements for Robust Manipulation,” *Micromachines*, vol. 8, no. 12, p. 350, Nov. 2017, doi: 10.3390/mi8120350.

[35] Y. Yamanishi *et al.*, “Maskless Gray Scale Lithography and its 3D Microfluidic Applications,” *J. Robot. Mechatron.*, vol. 23, no. 3, pp. 426–433, Jun. 2011, doi: 10.20965/jrm.2011.p0426.

[36] M. Nagai, K. Oohara, K. Kato, T. Kawashima, and T. Shibata, “Development and characterization of hollow microprobe array as a potential tool for versatile and massively parallel manipulation of single cells,” *Biomed. Microdevices*, vol. 17, no. 2, p. 41, Apr. 2015, doi: 10.1007/s10544-015-9943-z.

[37] M. Nagai, K. Kato, S. Soga, T. S. Santra, and T. Shibata, “Scalable Parallel Manipulation of Single Cells Using Micronozzle Array Integrated with Bidirectional Electrokinetic Pumps,” *Micromachines*, vol. 11, no. 4, p. 442, Apr. 2020, doi: 10.3390/mi11040442.

[38] R. Negishi *et al.*, “Gel-based cell manipulation method for isolation and genotyping of single-adherent cells,” *The Analyst*, vol. 144, no. 3, pp. 990–996, 2019, doi: 10.1039/C8AN01456F.

[39] T. Yoshino, T. Tanaka, S. Nakamura, R. Negishi, M. Hosokawa, and T. Matsunaga, “Manipulation of a Single Circulating Tumor Cell Using Visualization of Hydrogel Encapsulation toward Single-Cell Whole-Genome Amplification,” *Anal. Chem.*, vol. 88, no. 14, pp. 7230–7237, Jul. 2016, doi: 10.1021/acs.analchem.6b01475.

[40] R. Negishi, K. Takai, T. Tanaka, T. Matsunaga, and T. Yoshino, “High-Throughput Manipulation of Circulating Tumor Cells Using a Multiple Single-Cell Encapsulation System with a Digital Micromirror Device,” *Anal. Chem.*, vol. 90, no. 16, pp. 9734–9741, Aug. 2018, doi: 10.1021/acs.analchem.8b00896.

[41] M. B. Browning, S. N. Cereceres, P. T. Luong, and E. M. Cosgriff-Hernandez, “Determination of the *in vivo* degradation mechanism of PEGDA hydrogels: *In Vivo* Degradation Mechanism of PEGDAA,” *J. Biomed. Mater. Res. A*, p. n/a-n/a, Feb. 2014, doi: 10.1002/jbm.a.35096.

[42] M. Zhu, Y. Wang, G. Ferracci, J. Zheng, N.-J. Cho, and B. H. Lee, “Gelatin methacryloyl and its hydrogels with an exceptional degree of controllability and batch-to-batch consistency,” *Sci. Rep.*, vol. 9, no. 1, p. 6863, May 2019, doi: 10.1038/s41598-019-42186-x.

[43] V. A. Liu and S. N. Bhatia, “Three-Dimensional Photopatterning of Hydrogels Containing Living Cells,” *Biomed. Microdevices*, vol. 4, no. 4, pp. 257–266, 2002, doi: 10.1023/A:1020932105236.

[44] K. Yue, G. Trujillo-de Santiago, M. M. Alvarez, A. Tamayol, N. Annabi, and A. Khademhosseini, “Synthesis, properties, and biomedical applications of gelatin methacryloyl (GelMA) hydrogels,” *Biomaterials*, vol. 73, pp. 254–271, Dec. 2015, doi: 10.1016/j.biomaterials.2015.08.045.

[45] A. J. Berger, K. M. Linsmeier, P. K. Kreeger, and K. S. Masters, “Decoupling the effects of stiffness and fiber density on cellular behaviors via an interpenetrating network of gelatin-methacrylate and collagen,” *Biomaterials*, vol. 141, pp. 125–135, Oct. 2017, doi: 10.1016/j.biomaterials.2017.06.039.

[46] J. R. Rodrigues, N. M. Alves, and J. F. Mano, “Biomimetic polysaccharide/bioactive glass nanoparticles multilayer membranes for guided tissue regeneration,” *RSC Adv.*, vol. 6, no. 79, pp. 75988–75999, 2016, doi: 10.1039/C6RA14359H.

[47] B. Lee, N. Lum, L. Seow, P. Lim, and L. Tan, “Synthesis and Characterization of Types A and B Gelatin Methacryloyl for Bioink Applications,” *Materials*, vol. 9, no. 10, p. 797, Sep. 2016, doi: 10.3390/ma9100797.

[48] X. Zhao *et al.*, “Photocrosslinkable Gelatin Hydrogel for Epidermal Tissue Engineering,” *Adv. Healthc. Mater.*, vol. 5, no. 1, pp. 108–118, Jan. 2016, doi: 10.1002/adhm.201500005.

[49] J. Kopeček, “Hydrogel biomaterials: A smart future?,” *Biomaterials*, vol. 28, no. 34, pp. 5185–5192, Dec. 2007, doi: 10.1016/j.biomaterials.2007.07.044.

[50] Z. Wang, W. Yang, Y. Qin, W. Liang, H. Yu, and L. Liu, “Digital micro-mirror device -based light curing technology and its biological applications,” *Opt. Laser Technol.*, vol. 143, p. 107344, Nov. 2021, doi: 10.1016/j.optlastec.2021.107344.

[51] C. Yu *et al.*, “Photopolymerizable Biomaterials and Light-Based 3D Printing Strategies for Biomedical Applications,” *Chem. Rev.*, vol. 120, no. 19, pp. 10695–10743, Oct. 2020, doi: 10.1021/acs.chemrev.9b00810.

[52] C. Cha *et al.*, “Structural reinforcement of cell-laden hydrogels with microfabricated three dimensional scaffolds,” *Biomater Sci*, vol. 2, no. 5, pp. 703–709, 2014, doi: 10.1039/C3BM60210A.

[53] S. N. S. Alconcel, A. S. Baas, and H. D. Maynard, “FDA-approved poly(ethylene glycol)–protein conjugate drugs,” *Polym. Chem.*, vol. 2, no. 7, p. 1442, 2011, doi: 10.1039/c1py00034a.

[54] J. Ulbricht, R. Jordan, and R. Luxenhofer, “On the biodegradability of polyethylene glycol, polypeptoids and poly(2-oxazoline)s,” *Biomaterials*, vol. 35, no. 17, pp. 4848–4861, Jun. 2014, doi: 10.1016/j.biomaterials.2014.02.029.

[55] H.-W. Kang, Y. Tabata, and Y. Ikada, “Fabrication of porous gelatin scaffolds for tissue engineering,” *Biomaterials*, vol. 20, no. 14, pp. 1339–1344, Jul. 1999, doi: 10.1016/S0142-9612(99)00036-8.

[56] I. Pepelanova, K. Kruppa, T. Scheper, and A. Lavrentieva, “Gelatin-Methacryloyl (GelMA) Hydrogels with Defined Degree of Functionalization as a Versatile Toolkit for 3D Cell Culture and Extrusion Bioprinting,” *Bioengineering*, vol. 5, no. 3, p. 55, Jul. 2018, doi: 10.3390/bioengineering5030055.

[57] Y. Piao *et al.*, “Biomedical applications of gelatin methacryloyl hydrogels,” *Eng. Regen.*, vol. 2, pp. 47–56, 2021, doi: 10.1016/j.engreg.2021.03.002.

[58] R. N. Ghosh *et al.*, “An insight into synthesis, properties and applications of gelatin methacryloyl hydrogel for 3D bioprinting,” *Mater. Adv.*, vol. 4, no. 22, pp. 5496–5529, 2023, doi: 10.1039/D3MA00715D.

[59] J. Cui, H. Wang, Q. Shi, T. Sun, Q. Huang, and T. Fukuda, “Multicellular Co-Culture in Three-Dimensional Gelatin Methacryloyl Hydrogels for Liver Tissue Engineering,” *Molecules*, vol. 24, no. 9, p. 1762, May 2019, doi: 10.3390/molecules24091762.

[60] X. Zhao *et al.*, “Injectable Stem Cell-Laden Photocrosslinkable Microspheres Fabricated Using Microfluidics for Rapid Generation of Osteogenic Tissue Constructs,” *Adv. Funct. Mater.*, vol. 26, no. 17, pp. 2809–2819, May 2016, doi: 10.1002/adfm.201504943.

[61] H. Wang, H. Liu, H. Liu, W. Su, W. Chen, and J. Qin, “One-Step Generation of Core–Shell Gelatin Methacrylate (GelMA) Microgels Using a Droplet Microfluidic System,” *Adv. Mater. Technol.*, vol. 4, no. 6, p. 1800632, Jun. 2019, doi: 10.1002/admt.201800632.

[62] X. Gao *et al.*, “Acoustic quasi-periodic bioassembly based diverse stem cell arrangements for differentiation guidance,” *Lab. Chip*, vol. 23, no. 20, pp. 4413–4421, 2023, doi: 10.1039/D3LC00448A.

[63] Q. Hu *et al.*, “Heterogeneous tissue construction by on-demand bubble-assisted acoustic patterning,” *Lab. Chip*, vol. 23, no. 9, pp. 2206–2216, 2023, doi: 10.1039/D3LC00122A.

[64] X. Hu *et al.*, “On-chip hydrogel arrays individually encapsulating acoustic formed multicellular aggregates for high throughput drug testing,” *Lab. Chip*, vol. 20, no. 12, pp. 2228–2236, 2020, doi: 10.1039/D0LC00255K.

[65] P. Chansoria, S. Asif, K. Polkoff, J. Chung, J. A. Piedrahita, and R. A. Shirwaiker, “Characterizing the Effects of Synergistic Thermal and Photo-Cross-Linking during Biofabrication on the Structural and Functional Properties of Gelatin Methacryloyl (GelMA) Hydrogels,” *ACS Biomater. Sci. Eng.*, vol. 7, no. 11, pp. 5175–5188, Nov. 2021, doi: 10.1021/acsbiomaterials.1c00635.

[66] N. S. Kulkarni, G. Chauhan, M. Goyal, S. Sarvepalli, and V. Gupta, “Development of gelatin methacrylate (GelMa) hydrogels for versatile intracavitary applications,” *Biomater. Sci.*, vol. 10, no. 16, pp. 4492–4507, 2022, doi: 10.1039/D2BM00022A.

[67] N. B. Allen, B. Abar, L. Johnson, J. Burbano, R. M. Danilkowicz, and S. B. Adams, “3D-bioprinted GelMA-gelatin-hydroxyapatite osteoblast-laden composite hydrogels for bone tissue engineering,” *Bioprinting*, vol. 26, p. e00196, Jun. 2022, doi: 10.1016/j.bprint.2022.e00196.

[68] R. Negishi, H. Saito, R. Iwata, T. Tanaka, and T. Yoshino, “Performance evaluation of a high-throughput separation system for circulating tumor cells based on microcavity array,” *Eng. Life Sci.*, vol. 20, no. 11, pp. 485–493, Nov. 2020, doi: 10.1002/elsc.202000024.

[69] C. Sun, N. Fang, D. M. Wu, and X. Zhang, “Projection micro-stereolithography using digital micro-mirror dynamic mask,” *Sens. Actuators Phys.*, vol. 121, no. 1, pp. 113–120, May 2005, doi: 10.1016/j.sna.2004.12.011.

[70] A. Bertsch, H. Lorenz, and P. Renaud, “3D microfabrication by combining microstereolithography and thick resist UV lithography,” *Sens. Actuators Phys.*, vol. 73, no. 1–2, pp. 14–23, Mar. 1999, doi: 10.1016/S0924-4247(98)00249-0.

[71] L. Wu, L. Zhao, M. Jian, Y. Mao, M. Yu, and X. Guo, “EHMP-DLP: multi-projector DLP with energy homogenization for large-size 3D printing,” *Rapid Prototyp. J.*, vol. 24, no. 9, pp. 1500–1510, Nov. 2018, doi: 10.1108/RPJ-04-2017-0060.

[72] H. Quan, T. Zhang, H. Xu, S. Luo, J. Nie, and X. Zhu, “Photo-curing 3D printing technique and its challenges,” *Bioact. Mater.*, vol. 5, no. 1, pp. 110–115, Mar. 2020, doi: 10.1016/j.bioactmat.2019.12.003.

Publication list

Paper published

1. **Panneer Selvam Venkatesh Kumar**, Takeru Fukunaga, Yuya Suzuki, Shunya Okamoto, Takayuki Shibata, Tuhin Subhra Santra, and Moeto Nagai. "Single-Cell Screening through Cell Encapsulation in Photopolymerized Gelatin Methacryloyl." *Micro*, vol. 4, no. 2, pp. 295-304, 2024.

2. **Panneer Selvam Venkatesh Kumar**, Muhammad Luqman Arief Bin Kamaludin, Ghulam Murtaza, Rifat Hussain Chowdhury, Tanmay Debnath, Shunya Okamoto, Takayuki Shibata, Tuhin Subhra Santra, and Moeto Nagai. "Image-Based Gel Encapsulation of Suspended Single Cells for Parallel Single-Cell Screening." *Journal of Robotics and Mechatronics*, Vol. 35, no. 5, pp. 1177-1184, 2023.

International conferences

1. **Panneer Selvam VENKATESH KUMAR**, Shunya OKAMOTO, Takayaki SHIBATA, Moeto NAGAI, "Cell Encapsulation within Hydrogel Using LCD 3D Printer for Single-Cell Screening" The 19^{th} IEEE International Conference on Nano/Micro Engineered and Molecular system, Kyoto, Japan. May 2024.

Domestic conferences

1. **PANNEER SELVAM VENKATESH KUMAR**, Murtaza GHULAM, Muhammad KAMALUDIN, Shunya OKAMOTO, Takayuki SHIBATA, Moeto NAGAI, **"**Single-Cell Image-Based Screening with Integration of Motorized Stages and Digital Mirror Device**"** The Robotics and Mechatronics Conference 2022, Sapporo, Japan. June 2022.

2. **PANNEER SELVAM VENKATESH KUMAR**, Murtaza GHULAM, Muhammad KAMALUDIN, Shunya OKAMOTO, Takayuki SHIBATA, Moeto NAGAI, **"**Automation of Single-Cell Image-Based Screening Using Light Irradiation**"** 2021 Autumn Meeting of the Japan Society for Precision Engineering conference, Kobe, Japan. September 2021.

D